ENVIRONMENTALLY BENIGN FLAME RETARDANT NANOCOATINGS FOR FABRIC

A Dissertation

by

YU-CHIN LI

Submitted to the Office of Graduate Studies of
Texas A&M University
in partial fulfillment of the requirements for the degree of

DOCTOR OF PHILOSOPHY

May 2011

Major Subject: Materials Science and Engineering

Environmentally Benign Flame Retardant Nanocoatings for Fabric

Copyright 2011 Yu-Chin Li

ENVIRONMENTALLY BENIGN FLAME RETARDANT NANOCOATINGS FOR FABRIC

A Dissertation

by

YU-CHIN LI

Submitted to the Office of Graduate Studies of
Texas A&M University
in partial fulfillment of the requirements for the degree of

DOCTOR OF PHILOSOPHY

Approved by:

Chair of Committee,	Jaime C. Grunlan
Committee Members,	James D. Batteas
	Miladin Radovic
	Victor M. Ugaz
Intercollegiate Faculty Chair,	Ibrahim Karaman

May 2011

Major Subject: Materials Science and Engineering

ABSTRACT

Environmentally Benign Flame Retardant Nanocoatings for Fabric. (May 2011)

Yu-Chin Li, B.S., National Taiwan University;

M.S., National Taiwan University

Chair of Advisory Committee: Dr. Jaime C. Grunlan

A variety of materials were used to fabricate nanocoatings using layer-by-layer (LbL) assembly to reduce the flammability of cotton fabric. The most effective brominated flame retardants have raised concerns related to their toxicity and environmental impact, which has created a need for alternative flame retardant chemistries and approaches. Polymer nanocomposites typically exhibit reduced mass loss and heat release rates, along with anti-dripping behavior, all of which are believed to be due to the formation of a barrier surface layer. Despite these benefits, the viscosity and modulus of the final polymeric material is often altered, making industrial processing difficult. These challenges inspired the use of LbL assembly to create densely layered nanocomposites in an effort to produce more flame-retardant coatings.

Laponite and montmorillonite (MMT) clay were paired with branched poly(ethylenimine) to create thin film assemblies that can be tailored by changing pH and concentration of aqueous deposition mixtures. Both films can be grown linearly as a function of layers deposited, and they contained at least 70 wt% of clay. When applying these films to cotton fabric, the individual fibers are uniformly coated and the fabric has

significant char left after burning. MMT-coated fabric exhibits reduced total heat release, suggesting a protective ceramic surface layer is created.

Small molecule, POSS-based LbL thin films were also successfully deposited on cotton fabric. With less than 8 wt% added to the total fabric weight, more than 12 wt% char remained after microscale combustion calorimetry. Furthermore, afterglow time was reduced and the fabric weave structure and shape of the individual fibers were highly preserved following vertical flame testing. A silica-like sheath was formed after burning that protected the fibers.

Finally, the first intumescent LbL assembly was deposited on cotton fabric. SEM images show significant bubble formation on fibers, coated with a 0.5 wt% PAAm/1 wt% PSP coating after burning. In several instances, a direct flame on the fabric was extinguished. The peak HRR and THR of coated fabric has 30 % and 65 % reduction, respectively, compared to the uncoated control fabric. These anti-flammable nanocoatings provide a relatively environmentally-friendly alternative for protecting fabrics, such as cotton, and lay the groundwork for rendering many other complex substrates (*e.g.*, foam) flame-retardant without altering their processing and desirable mechanical behavior.

DEDICATION

To

My father;

Without your encouragement

to continue on with my graduate studies,

I may have never reached this milestone.

Rest in peace.

ACKNOWLEDGEMENTS

I would like to thank my graduate advisor, Dr. Jamie Grunlan, for his guidance, inspiration, and financial support. The topic of the projects presented here is one of the most exciting and challenging that I have studied so far, and I am grateful to have enjoyed this opportunity to develop and showcase my strengths and competencies both in and out of the lab.

I would also like to thank for my graduate committee members, Dr. James Batteas, Dr. Miladin Radovic, and Dr. Victor Ugaz, for their valuable suggestions that helped steer my research.

The great help and dedication of two of my undergraduate research assistants, Sarah Mannen and Jessica Schulz, deserves to be featured in these acknowledgements as well, for without them the work would not have been done so efficiently. Thanks also go to my former and current colleagues in the Grunlan group: Yeon Seok Kim and You-Hao Yang, for their assistance with SEM imaging; Charlene Dvoracek, Yong Tae Park, and Morgan Priolo for their assistance with TEM imaging; and all other members of our research group for their support.

Finally, I must mention the great appreciation that I have for the love and encouragement that I have received from my family and friends; without you, I would not be able to complete this journey in pursuit of the Ph.D. degree. Thank you for being there!

NOMENCLATURE

AFM	Atomic Force Microscopy
AP	Aminopropyl Silsesquioxane Oligomer
ASTM	American Society for Testing and Materials
BPEI	Branched Polyethylenimine
FTIR	Fourier Transform Infrared Spectroscopy
LbL	Layer-by-Layer
MCC	Microscale Combustion Calorimeter
MMT	Montmorillonite
PAAm	Poly(allylamine)
POSS	Polyhedral Oligomeric Silsesquioxane
PSP	Poly(sodium phosphate)
QCM	Quartz Crystal Microbalance
SEM	Scanning Electron Microscopy
TEM	Transmission Electron Microscopy
TGA	Thermogravimetric Analysis
XRD	X-Ray Diffraction

TABLE OF CONTENTS

Page

ABSTRACT iii

DEDICATION v

ACKNOWLEDGEMENTS vi

NOMENCLATURE vii

TABLE OF CONTENTS viii

LIST OF FIGURES xi

LIST OF TABLES xvii

CHAPTER

I INTRODUCTION 1

1.1 Background 1
1.2 Objective and Dissertation Outline 4

II LITERATURE REVIEW 7

2.1 Polymer Combustion and General Flame Retardant Mechanism 7
2.2 Types of Flame Retardants 8
2.2.1 Halogenated FR 8
2.2.2 Phosphorus-Containing FR 10
2.2.3 Inorganic Hydroxides FR 11
2.2.4 Polymer Nanocomposites 12
2.3 Flame Retardant Strategies for Textiles 18
2.4 Layer-by-Layer Assembly 23
2.5 Flammability Testing Methods 27
2.5.1 Vertical and Horizontal Flame Tests (ASTM D6413 and D 5132) 28
2.5.2 Pill Test (ASTM D 2859) 30
2.5.3 Cone and Microscale Combustion Calorimetry (ASTM E 1354 and D 7309) 31

CHAPTER Page

III POLYELECTROLYTE/CLAY THIN FILM ASSEMBLIES: INFLUENCE OF PH ON GROWTH, MECHANICAL BEHAVIOR, AND FLAME RETARDANT BEHAVIOR ON COTTON FABRIC 35

3.1 Introduction 35
3.2 Experimental 37
3.2.1 Preparation of Deposition Mixtures 37
3.2.2 Substrates 37
3.2.3 LbL Film Deposition 38
3.2.4 Film Characterization 39
3.2.5 Thermal, Flammability and Combustibility 40
3.2.6 Analysis of Fabric Properties 41
3.3 Results and Discussion 42
3.3.1 Film Growth and Structure of BPEI/Laponite 42
3.3.2 Mechanical Behavior of BPEI/Laponite Assemblies 51
3.3.3 Flame Resistance of BPEI/Laponite-Coated Fabric 54
3.3.4 Film Growth and Structure of BPEI/MMT 58
3.3.5 Flame Resistance of BPEI/MMT-Coated Fabric 62
3.3.6 Physical Properties of Fabric 73
3.4 Conclusions 78

IV GROWTH AND FIRE PROTECTION BEHAVIOR OF POSS-BASED MULTILAYER THIN FILMS 80

4.1 Introduction 80
4.2 Experimental 82
4.2.1 Chemical Reagents and Substrates 82
4.2.2 Layer-by-Layer Deposition 83
4.2.3 Film Growth Characterization 83
4.2.4 Thermal Stability, Flammability, Combustibility and Ignition Testing of Fabrics 84
4.2.5 Analysis of Fabric 84
4.3 Results and Discussion 85
4.3.1 Growth and Structure of Si-Based Assemblies 85
4.3.2 Thermal Properties of Coated Fabric 89
4.3.3 Characterization of Burned Fabric 96
4.4 Conclusions 102

V INTUMESCENT LAYER-BY-LAYER COATINGS ON COTTON FABRIC 103

5.1 Introduction 103

CHAPTER Page

5.2 Experimental 104
5.2.1 Chemical Reagents and Substrates 104
5.2.2 Layer-by-Layer Deposition 105
5.2.3 Film Growth and Fabric Characterization 106
5.2.4 Thermal Stability, Flammability and Combustibility Testing of Fabric 106
5.3 Results and Discussion 106
5.3.1 Film Growth and Characterization 106
5.3.2 Thermal Stability of Coated Fabric 109
5.3.3 Flame Testing of Coated Fabric 113
5.3.4 Calorimetry of Coated Fabric 121
5.4 Conclusions 126

VI CONCLUSIONS AND FUTURE WORK 128

6.1 Polyelectrolyte/Clay Thin Film Assemblies 128
6.2 POSS-Based Multilayer Thin Film Assemblies 129
6.3 Intumescent Layer-by-Layer Assemblies 130
6.4 Future Research Plan 131
6.4.1 Improved, Softer Intumescent Coatings 131
6.4.2 Improvement of Nanocoating Durability 134
6.4.3 Commercial Scale Production 135

REFERENCES AND NOTES 137

VITA 171

LIST OF FIGURES

FIGURE Page

1.1 Layer-by-layer deposition process used to prepare functional thin films. Step 1 – 4 are repeated until the desired number of bilayers are generated on a substrate 3

2.1 Polymer combustion process 7

2.2 Free radical generation during the combustion of ethane 9

2.3 Structure of smectites 14

2.4 General structure of POSS 15

2.5 A schematic illustration of defined morphology of the polymer nanocomposites. Immiscible (a), intercalated (b), and exfoliated (c) 16

2.6 Flame retardant mechanism of polymer/clay nanocomposites 18

2.7 LbL assembly on colloidal particles are used to form hollow capsules..... 25

2.8 SEM (a) and TEM (b and c) images of hollow Laponite spheres..... 25

2.9 Nanotubes synthesis through LbL assembly on a porous template (a). SEM images of nanotubes, made by polyelectrolyte and Au nanoparticles, after removal of 400 nm-diameter pored polycarbonate template, and removal of the coated film on the top and bottom surfaces. 25

2.10 TEM images of cotton fiber coated with 20 BL of PSS/PAH. This conformal coating thickness, from A to C, is 365, 395, and 313 nm, respectively (a). High resolution TEM images of PSS/PAH film, with 18 to 22 nm thickness (b) 26

2.11 Schematic of TiO_2/POSS coated electrospun polymer fibers using LbL assembly (a). TEM images of TiO_2-coated electrospun fibers: PS (b) and PSEI (c) 27

2.12 Vertical (a) and horizontal (b) flammability testing apparatus 29

FIGURE Page

2.13 Images of 50/50 cotton polyester blend carpet with (left) and without (right) FR treatment after pill test 30

2.14 Schematic of cone calorimeter 32

2.15 Schematic diagram of MCC apparatus..... 34

3.1 Film thickness as a function of the number of bilayers deposited for LbL assemblies made with varying BPEI (a) and Laponite (b) deposition mixture pH. Only one ingredient's pH was varied at a time, while the other was held at its unadjusted pH (10.3 for BPEI and 10.1 for Laponite) 44

3.2 BPEI-Laponite film thickness as a function of bilayers deposited with varying NaCl concentration. The BPEI solution was maintained at pH 8 and Laponite pH was unadjusted 46

3.3 Film mass as a function of layers deposited for three different BPEI/ Laponite systems. In all cases, BPEI is odd layers and Laponite is even. When no pH is specified for BPEI or Laponite, it means the unadjusted pH was used 46

3.4 TEM cross-sectional images of 30 BL assemblies made with Laponite and BPEI at pH 10 (a) and pH 8 (b) and BPEI and Laponite at pH 6 (c) .. 48

3.5 AFM height (a), (c) and phase (b), (d) surface images of a 10 BL BPEI (pH 7) /Laponite film. (a), (b) are under 3 μm scale and (c), (d) are under 1 μm scale..... 49

3.6 X-ray diffraction patterns for neat Laponite, and 30 BL films made by varying the pH of the BPEI and Laponite solutions..... 50

3.7 Load-displacement curves (a), and mechanical properties ((b) hardness and (c) elastic modulus) of 40 BL thin films 53

3.8 Weight loss as a function of temperature for cotton fabrics coated with 10 bilayers of BPEI/Laponite (pH 6) and BPEI (pH 8)/Laponite. These results were obtained using TGA at a heating rate of 20 °C/min..... 55

3.9 Images of uncoated and coated cotton fabrics following the vertical flame test. Coated fabric is 10 BL of a given recipe 56

FIGURE Page

3.10 SEM images of virgin fabric before (a) and after (b) flame test; (c) coated fabric after flame test (BPEI (pH 8)/Laponite) 57

3.11 SEM images of fabrics before ((a)-(c)) and after flame test ((d)-(f)). (a) and (d) are uncoated fabrics, (b) and (e) are fabric coated with 10 BL of BPEI (pH 8)/Laponite, and (c) and (f) are fabric coated with 10 BL of BPEI/Laponite (pH 6) 58

3.12 Film thickness as a function of the number of bilayers deposited, for a series of LbL assemblies made with varying pH of the BPEI solution and concentration of the MMT mixture. MMT was used at its unadjusted pH of 9.8 59

3.13 Film mass as a function of individually deposited clay and polymer layers for four different BPEI/MMT systems. In all cases, odd layers are BPEI and even layers are MMT. 61

3.14 AFM height (a) and phase (b) surface images of a 30 BL BPEI pH 10/ 1 wt% MMT film; height (c) and phase (d) images of a 30 BL BPEI pH 7/1 wt% MMT film; and TEM cross-section (e) of a 40 BL assembly made with BPEI pH 10/0.2 wt% MMT 62

3.15 SEM images of cotton fabric coated with 20 BL of BPEI/MMT. These coatings were made using BPEI at pH 10 (a) and 7 (b). Both coatings were prepared with a 1 wt% MMT deposition mixture 63

3.16 Weight loss as a function of temperature for cotton fabrics coated with 5 BL (a) and 20 BL (b) of 0.1 wt% BPEI (pH 10 and 7) with 0.2 and 1 wt% MMT. These results were obtained using TGA at a heating rate of 20 °C/min under an air atmosphere. 65

3.17 Images of vertical flame testing of the uncoated and coated cotton fabrics 5 seconds after ignition. The coated fabrics are 20 BL of a given recipe 67

3.18 Images of uncoated and 20 BL coated cotton fabrics following the vertical flame test 67

3.19 SEM images of uncoated fabric before (a) and after (c) the vertical flame test. 5 BL-coated fabric (BPEI pH 10/0.2 wt% MMT) before (b) and after (d) flame test is also shown 69

FIGURE Page

3.20 Low magnification SEM images highlighting the weave structure of fabrics before and after burning: coated fabric before burning (a), ash from control fabric after burning (b), residues from fabric coated with 5 (c) and 20 BL (d) of BPEI pH 7/1 wt% MMT, and residue from fabric coated with 20 BL of BPEI pH 10/1 wt% MMT (e) 71

3.21 X-ray diffraction patterns for neat MMT, 20 BL BPEI pH 7/1 wt% MMT coated fabric, before and after burning, and the control fabric 71

4.1 Chemical structures of deposition materials and schematic of the LbL deposition process used to prepare Si-based assemblies. Steps 1 – 4 are repeated until the desired number of bilayers is deposited 83

4.2 Film thickness as a function of the number of bilayers deposited. Films were assembled from aqueous solutions with 1 wt% AP at pH 10 or 10 mM (+)POSS at pH 7.5, paired with 10 mM (–)POSS at pH 10 86

4.3 Accumulated film mass as a function of deposited layers for the two 10 mM (–)POSS (pH 10)-based films 87

4.4 AFM height (a) and phase (b) surface images of a 30 BL AP/(–) POSS film. Height (c) and phase (d) images of a 30 BL (+)POSS/(–) POSS film are also shown 88

4.5 Weight loss as a function of temperature for cotton fabrics coated with 5, 10, 20 and 30 BL of AP/(–)POSS (a) and (+)POSS/(–)POSS (b). Control refers to the uncoated cotton fabric 90

4.6 Images of vertical flame testing of the uncoated and coated cotton fabrics 6 seconds after ignition. The coated fabrics are 10 BL of a given recipe 93

4.7 Images of control, 5, 10, and 20 BL-coated cotton fabrics following the vertical flame test. Residues of fabrics coated with AP/(–)POSS (a), and (+)POSS/(–)POSS (b), are shown 94

4.8 Pill test images of post-burn control fabric (a), 10 BL AP/(–) POSS coated fabric (b), and 10 BL of (+)POSS/(–)POSS coated fabric (c) 96

FIGURE Page

4.9 SEM images of 5, 10 and 20 BL of AP/(–)POSS coated fabrics. The top row images are coated fabrics before flame testing, while bottom row images show the weave structure of residues after burning the coated fabrics in the vertical flame test 97

4.10 SEM images of 5, 10 and 20 BL of (+)POSS/(–)POSS pH 10 coated fabrics. The top row images are coated fabrics before flame testing, while bottom row images show the weave structure of residues after burning the coated fabrics in the vertical flame test..... 98

4.11 Residue of 20 BL of AP/(–)POSS coated fabric after vertical flame testing (a), SEM image of the white char (b), higher magnification SEM image of the hollow siliceous fiber tube (c), and EDX analysis of the hollow tube (d) 99

4.12 FTIR spectrum of control and AP/(–)POSS coated fabrics, at 5 and 20 BL (a). Spectrum comparison of AP/(–)POSS 20 BL coated fabric, and char 101

5.1 Structures of PAAm and PSP..... 105

5.2 Film thickness as a function of the number of bilayers deposited. Films were assembled with low and high concentration of PAAm pH 7and PSP pH 7, and a film made with 10 BL of BPEI pH 10 and MMT plus 20 BL of high concentration PAAm/PSP..... 108

5.3 Accumulated film mass as a function of deposited layers for the high concentration PAAm pH 7/PSP pH 7 system and with 10 BL of BPEI pH 10/MMT combined with 20 BL of high concentration PAAm/PSP 109

5.4 Weight loss as a function of temperature for fabric coated with different bilayers of low (a) and high (b) concentration PAAm/PSP, and $(BPEI/MMT)_{10}(PAAm/PSP)_{10n}$ (c) 112

5.5 Images of coated fabrics following vertical flame testing. Residue of fabrics coated with low (a) and high (b) concentration PAAm/PSP, and the combined system (c) are shown 114

FIGURE Page

5.6 Images of in progress horizontal flame testing of control (a), 20 BL of high concentration PSP-coated (b), and $(BPEI/MMT)_{10}(PAAm/PSP)_{20}$ coated (c) fabric. These images were taken 30 seconds after the flame passed the first scribed line. Post-test images of the control (d), 30 BL of high concentration PSP-coated (e), and $(BPEI/MMT)_{10}(PAAm/PSP)_{30}$ coated (f) fabric are also shown 116

5.7 Weave structure of control fabric (a), 10 (b) and 30 (c) BL of high concentration PSP-coated fabric, before burning, and the residue of 10 (d) and 30 (e) BL fabric after burning 117

5.8 SEM images of control fabric (a) and fabric coated with 10 (b), 20 (c), 30 (d), and 40 (e) BL of high concentration PSP before burning 118

5.9 SEM images of 10 (a), 20 (b), 30 (c) and 40 (d) BL of high concentration PSP-coated fabric after burning 119

5.10 Digital and SEM images of 20 (a), 30 (b), and 40 (c) BL high concentration PSP-coated fabric after burning 120

5.11 Heat release rate as a function of temperature for control, 10 and 30 BL of high concentration PSP-coated cotton fabric 122

5.12 Heat release rate as a function of time of control (a), 10 BL (b), and 30 BL (c) of high PSP-coated fabrics 126

6.1 Structures of hydroxyl-rich molecules 132

6.2 Covalent bonds formed between glutaraldehyde and amine or hydroxide groups 134

6.3 Schematic continuous roll-to-roll process (a) and an actual pilot scale production unit for continuous layer-by-layer assembly (b) 136

LIST OF TABLES

TABLE Page

2.1 Flame retardant fibers in common use 20

3.1 Thickness per bilayer for various BPEI/Laponite recipes..... 43

3.2 Film density and composition for various BPEI/Laponite recipes 45

3.3 Weight added by coating fabrics, and residue amounts after heat treatment..... 66

3.4 Microscale combustion calorimeter results for various coated fabrics..... 73

3.5 Fabric counts of uncoated and coated fabrics 74

3.6 Tearing force and tensile breaking force of uncoated and coated fabrics.. 76

3.7 Vertical wicking rate of fabrics..... 77

4.1 Thermogravimetric analysis of control and eight different coated fabrics 92

4.2 Microscale combustion calorimetry results for various coated fabrics..... 95

5.1 Thermogravimetric analysis of control and coated fabrics 111

5.2 Measurement of coated fabrics from vertical flame testing..... 115

5.3 Burning rate of control and coated fabrics from horizontal flame testing . 116

5.4 Microscale combustion calorimetry measurement for high PSP-coated fabric..... 122

5.5 Cone calorimeter data of control, 10 and 30 BL of high PSP-coated fabric 124

6.1 Potential ingredients for intumescent systems 133

CHAPTER I

INTRODUCTION

1.1 Background

A wide range of commonly used materials that adds to the quality of modern life, such as plastics and textiles, are highly flammable. In the United States, fire has killed more people than all natural disasters combined. According to a report from the National Fire Protection Association (NFPA), there were an estimated 1.3 million fires in 2009 that resulted in 3,010 civilian deaths (one every 175 minutes), and 17,050 injuries (one every 31 minutes).[1] Direct property loss due to fires was estimated at $12.5 billion. These issues have created a great need to produce materials that can reduce fire risk and significantly contribute to saving lives and resources.

Although the number of fire-related fatalities and amount of property damage has declined gradually as legislation has forced a variety of polymeric materials to be rendered flame retardant,[2-3] the need for new flame retardants continues unabated as new fire risk scenarios occur. As of 1998, flame retardants were second only to plasticizers in terms of quantity added to plastics.[4] Brominated compounds are the most commonly used flame retardants, but they may give rise to toxic, acidic and dense smoke.[5] Both the European Union and the United States government have expressed concern about the toxicity and environmental impact that halogenated additives create. These concerns

---

This dissertation follows the style of *ACS Nano.*

have led to significant research into the use of alternate flame retardant chemistries and approaches, including polymer nanocomposites prepared with more environmentally benign nanoparticles like clays[6-8] and carbon nanotubes.[9-10] These polymer nanocomposites typically exhibit reduced mass loss and heat release rates, along with anti-dripping behavior, all of which is believed to be due to the formation of a barrier surface layer in the case of clay[7] and a gel-like network in the case of nanotubes.[11] Despite this improved thermal behavior, adding these particles is known to increase viscosity and modulus of the final polymeric material, making industrial processing difficult.[12] These adverse side effects make their use in the protection of highly flammable flexible foams and fabrics prohibitive, and create a vitally important need for an alternative technology.

It has been proposed that the combustion process in polymer/clay systems involves a protective charred ceramic surface layer that is created during polymer ablation. Such a layer is presumably formed by the reassembly of the finely dispersed clay, which results in 70 to 80 % reduction in heat release for nanocomposites made at low clay loadings (typically 2 to 5 wt%).[13] Nanotubes have shown similar behavior by a similar mechanism.[11] It was this ceramic char-layer nanocomposite theory of flame-suppression that inspired the use of layer-by-layer (LbL) assembly to create densely layered nanocomposites in an effort to produce more flame-retardant materials.

Over the past two decades, layer-by-layer assembly has been studied extensively as a simple and versatile method to develop multifunctional thin films.[14-17] The LbL process typically involves alternately dipping substrates into aqueous mixtures of

positively- and negatively-charged polymers and/or particles (typically < 1wt% in water), as shown in Figure 1.1. Electrostatic attraction causes the charged substances to adsorb onto the surface one nano layer at a time, often creating a multilayer film less than one micron thick. The process is continued until the desired number of bilayers (BL) is reached. Some films exploit other forces such as covalent[18-19] or hydrogen bonds[20-21] instead of, or in addition to, electrostatic attraction. Spray coating[22] and spin coating[23-24] have been successfully used as alternatives to dipping the substrates. Film properties can be controlled by adjusting the deposition mixture conditions such as pH,[25-26] ionic strength,[27] and molecular weight[27-28] of the species, or by altering the temperature.[29-30] LbL films have been studied for applications that include sensing,[31-33] antimicrobial surfaces,[34] drug delivery and biomedical applications,[35-37] battery electrolytes,[38-39] superhydrophobic surfaces[40-41] and oxygen barrier layers.[42-43]

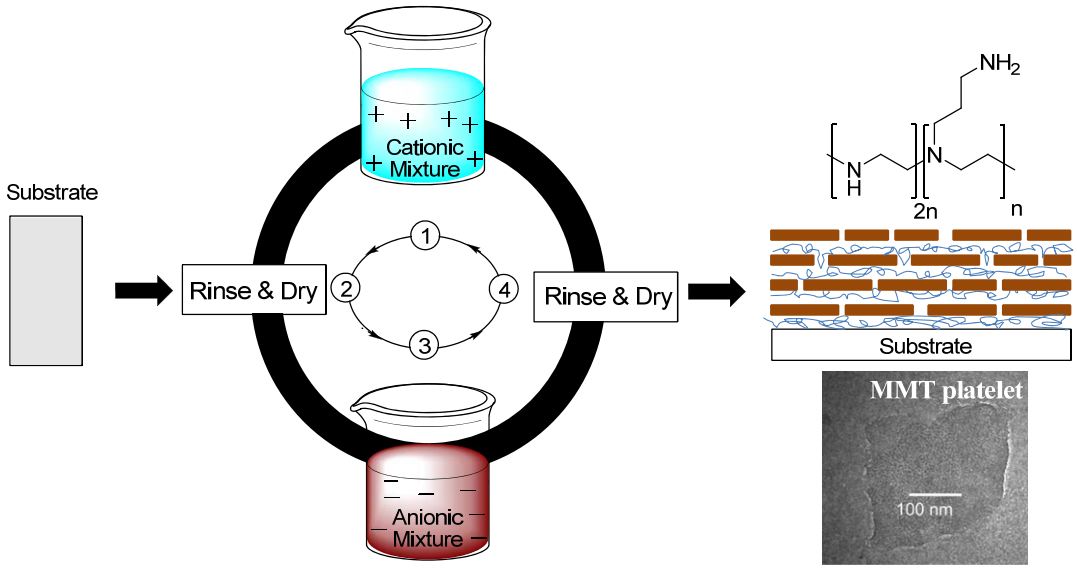

Figure 1.1. Layer-by-layer deposition process used to prepare multilayer thin films. Step 1 – 4 are repeated until the desired number of bilayers are generated on a substrate.

1.2 Objective and Dissertation Outline

Cotton fabric is the model substrate used throughout this study. It is one of the most natural textile fibers used to produce apparel, home furnishings, and industrial products, but this cellulosic material has a low limiting oxygen index (LOI) and combustion temperature (360 – 425 °C) that makes it highly flammable.[44] Cotton textiles burn rapidly once ignited, and the flame spreads quickly, potentially causing fatal burns within 15 seconds of ignition.[45] By coating cotton fabrics with a flame retardant thin film, we intend to slow down the burning process of the fabric to reduce injury and damage as a result of exposure to fire. The objective of this study is to develop and examine the efficacy of flame retardant nanocoatings deposited on the three-dimensional surface of virgin cotton fabric *via* layer-by-layer assembly. These thin coatings serve as a protective barrier against direct flame and heat. The ultimate goal of this study is to create a coating system that will be able to coat any type of substrate (with proper surface pre-treatment) and extinguish flame on the coated substrate when exposed to the fire.

Chapter II is a brief review of the flame retardant and layer-by-layer assembly literature. The combustion process of polymers and the flame retardant methods and mechanism are first presented, followed by flame retardant strategies for textiles. The second part of this review covers the basics of LbL assembly, with special emphasis on the use of complex surface (*e.g.*, fibers, patterned/textured surfaces, particles, etc.), and the flame testing methods used in this dissertation.

Chapter III describes two different clays (synthetic laponite and natural montmorillonite) paired with branched polyethylenimine (BPEI), as the components of multilayer assemblies. The influence of pH on polymer/clay growth and mechanical properties are examined, as well as the flammability of the coating on cotton fabric. Additional investigation of the flame retardant behavior of polymer/clay coatings was conducted by varying the concentration of the montmorillonite deposition solution. Ellipsometry and quartz crystal microbalance (QCM) were used to measure the thickness and the mass composition of the assemblies. Surface morphologies were imaged by atomic force microscopy (AFM) and the lateral spacing of clay in the films was analyzed by x-ray diffraction (XRD).

Chapter IV examines the use of silicon-containing materials in these flame retardant nanocoatings. Aminopropyl silsesquioxane (AP) or OctaAmmonium POSS® ((+)POSS) (both positively-charged in water), and OctaTMA POSS® ((–)POSS, negatively-charged in water), are the components of these assemblies. Two coating systems, AP/(–)POSS and (+)POSS/(–)POSS thin films, were first grown and characterized on a silicon wafer before depositing them onto fabric. Thermogravimetric analysis (TGA), microscale combustion calorimetry (MCC) and vertical flame testing (ASTM D6413) were used to examine the flammability of the coated fabrics. Scanning electron microscopy (SEM) and Fourier transform infrared spectroscopy (FTIR) were used to analyze the coating on the fabrics before and after burning.

Chapter V describes the first ever intumescent nanocoatings created by LbL assembly. Poly(allylamine) and poly(sodium phosphate) are the N-rich and P-rich

components necessary for such a coating. TGA and vertical flame tests of coated fabrics demonstrate evidence of intumescent flame retardant behavior. The concentration of the deposition solutions and the number of deposited bilayers were adjusted to optimize the flame retardant effect. Burning rate (by horizontal flame test), time to ignition and heat release measurements (by cone calorimeter) were used to evaluate anti-flammable performance. Polymer/clay layers were also added underneath the intumescent systems in an effort to evaluate the synergy between intumescent and barrier layers.

Chapter VI provides some conclusions for this work and future research directions. This dissertation lays the groundwork for creating flame retardant nanocoatings via LbL assembly. Three different types of flame retardants were studied, with each system providing some added level of anti-flammability. To further improve these coatings, additional ingredients will need to be evaluated with regard to chemistry, concentration and number of layers deposited. Improving coating durability is another important topic to be studied, especially if this technology will be used commercially.

CHAPTER II

LITERATURE REVIEW

2.1 Polymer Combustion and General Flame Retardant Mechanism

All organic polymeric materials are combustible. They decompose or pyrolyze when exposed to sufficient heat, generating flammable volatiles. When these volatiles mix with air (oxygen), ignition occurs. Figure 2.1 summarizes the polymer combustion process. With sufficient heat, polymers will go through an endothermic process, known as pyrolysis, which causes bond-breaking (200 – 400 kJ/mol). The products from pyrolytic decomposition include combustible gases, non-combustible gases, and carbonaceous char. When the combustible gases (fuel) mix with oxygen, ignition occurs due to the presence of an external flame or spark. Flame and heat are generated after ignition, and some of the heat is transferred back to the polymer pyrolysis process. This cycle leads to an increasing supply of fuel to the flame, which then spreads over the polymer surface.[46]

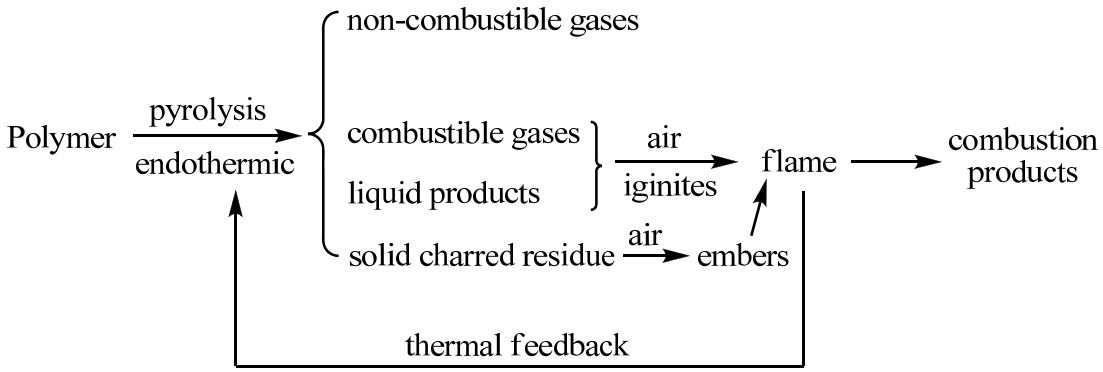

Figure 2.1. Polymer combustion process.[47]

The mechanism of flame retardant behavior can be divided into two different modes of action that break the polymer combustion cycle. A condensed-phase mechanism occurs when a flame retardant agent chemically interacts with the polymer to generate char (or the polymer physically retains its condensed phase after thermal decomposition). Another form of the condensed phase mechanism involve an additive creating a physical barrier that interrupts the pyrolytic path of the polymers, reduces the combustible gases, and slows the heat and mass transfer.[48-49] Gas-phase is the other mechanism that can happen chemically and/or physically. Active flame retardants scavenge free radicals from chain-branching reactions (*i.e.*, the active intermediates increase after each propagation step) in the flame. Inert flame retardants can generate large amount of non-combustible gases, to dilute the flammable gases, and decrease the burning temperature by absorbing heat when endothermic dissociation happens.[50]

2.2 Types of Flame Retardants

Several types of flame retardants (FR) have been used for suppression of the combustion process. Traditional flame retardants include halogenated, phosphorus-containing, and inorganic metal hydroxides. Polymer nanocomposites, containing particles such as clay, are a newer development in the area of flame retardancy.

2.2.1 Halogenated FR

When polymers are exposed to sufficient heat, highly reactive H• and OH• radicals are generated that propagate chain branching reactions, leading to

decomposition and burning.[50] Figure 2.2 shows an example of how free radicals are generated and propagate from ethane.

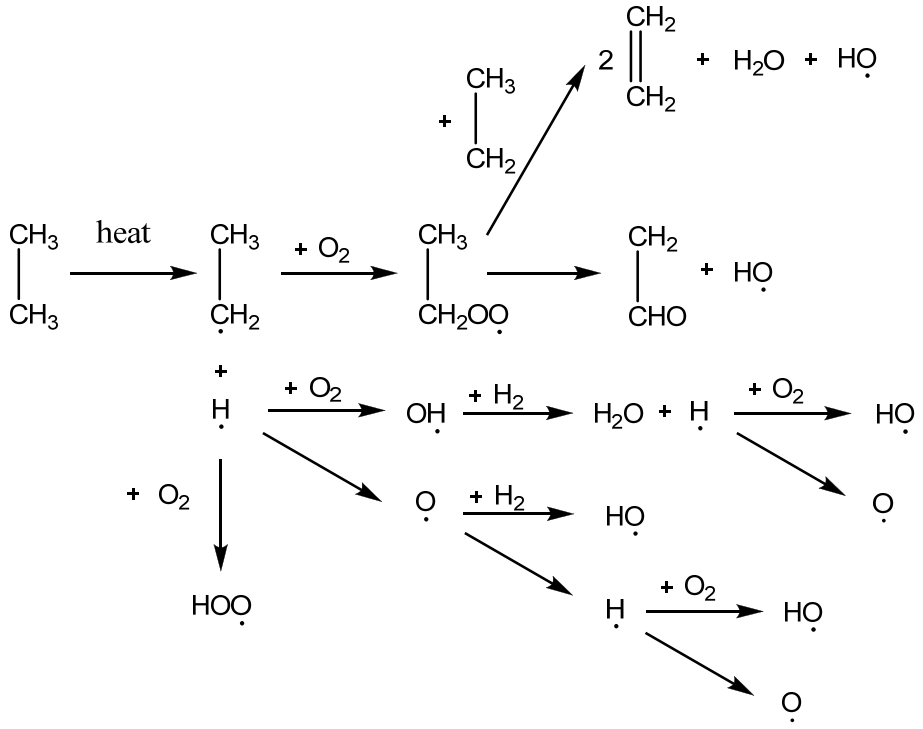

Figure 2.2. Free radical generation during the combustion of ethane.[51]

Halogenated compounds, most commonly brominated,[52-54] are often mixed into polymers as additives or introduced by copolymerization.[47, 52] The primary halogenated flame retardant mechanism is chemical reaction in the gas phase. Halogenated FR degrades (or volatilizes) when the temperature increases and they release halogen radicals X• (1), and these radicals can abstract hydrogen atoms from polymers to form hydrogen halides (2). These hydrogen halides are the actual flame inhibitor because they quench the radicals that cause chain branching propagation (3), (4).

$$R—X \rightarrow X\bullet + R\bullet \quad (1)$$

$$RH + X\bullet \rightarrow HX + R\bullet \quad (2)$$

$$H\bullet + HX \rightarrow H_2 + X\bullet \quad (3)$$

$$OH\bullet + HX \rightarrow H_2O + X\bullet \quad (4)$$

A physical flame retardant action can happen in the gas phase as hydrogen halides dilute the concentration of combustible gases and decrease the temperature of the flame.[55] In the condensed phase, after abstracting the hydrogen by halogen radicals, newly unsaturated polymers form double bonds that are known to be the precursors of char formation.[56]

2.2.2 Phosphorus-Containing FR

Phosphorus-containing flame retardants include elemental red phosphorus,[57] inorganic phosphates,[58] and organophosphates.[59] It is believed these flame retardants are significantly more effective in oxygen-containing polymers (*e.g.*, cellulose and rigid polyurethane foam).[60-61] Phosphorus compounds will decompose thermally in the condensed phase to phosphoric and polyphosphoric acids, which can phosphorylate the hydroxyls and also release water. Phosphorylated molecules break down further to form the char that protects a polymer surface from flame and oxygen.[50] Besides promoting char formation, phosphorus-based flame retardants can coat the char to prevent burning by obstruction of the surface that results in an inhibition of smoldering, which is known as glowing combustion of the char.[62-63] Volatile phosphorus compounds ($HPO_2\bullet$, $PO\bullet$, $PO_2\bullet$ and $HPO\bullet$) in the gas phase act as scavengers of $H\bullet$.or $OH\bullet$ radicals and they are

five times more effective than bromine, and 10 times more effective than chlorine, in flame retardancy.[64]

Intumescent systems are another category of flame retardants that use phosphorus compounds.[65-66] When polymers do not have reactive groups, coadditives are needed to create a viscous swollen char on the surface when burning and protect the underlying polymer. Three ingredients are necessary for the intumescent effect: an acid source (precursor for catalytic acidic species, [*e.g.*, ammonium polyphosphate and melamine phosphate, etc.]), a char-forming agent (polyhydric compounds, [*e.g.*, starch, dextrins, and pentaerylthritol], to undergo the phosphorylation), and a blowing agent (*e.g.*, urea or melamine) that decomposes to generate gases and cause the char to swell.)[65] It has been suggested that amines/amides catalyze the reactions leading to the formation of char.[66] Some studies have also shown that the combination of phosphorus and certain nitrogen compounds can interact synergistically and improve the anti-flammability of cellulose[67-68] and thermoplastics.[69-70] P–N synergism can increase the rate of phosphorylation on hydroxyls, and P–N bonds are more reactive than P–O bonds in the phorphorylation process.[71]

2.2.3 Inorganic Hydroxides FR

Inorganic hydroxides, such as aluminum trihydroxides (ATH) and magnesium hydroxide, can undergo endothermic decomposition (5), (6) to produce water upon heating above 200 °C.[72] This energy absorption is one of the key reasons these materials are flame retardant.

$$2\ Al(OH)_3 \rightarrow Al_2O_3 + 3\ H_2O \quad 1.17\ kJ/g \tag{5}$$

$$Mg(OH)_2 \rightarrow MgO + H_2O \quad 1.356\ kJ/g \tag{6}$$

As water releases into the vapor phase it dilutes the concentration of combustible gases produced by polymer decomposition, and limits the heat being fed back to the surface of the polymer.[73] Anhydrides can act as an acid catalyst to promote charring. Moreover, these minerals can reflect the heat when they accumulate on the surface. All inorganic hydroxides are relatively nontoxic, but they generally require more than 50 % by weight of the substrates to pass the flame retardancy tests.[74]

2.2.4 Polymer Nanocomposites

Nanocomposites terminology was first reported in the 1960s by Blumstein.[75-76] There are two components that differentiate these materials from macroscopic composites (or microcomposites): nanoparticles (at least one dimension < 100 nm, 1 to 10% mass fraction) and the interfacial polymer associated with them. When properly formed, with nanoparticles evenly dispersed throughout the polymer, no bulk polymer exists. Nanoparticles used in polymer nanocomposites are often described by the number of nanoscale dimensions. There are layered materials (2D), tube/rods (1D) and spherical/colloidal solids (0D).[77-78] There are several examples of 2D nanoparticles, such as layered double hydroxides (LDH),[79] layered zirconium phosphate,[80] layered titanates[81] and layered silicates,[82] or clay, which is the most widely studied.[12, 83-84] Nanocomposites exhibit superior properties to more macroscopic composites and pure polymers, such as high modulus and strength, decreased gas permeability, increased

solvent resistance, increased thermal stability and high transparency.[84-85] Some of these improved properties have inspired the study of nanocomposites as flame retardant materials.

Montmorillonite clay is by far the most studied platelet filler for polymer nanocomposites, having been used to enhance mechanical properties,[84, 86-87] reduce gas permeability,[88-90] and improve anti-flammability.[7-8, 91-92] MMT is a member of the smectite family in which an individual clay platelet (elementary sheet) is composed of one central layer of $Al(OH)_6^{-3}$ or $Mg(OH)_6^{-4}$ octahedra, sandwiched between two layers of $Si_2O_5^{-2}$ tetrahedra, as shown in Figure 2.3. The clay has a negative surface charge that is balanced by cations such as Na^+ or K^+ in the gallery space between layers,[93] which can be exchanged with various organic cations. Those organic cations can make organosilicates more compatible with polymers.[85] The thickness of these individual clay units (*i.e.*, platelets) is approximately one nanometer.

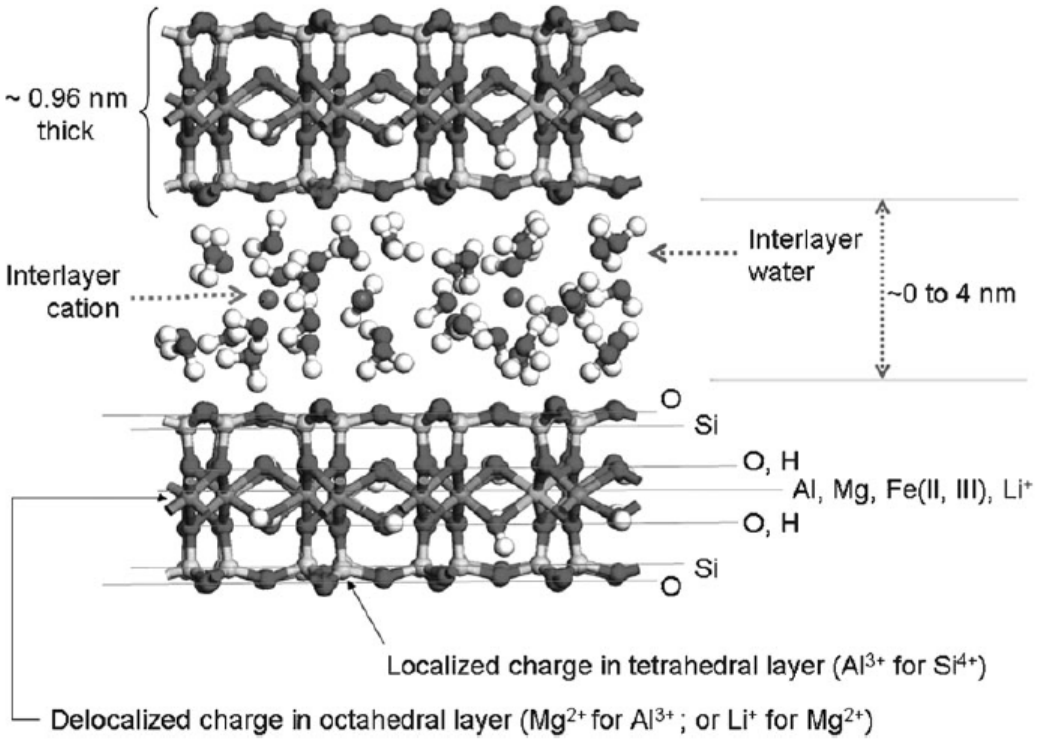

Figure 2.3. Structure of smectites.[93]

In addition to the layered silicates (i.e., clay), carbon nanotubes (CNTs) and nanofibers are becoming more commonly used in polymer nanocomposites.[94-96] CNTs are nano-cylindrical carbon molecules and have a very high aspect ratio (often > 1000).[10] CNTs have unique mechanical, electrical and thermal properties that make them good candidates to replace the conventional nanofillers in the fabrication of polymer nanocomposites.[11, 97-98] Because of strong attractive Van der Walls forces, CNTs are typically aggregated, requiring surface treatment with various species, such as functionalization or grafting on the surface that leads to improved dispersion.[94, 99] CNTs

appear to be the second most investigated nanoparticles to reduce the flammability of polymers.[11, 100-101]

Polyhedral oligomeric silsesquioxane (POSS) is one example of a zero-dimensional nanoparticle, whose general structure is shown in Figure 2.4. POSS is an inorganic-organic hybrid, containing an inorganic siloxane-like core, Si_8O_{12}, and organic substituents that can be modified with various groups. These molecules/particles can reinforce polymer chain segments and control chain motions by maximizing surface area and interaction with polymers in composites.[102-103] Varied POSS chemistries have been studied with polymers to improve mechanical behavior,[104] thermal stability,[105] low dielectric constant,[106] and reduced flammability.[107-108]

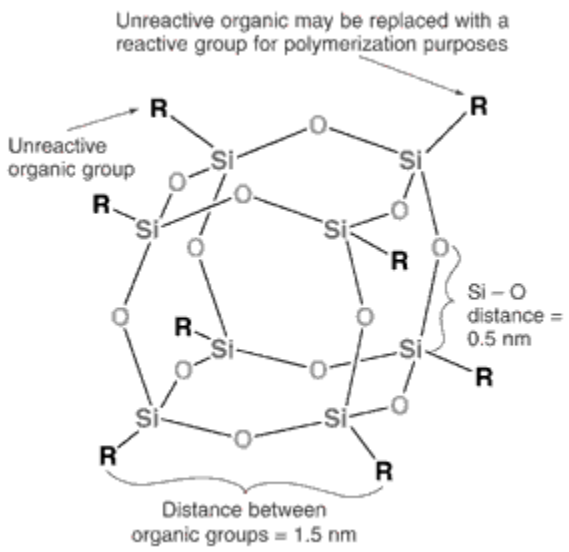

Figure 2.4. General structure of POSS.[109]

Simple physical mixing of a polymer and nanoparticles does not typically result in a nanocomposite, but rather creates a conventional composite with relatively poor

mechanical and thermal properties because of micro (or macro) phase separation. There are three ways to successfully create a true the polymer nanocomposite: by *in-situ* polymerization,[110] solvent blending[89] and melt compounding.[83] The key issue is to break up the agglomerates into single nanoparticles and uniformly disperse them in the polymer matrix. In the case of clay, three morphologies are possible (Fig. 2.5): immiscible (clay is not well-dispersed and this is more like a conventional composite), intercalated (good dispersion of the clay in the polymer, periodic spacing between clay layers is expanded), and exfoliated (the spacing between clay layers has been lost and individual platelets are randomly dispersed).[111-112] There is not much difference in fire retardancy when the nanocomposites are either in the exfoliated or intercalated state.[77]

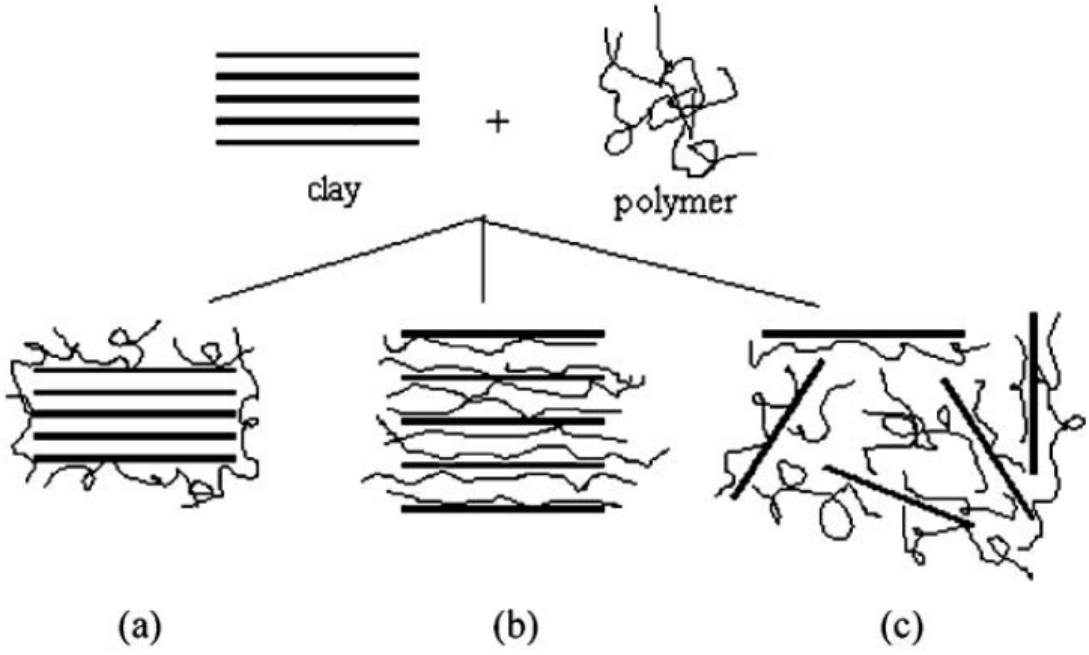

Figure 2.5. A schematic illustration of defined morphology of the polymer nanocomposites. Immiscible (a), intercalated (b), and exfoliated (c).[111]

All polymer nanocomposites use a similar method to reduce flammability. In general, the nanoparticles reduce mass loss rate by slowing the rate of polymer pyrolysis, which in turn lowers the heat release rate when the polymer burns.[77] The reason for the lowered mass loss rate is the protective barrier formed when the polymer nanocomposites decompose. For polymer-clay composites, a protective clay-rich barrier is formed shortly after exposure to heat/flame.[91, 113] It is believed that clay is pushed by the numerous bubbles of degradation products and migrates to the surface of the polymer matrix.[114-115] This clay-rich layer also provides thermal insulation for the condensed phase.[7] Figure 2.6 summarizes the various stages of clay-filled polymer degradation and the associated barrier protection.[116] As discussed throughout this dissertation, it was the realization that fire protection is largely a surface issue that inspired the use of layer-by-layer assembly (Section 2.4) to put anti-flammable materials directly where they are needed. This is especially important for fabrics, whose need for flexibility and complex surface makes them difficult to render highly flame retardant.

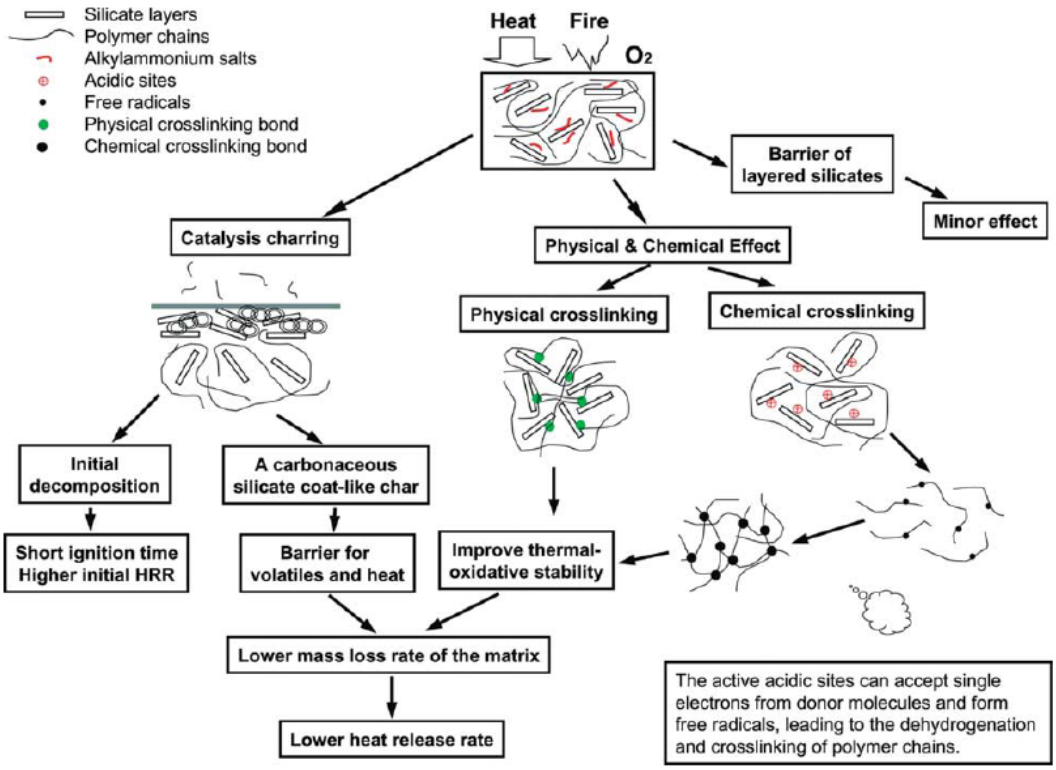

Figure 2.6. Flame retardant mechanism of polymer/clay nanocomposites.[116]

2.3 Flame Retardant Strategies for Textiles

Fibers used in fabric have varied burning behavior depending on their physical and chemical properties. All organic materials ultimately degrade under intense and prolonged heat. Individual fibers are typically 10 – 30 µm in diameter and yield fabrics with thickness from 100 µm up to several millimeters when woven together. High fiber surface-to-mass ratio creates a low temperature gradient and causes the combustion process to occur very quickly.[117] In addition to fiber size and chemistry, burning behavior depends on the fabric density, weave structure, finish, garment design, ignition source and intensity, and orientation. As a result of so many variables, a specific flame

retardant system is required for a given end use and fabric type. As shown in Figure 2.1, the combustion cycle of textiles is the same as bulk polymers, and there are several ways to break this cycle:[118]

- Removal of heat
- Increased decomposition temperature
- Decreased formation of flammable volatiles (increases char)
- Reduced access to oxygen (or flame dilution)
- Interference with flame chemistry and/or increased fuel ignition temperature

Flame retardants function in more than one mode, as described in Section 2.2. Several practical examples of flame retardant fibers are shown in Table 2.1.[118]

There are numerous strategies used to make textile fibers flame retardant: surface treatment, fire retardant additives/comonomers in synthetic fibers, nanocomposite-based, heat resistant and inherently fire retardant fibers, and fiber blending.[117] Presently, FR additives are used to increase the flame retardancy of synthetic polymers by either attaching them to the polymer chain during polymerization or introducing them in the polymer melt or in solution before extrusion.[117-118] As shown in Table 2.1, the additives for viscose (or rayon), polyester, and polypropylene are phosphorus-based, and their mode of action is through the condensed phase. Clay-polymer nanocomposites are well studied as a good thermal and physical barrier, but the thin fibers in textile does not allow enough time for clay to make a barrier during burning. Several synthetic fibers have been studied by adding clay[119-122] and POSS[123] as the flame retardant, but there are currently no commercial nanocomposite textiles.

Table 2.1. Flame retardant fibers in common use[118]

Fiber	Flame retardant structural components	Mode of introduction
Natural:		
cotton	Organophosphorus and nitrogen-containing monomeric or reactive species, e.g. Proban CC (Rhodia), Pyrovatex CP (Ciba), Aflammit P and KWB (Thor), Flacavon WP (Schill & Seilacher)	chemical finish
	Antimony-organo-halogen systems, e.g. Flacavon F12/97 (Schill & Seilacher), Myflam (B F Goodrich)	chemical finish
wool	Zirconium hexafluoride complexes, e.g. Zirpro (IWS); Pyrovatex CP (Ciba), Aflammit ZR (Thor)	chemical finish
Regenerated:		
viscose	Organophophorus and nitrogen/sulphur-containing species, e.g. Sandoflam 5060 (Clariant), in FR Viscose (Lenzing); polysilicic acid and complexs e.g. Visil AP (Sateri)	additive introduced during fiber production
Inherent Synthetic:		
polyester	Organophosphorus species: Phosphinic acidic comonomer, e.g. Trevira CS (Trevira GmbH); phosphorus-containing additive, Fidion FR (Montefibre)	copolymeric modification
acrylic	Halogenated comonomer (35-50% w/w) plus antimony compound, e.g. Velicren (Montefibre); Kanecaron (Kaneka Corp.)	copolymeric modification
polypropylene	Halo-organic compounds usually as brominated derivatives, e.g. Sandoflam 5072 (Clariant)	additive introduced during fiber production
polyhaloalkenes	Polyvinl choloride, e.g. Clevyl (Rhone-Poulenc. Polyvinylidene chloride, e.g. Saran (Sarah Corp.)	homopolymer
High Heat and Flame Resistant (Aromatic):		
polyaramids	Poly(m-phenylene isophthalamide), e.g. Nomex (Du Pont), Conex (Teijin). Poly(p-ohenylene terephthalamide), e.g. Kevlar (Du Pont), Twaron (Acordis)	aromatic homo- or copolymer
poly(aramid-arimid)	e.g. Kermel (Rhone-Poulenc)	aromatic homo- or copolymer
polybenzimidazole	e.g. PBI (Hoechst-Celanese)	

Inherently flame and heat resistant fibers are either all aromatic polymeric structures or inorganic and mineral based. Aramids, which have aromatic repeat units, bonded with either amide or imide, have decomposition temperatures above 375 °C.[118] As shown in Table 2.1, the most commonly used aramids are Nomex and Kevlar. Inorganic fibers include glass, carbon and ceramic. Glass fiber is nonflammable, but melts at 600 °C,[124] while carbon fibers have extremely high heat resistance with a melting temperature near 4000 °C.[125] Ceramic fibers, such as SiC, silicon and alumina, have been developed to withstand temperatures above 1000 °C.[126] Fiber blending is another method to reduce the flammability of fabric. For example, polyester or nylon are often blended with cotton to reduce flammability.[127-128] Aircraft seats and fire fighters' protective garments show better performance when Nomex is blended with other FR fibers.[129-130]

Surface treatment, in the form of finishes and coatings, are the oldest methods to reduce textile flammability. Most of finishes were developed between 1950 and 1970,[118, 125, 129] and applied by a pad-dry method that impregnates the fabrics in an aqueous solution of chemicals. Ammonium phosphates create the most effective flame retardant finish for cotton. The water-solubility of AP makes it a non-durable treatment, which is useful for disposable fabrics, insulation, wall boards, packaging material, and paper.[117] Ammonium polyphosphates (APP), paired with urea, provide semi-durable finishes by curing at 160 °C to induce phosphorylation. This type of finish is useful for materials that do not require frequent washings, such as mattresses, drapes, upholstery, and carpets. Durable finishes are chemically cured, and the most successful examples are

listed in Table 2.1. Pyrovatex CP type treatments can crosslink with cellulose and they have strong affinity to dyes, which make them useful for curtains and apparel. Proban CC type treatments create a highly crosslinked three-dimensional polymer network, providing greater fabric strength.[117, 129]

Coatings are applied as a continuous or discontinuous layer on the surface of a fabric, to generate heterogeneous fabric/polymer composites.[131] Properties such as water resistance, flexibility and moisture permeability, can be imparted by these coatings. It is important to have FR additives present to protect these functional coatings as well as the underlying fabric. Back-coating is the most well-established method, where FR compounds are in a bonding resin and applied on the reverse surface of the fabrics as a paste or foam. Brominated compounds are the most common FR for back-coating due to their effectiveness in various fabrics (*e.g.*, nylon, polypropylene, acrylics and many blends).[131-132] Due to environmental concerns, phosphorus-based and intumescent coatings have been developed more recently,[133-134] including microencapsulation of ammonium phosphate in polyurethane coating on textiles.[135-136] Most commercial flame retardants contain 8 – 20 % P and the total amount of material added on the fabric surface ranges from 5 to 25 wt%, with respect to the textile weight.[137] The bonding resin is usually flammable, unless it is inherently flame retardant, so the amount of the flame retardant present in coating is often higher than is necessary to be effective on the fabric alone. Smarter forms of flame retardant coating are needed to overcome these issues.

Plasma offers a way to achieve improved coatings by activating the fabric surface. Plasma-induced-graft-polymerization, in which the plasma is used to activate

the surface and plasma of the inert gas is used to initiate polymerization of the monomers on the surface of the substrates, was used for grafting rayon, polyacrylonitrile, and cotton fabrics with phosphorus-containing molecules.[138-140] Other nanotechnologies such as liquid phase deposition,[141] Langmuir-Blodgett films,[142] the sol-gel technique,[143] physical vapor deposition,[144] chemical vapor deposition,[145] surface grafting of polymer nanofilms,[146] synthesis of smart switchable hybrid polymer nanolayers,[146-147] and layer-by-layer self-assembly of nanolayer films,[148] have also been developed to modify surfaces for different applications. By coating only individual fiber surfaces, instead of being applied on the bulk textile surface, layer-by-layer assembly provides one the most effective ways to apply high concentrations of flame retardants precisely where needed to enhance anti-flammability.

2.4 Layer-by-Layer Assembly

As mentioned in Chapter I, layer-by-layer assembly has become a popular method to fabricate multifunctional films that are typically less than one micrometer thick. A variety of LbL-assembled functional thin films are currently being evaluated for various applications. The concept of LbL assembly was first introduced by Iler using anionic and cationic colloidal particles to build multilayerd assemblies.[149] Decher later used linear polyelectrolytes to realize this concept.[150-151] Since the 1990s, a wide range of materials have been extensively studied, including conventional polyelectrolytes,[25, 152] conductive polymers,[153-154] dendrimers,[155] proteins,[156-157] nucleic acids,[158] saccharides,[159] virus particles,[160] inorganic colloidal particles,[161-162] quantum dots,[163] clay platelates,[164-

[165] nanosheets,[81, 166] nanorods,[167-168] nanowires,[169] nanotubes,[31, 170-171] organic dyes,[172-173] micelles,[174] vesicles[175] and lipid membranes.[32]

In the early days of LbL technology, researchers assembled films on a flat solid support of macroscopic dimensions, but the mechanism of LbL assembly does not limit the size and shape of the substrate. The highly conformal nature of LbL assembly allows multilayered thin films to be deposited on both three-dimensional structures and nano/micro-sized objects. One example of 3-D conformal LbL assemblies uses colloidal particles to generate hollow capsules,[176] as shown in Figure 2.7. Titanium dioxide, silica, and Laponite nanoparticles were used as the inorganic building blocks for multilayer formation on polystyrene (PS) sphere templates. The type, shape (spherical to sheet-like) and size (3 – 100 nm) of nanoparticles, and the diameter of the PS templates (210 – 640 nm) were used to study the multilayer formation on spheres.[177] These hybrid core-shell particles were then calcined to create hollow spheres. Figure 2.8 shows hollow Laponite spheres that were obtained after calcinations of PS spheres (640 nm) coated with 5 BL of Laponite/poly(diallydimethylammonium chloride) (PDDA). A similar template synthesis was applied to nanotube formation, as shown in Figure 2.9(a). Self-assembled nanotubes are achieved when the template contains regular pores. Template removal can also result in a self-standing tubular structure. Figure 2.9(b) shows nanotubes assembled with polyelectrolytes and gold nanoparticles after removal of a polycarbonate membrane with 400 nm diameter pores.[178]

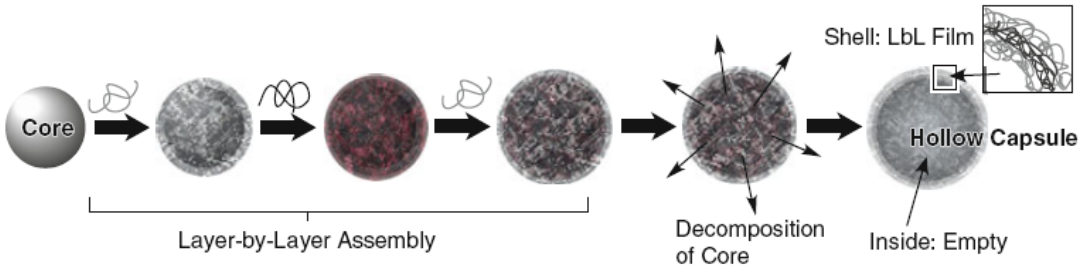

Figure 2.7 LbL assembly on colloidal particles are used to form hollow capsules.[14]

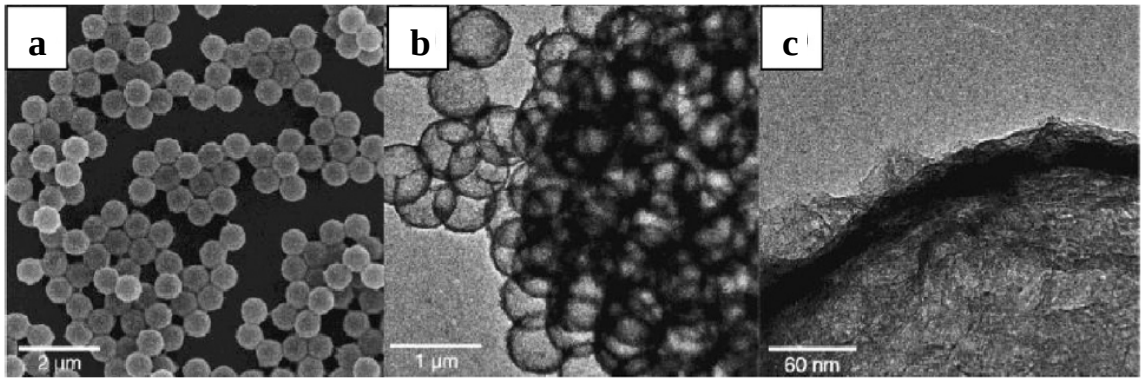

Figure 2.8 SEM (a) and TEM (b and c) images of hollow Laponite spheres.[177]

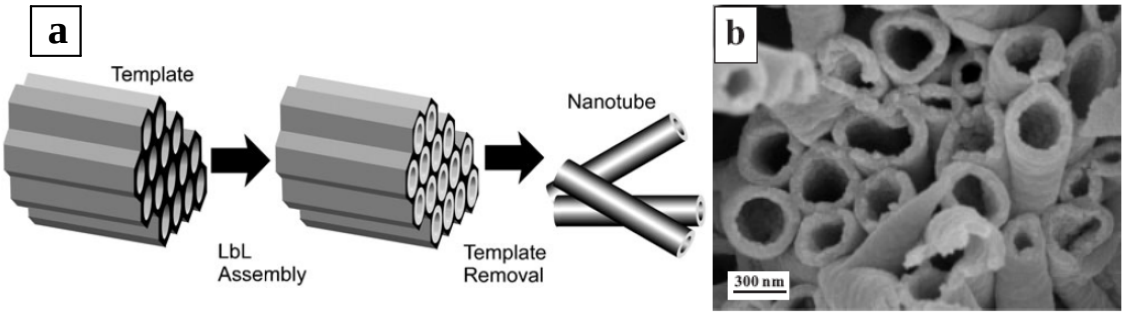

Figure 2.9. Nanotube synthesis through LbL assembly on a porous template (a).[14] SEM images of nanotubes, made by polyelectrolyte and Au nanoparticles, after removal of 400 nm-diameter pored polycarbonate template, and removal of the coated film on the top and bottom surfaces.[178]

Besides coating on templates, like cores and pores, several studies coat on the complex substrates such as fibers, fabrics and papers.[40, 148, 179-183] Cotton fibers have been coated with polystyrene sulfonate (PSS) and polyallylamine hydrochloride (PAH) through LbL assembly.[184] The cotton fibers were initially treated with 2,3-epoxypropyltrimethylammonium chloride to positively charge the surface. X-ray photoelectron spectroscopy (XPS) and TEM indicate that uniform coating of PSS and PAH was achieved on the cotton surface, as shown in Figure 2.10. Moreover, the LbL assembly was found to be more dependent on the nature of polyelectrolytes than that of substrate.[184] Different surface charge density levels on cotton fibers were also prepared, and the elemental analysis and XPS data show that PSS/PAH deposition is not significantly influenced by charge density on cotton. This uniform nanocoating was also found to be insensitive to the charge on the substrate surface once a critical number of layers was deposited.[148]

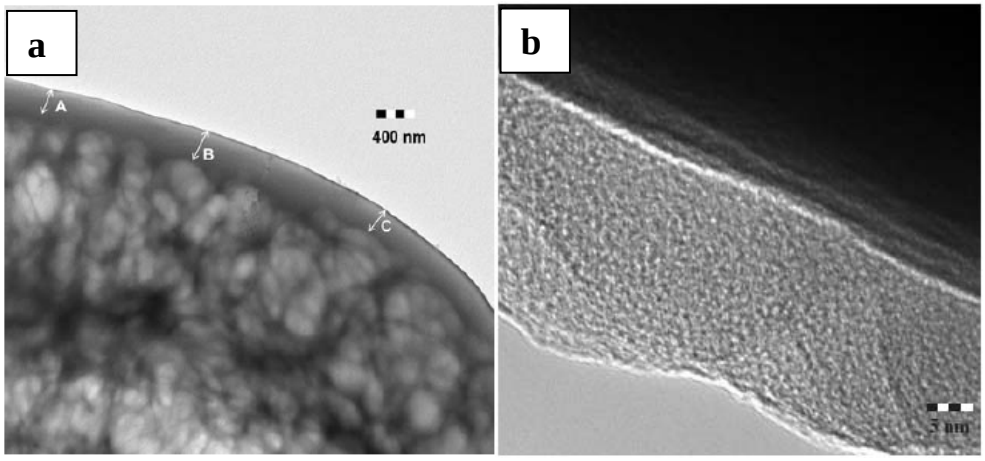

Figure 2.10. TEM images of cotton fiber coated with 20 BL of PSS/PAH. This conformal coating thickness, from A to C, is 365, 395, and 313 nm, respectively (a).[148] High resolution TEM images of PSS/PAH film, with 18 to 22 nm thickness (b).[184]

LbL assembly can also be applied to electrospun nanofibers.[22, 181] Polystyrene (PS), polyacylonitrile, a blend of poly(methyl methacrylate) and poly(ethylene oxide), and poly(dimethylsiloxane-*b*-etherimide) (PSEI) were treated with plasma before coating with TiO_2 nanoparticles and positively charged polyhedral oligosilsesquioxane (POSS), as shown in Figure 2.11(a). This type of nanoparticle/small molecule LbL system can also be coated on nanofibers conformally, as shown in Figure 2.11(b) and (c).[181] These studies lay the groundwork for the anti-flammable systems studies in this dissertation.

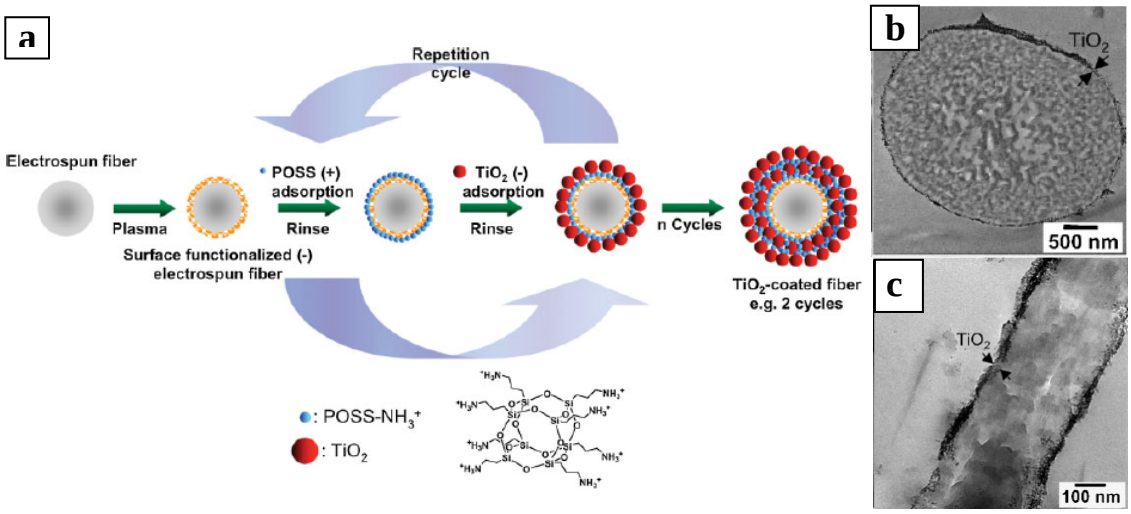

Figure 2.11. Schematic of TiO_2/POSS coated electrospun polymer fibers using LbL assembly (a). TEM images of TiO_2-coated electrospun fibers: PS (b) and PSEI (c).[181]

2.5 Flammability Testing Methods

A large number of flammability tests have been developed by several standards organizations (ASTM, NFPA, UL, ISO, IEC, etc.) to evaluate the ignition tendency and

burning parameters of a wide range of materials. There are three primary types of flammability tests: small heat source ignition tests, bench-scale reaction-to-fire tests, and large-scale reaction-to-fire tests.[185] In small heat source ignition tests, a specimen is exposed to a small heat source (Bunsen burner type flame, hot wire, etc.) for a short duration (seconds) to evaluate the ignition, flaming droplets formation, and/or flame or smolder sustention after removal of the heat source. Bench- and large-scale fire tests are used to characterize the behavior of materials under more severe thermal exposure conditions (how a material responds to the temperatures and heat flux in a growing fire).[185] In this dissertation, vertical and horizontal flame tests, and the pill test are used as small heat source ignition tests. Cone and microscale combustion calorimeter are used as bench-scale reaction-to-fire tests. All tests follow the ASTM (the American Society for Testing and Materials) standards.

2.5.1 Vertical and Horizontal Flame Tests (ASTM D 6413 and D 5132)

ASTM D 6413 is used to measure the vertical flame resistance of textiles, and also evaluates after-flame and afterglow characteristics. A specimen (76 × 300 mm) is clamped in the sample holder and positioned vertically above (19 mm) a controlled flame and exposed for 12 seconds. Five specimens are needed for each sample to gather the afterflame (the length of time for which a material continues to flame after the ignition source has been removed) and afterglow (the time glowing continues after the removal of the ignition source and the cessation of flaming) times. The actual tester and schematic of the sample holder are shown in Figure 2.12(a).

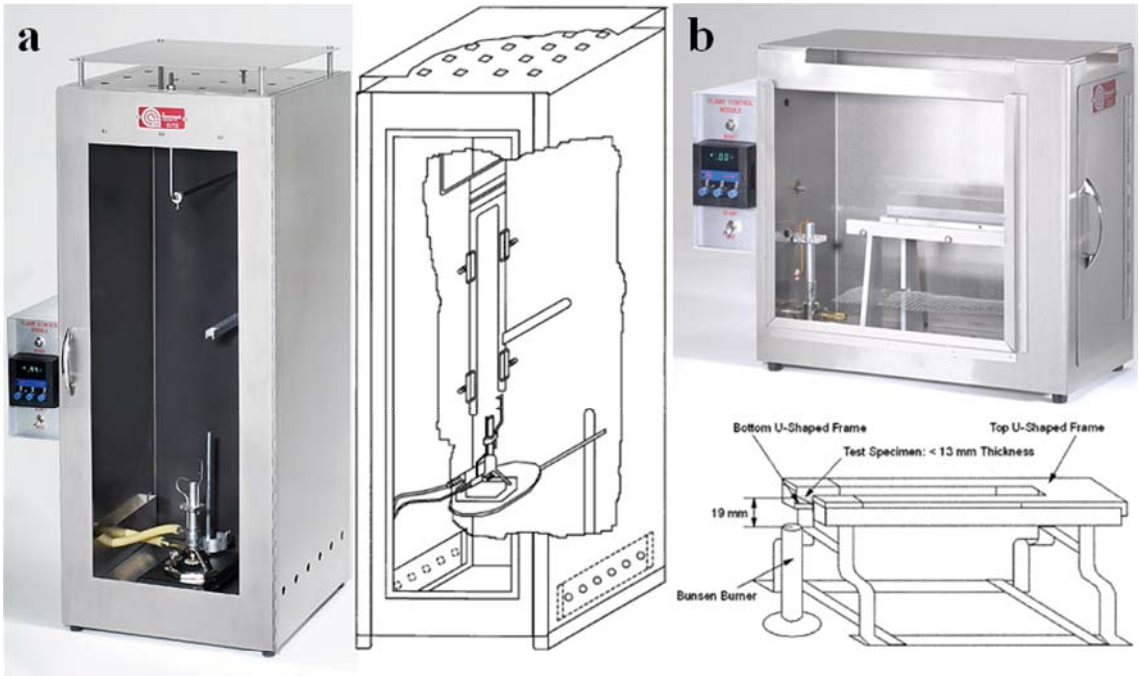

Figure 2.12. Vertical (a) and horizontal (b) flammability testing apparatus.[186]

ASTM D 5132 is intended for use in a small-scale laboratory for comparing the relative horizontal burning rates of polymeric materials. This test method employs a standard test specimen (100 × 300 nm) with a thickness up to 13 mm, mounted in a U-shape metal frame. The specimen is ignited with a 38-mm high flame for 15 seconds, and the burning rate is determined by measurements of the horizontal distance burned (tow scribed marks on sample holder, as shown in Fig. 2.12(b)) in relation to the time of burning (from the flame front reaching the first scribed mark to the second one). Five specimens are needed and the burning rate is calculated as follows:

$$B = D / T \times 60 \qquad (2.1)$$

where B is the burning rate (in mm/min), D is the length the flame traveled, starting from the first scribed line (in mm) and T is the time for the flame to travel distance D (in s).

2.5.2 Pill Test (ASTM D 2859)

This fire-test-response standard is to determine the flammability of finished textile floor covering materials when exposed to an ignition source under controlled laboratory conditions. Eight specimens (230 mm square) are required. Methenamine burning tablets are the ignition source, with a diameter of 6.35 mm, and the burning time of tablet is 130 s. A tablet is placed in the center of the specimen, which is ignited by touching a lighted match to the top of the tablet. Once the ignition flame and any propagated flame gas burned out, the test is determined to be passed if the charred portion of the tested specimen has not extended beyond 25 ± 0.5 mm of the edge of the hole. Figure 2.13 shows an example of the pill test used to evaluate polyester carpet.

Figure 2.13. Images of 50/50 cotton polyester blend carpet with (left) and without (right) FR treatment after pill test.[187]

2.5.3 Cone and Microscale Combustion Calorimetry (ASTM E 1354 and D7309)

The cone calorimeter was developed at the National Bureau of Standards (NBS), currently the National Institute of Standards and Technology (NIST) (Fig. 2.14). It is a fire testing instrument which quantitatively measures the inherent flammability of material through the use of oxygen consumption calorimetry, and is a standard technique under ASTM E 1354/ISO 5660. The test specimen is 100 × 100 mm and can have a thickness between 6 and 50 mm. It is exposed to a heat flux from the electric heater in the range of 10 – 100 kW/m^2. An electric spark is used to ignite the pyrolysis products released by the specimen, and is removed once the sustained flame is observed. All combustion products and air are collected by the hood, and a gas sample is taken and analyzed for oxygen concentration. Mass flow rate of the exhaust gas can be calculated by the measurements of the gas temperature and differential pressure, and the heat release rate can be determined by the oxygen depletion and mass flow rate. The cone calorimeter is equipped with a laser for smoke measurements and CO_2/CO detection. A load cell is used to measure mass loss as the sample pyrolyzes during heat exposure. The key parameters obtained from the cone calorimeter are:

- Time to ignition (TTI): this is the time to sustain ignition of the sample (measured in seconds).
- Heat release rate (HRR): the rate of heat release (in units of kW/m^2), as measured by oxygen consumption calorimetry.
- Peak heat release rate (Peak HRR): the maximum value of the heat release rate during sample combustion. The higher the peak HRR, the more likely that flame

will self-propagate on the sample in the absence of an external flame or ignition source.

- Total mass loss: taken from the load cell of the cone calorimeter at the beginning and end of the experiment to see how much total material from the sample was pyrolyzed/burned away during the experiment.
- Total heat release (THR): the area under the heat release rate curve (measured in units of MJ/m^2), representing the total heat released from the sample during burning from TTI to flameout. The higher the THR, the higher the energy content of the tested sample.
- Total smoke release: the total amount of smoke generated by the sample during burning in the cone calorimeter. The higher the value, the more smoke generated either due to incomplete combustion of the sample, or due to polymer chemical structure.

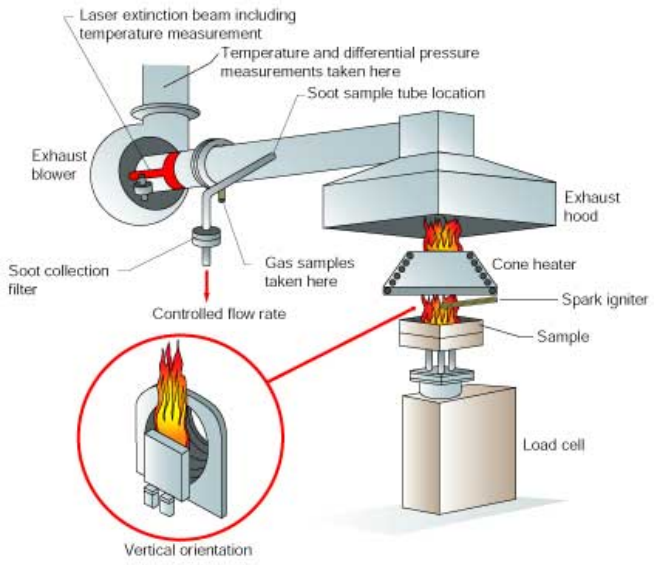

Figure 2.14. Schematic cone calorimeter.[188]

The U.S. Federal Aviation Administration (FAA) developed the microscale combustion calorimeter (MCC) to assist with the development of fire-resistant polymers for use in commercial passenger aircraft. A schematic of the MCC apparatus is shown in Figure 2.15. A 1 – 10 mg specimen is heated at a constant rate between 0.2 and 2 K/s in the lower chamber. Decomposition can take place in nitrogen (method A) or in a mixture of nitrogen and oxygen (method B). When method A is used, charforming specimens do not decompose completely and leave a solid residue. In the case of method B, the specimen is completely consumed. The generated gases then mix with excess oxygen, and completely oxidize in a high temperature furnace. Key parameters obtained from method A are:

- Char yield: obtained by measuring the sample mass before and after pyrolysis. The higher the char yield, the more carbon/inorganic material left behind (resulting in decreased total heat release).
- Peak HRR
- Peak HRR temperature
- THR

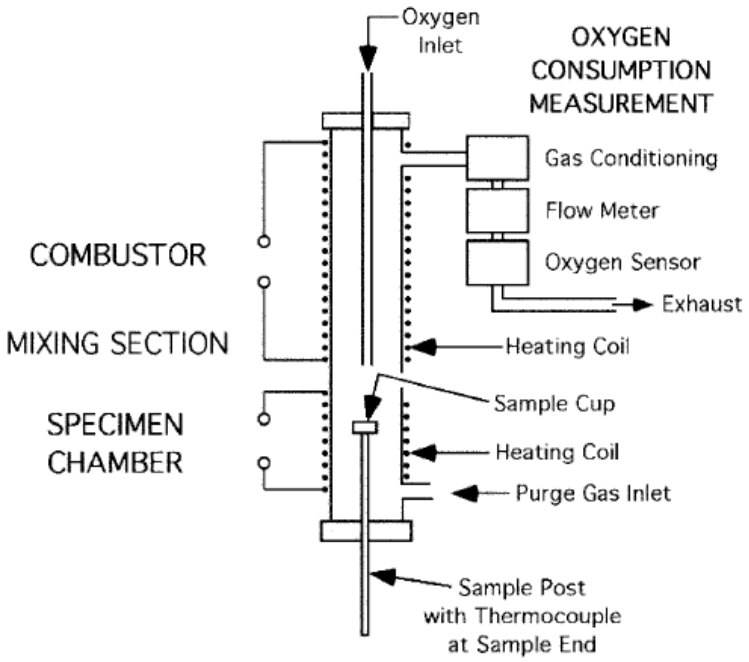

Figure 2.15. Schematic diagram of MCC apparatus.[189]

CHAPTER III

POLYELECTROLYTE/CLAY THIN FILM ASSEMBLIES: INFLUENCE OF PH ON GROWTH, MECHANICAL BEHAVIOR, AND FLAME RETARDANT BEHAVIOR ON COTTON FABRIC*

3.1 Introduction

Thin films of synthetic Laponite clay and branched polyethylenimine (BPEI) are examined here, with a focus on the influence of the pH of the aqueous deposition mixtures and the concentration of sodium chloride in the BPEI solution at a given pH. Film growth, hardness, and antiflammability of these films are evaluated under various deposition conditions. As an extension of the Laponite study, natural montmorillonite (MMT) clay was also deposited with BPEI to generate nanocomposite assemblies on cotton fibers and the flame retardant properties are evaluated. Laponite and MMT are smectite clays, which have been widely studied in LbL thin films.[42, 190-198] Each individual clay platelet (approximately one nanometer thick) is composed of one central layer of AlO_6 octahedra, sandwiched between two layers of SiO_4 tetrahedra, with swelling and ion exchange properties that allow for exfoliation of the platelet and for its surface to become negatively charged when immersed in water.[93]

---

* Reprinted with permission from "Polyelectrolyte/nanosilicate thin-film assemblies: influence of pH on growth, mechanical behavior, and flammability" by Yu-Chin Li *etc*., *ACS Appl. Mater. Interfaces* **2009**, *1*, 2338-2347, and from "Flame retardant behavior of polyelectrolyte-clay thin film assemblies on cotton fabric" by Yu-Chin Li *etc*., *ACS Nano* **2010**, *4*, 3325-3337. © 2009 & 2010 ACS.

Laponite is a synthetic clay with uniform disc-shaped platelets that are approximately 25 nm in diameter,[199-200] and MMT platelets are 10 – 1000 nm in diameter (average is around 200 nm).[201] Quartz crystal microbalance (QCM) data indicate that Laponite content in these films can be varied between 62 and 83 wt%, although no clear correlation between clay content and mechanical behavior is observed. Nanoindentation was performed on four different recipes to highlight the ability to tailor the mechanical behavior of these films with pH, which may be useful in applications such as scratch-resistant coatings for flexible electronics. Four different BPEI-MMT formulations were applied to cotton fabric and the flame-retardant properties were studied by thermogravimetric analysis (TGA), vertical flame testing, and microcombustion calorimetry. Additionally, the mechanical properties and water-wicking ability of the coated fabrics were also examined. High assembly pH and clay concentration result in a fabric with the best flame resistance. 5 BL of pH 10 BPEI and MMT (0.1 and 1 wt% in water) added 2 wt% to the cotton fabric, which maintained 11 % of its weight at 500 °C and a significant level of fiber and fabric weave structure was maintained following vertical burn. This work represents the first in-depth study of an LbL-based flame retardant. The use of MMT is a dramatic improvement over the much smaller Laponite,[202] which was used in the only other mention of layer-by-layer assembly for imparting flame resistance to fabric. A framework is provided for improving the anti-flammability of cotton (and other flammable materials such as foam insulation) that could result in significant savings of both life and property.

3.2 Experimental

3.2.1 Preparation of Deposition Mixtures

Cationic deposition solutions were prepared by dissolving 0.1 wt% branched polyethylenimine (BPEI, structure is shown in Fig. 1.1), with a molecular weight of 25,000 g/mol (Aldrich, Milwaukee, WI), into 18.2 MΩ deionized water from a Direct-QTM 5 Ultrapure Water System (Millipore, Bellerica, MA). Synthetic Laponite®RD clay and montmorillonite (Southern Clay Product, Inc., Gonzales, TX) was exfoliated (0.2 and/or 1 wt%) in deionized water, by simply adding it to water and slowly rolling for 24 h, to produce the anionic deposition mixtures. 1M hydrochloric acid (36.5 – 38 % HCl; Mallinckrodt Chemicals, Phillipsburg, NJ) was used to adjust the pH of deposition solutions. 1, 10, 100 and 1000 mM of sodium chloride (reagent plus >99.5 %, Aldrich) solutions were prepared and used for preparation of the BPEI (at pH 8) and Laponite deposition solutions for different ionic strength. The pH was measured with an Accumet® Basic AB15 pH meter (Fisher Scientific, Pittsburgh, PA).

3.2.2 Substrates

Silicon wafers (University Wafer, South Boston, MA) were used as deposition substrates for films characterized with ellipsometry, AFM, scanning electron microscopy (SEM), and X-ray diffraction (XRD). Polished Ti/Au crystals with a resonance frequency of 5 MHz were purchased from Maxtek, Inc. (Cypress, CA) and used as deposition substrates for quartz crystal microbalance characterization. TEM imaging of these films required the use of 125 μm polystyrene (PS) film (Goodfellow, Oakdale, PA)

as the substrate for deposition. Prior to deposition, silicon wafers were cleaned by immersion into "piranha" solutions (3:1 H_2SO_4/H_2O_2; dangerous if contacted with organics) for 1 h, followed by rinsing with deionized water. In the case of PS substrates, the film was rinsed with methanol and deionized water, and dried with air. The clean PS substrates were then corona-treated with a BD-20C Corona Treater (Electro-Technic Products Inc., Chicago, IL) for 2 minutes. Corona treatment oxidizes the PS film surface and creates a negative surface charge,[203-204] which improves adhesion of the first BPEI layer. Scoured and bleached plain-woven cotton fabric, that was coated and tested for thermal stability, was supplied by the United States Department of Agriculture (USDA) Southern Regional Research Center (SRRC, New Orleans, LA). The fabric was a balanced weave with approximately 80 threads per inch in both the warp and fill direction, with a weight of 119 g/m^2. The control fabric referred to in this paper was treated by laundering through a cold water cycle, with no detergent, in a standard commercial high-efficiency clothes washer and dried for approximately 30 minutes in a commercial electric clothes dryer (Whirlpool Corporation, Benton Harbor, MI). The wet processing of the control fabric was intended to eliminate any changes in physical construction of the fabric due to the wet processing of the fabric during the LbL deposition and was then used as the uncoated fabric in all tests.

3.2.3 LbL Film Deposition

All films were assembled on a given substrate using the procedure shown in Figure 1.1. The substrate was dipped into the ionic deposition solutions, alternating

between the BPEI (cationic) and Laponite(or MMT) (anionic), with each cycle corresponding to one bilayer. The first dip into each mixture was for 5 min, beginning with the cationic solution. Subsequent dips were for one minute each. Every dip was followed by rinsing with deionized water for 30 seconds and drying with a stream of filtered air for 30 seconds. In the case of the fabrics, the drying step involved wringing the water out instead of air-drying. After achieving the desired number of bilayers, the coated wafers were dried with filtered air, whereas the fabrics were dried in an 80 °C oven for 2 hours.

3.2.4 Film Characterization

Film thickness was measured on silicon wafer using a PhE-101 Discrete Wavelength Ellipsometer (Microphotonics, Allentown, PA). The HeNe laser (632.8 nm) was set at an incidence angle of 65°. A Maxtek Research Quartz Crystal Microbalance (QCM) from Infinicon (East Syracuse, NY), with a frequency range of 3.8 – 6 MHz, was used in conjunction with 5 MHz quartz crystals to measure the weight per deposited layer. The crystal, in its holder, was dipped alternately into the positively and negatively-charged solutions. Between each dip, the crystal was rinsed, dried, and left on the microbalance for five minutes to stabilize. Cross-sections of the clay-polymer assemblies were imaged with a JEOL 1200 EX TEM (Mitaka, Tokyo, Japan), operated at 110 kV. Samples were prepared for imaging by embedding a piece of coated PS in epoxy and sectioning it with a microtome equipped with a diamond knife. Surface structures were imaged with a Nanosurf EasyScan 2 Atomic Force Microscope (AFM) (Nanoscience

Instruments, Inc., Phoenix, AZ). AFM images were gathered in tapping mode with a XYNCHR cantilever tip. A Bruker-AXS D8 Advanced Bragg-Brentano X-ray Powder Diffractometer (Cu Kα, λ= 1.541Å) (BRUKER AXS Inc., Madison, WI) was used for both powder diffraction and glancing angle XRD. Contact angle measurements were done using a CAM 200 Optical Contact Angle Meter (KSV Instruments Ltd., Helsinki, Finland). Nanoindentation was performed by Hysitron, Inc. (Minneapolis, MN) using a TI-700 UBI® nanomechanical test instrument to determine the hardness and reduced modulus of films on silicon with a diamond Cube-Corner indenter probe. Fifteen to twenty indentation tests were performed on each sample. Each indent consisted of a 5 second loading segment, a 2 second hold segment and a 5 second unloading segment. An indentation depth of 10 nm was used in most cases, which is the shallowest depth that can give reliable hardness and modulus values. Surface images of coated fabrics, as well as of the chars from fabrics (after direct exposure to flame), were acquired with a Quanta 600 FE-SEM (FEI Company, Hillsboro, OR).

3.2.5 Thermal, Flammability, and Combustibility

All tests were conducted in triplicate for each system to obtain the reported averages. The thermal stability of uncoated and coated fabrics was measured in a Q50 Thermogravimetric Analyzer (TA Instruments, New Castle, DE). Each sample was approximately 20 mg and was tested in an air atmosphere, from room temperature to 600 °C, with a heating rate of 20 °C/min. Vertical flame testing was performed on 3 ×12 in. sections of uncoated and coated fabrics according to ASTM D6413. An Automatic

Vertical Flammability Cabinet, model VC-2 (Govmark, Farmingdale, NY), was used to conduct this testing. The Bunsen burner flame, 19 mm below the fabric sample, was applied for twelve seconds, after which the after-flame and afterglow times were measured. Microscale combustibility experiments were carried out in a Govmark MCC-1 Microscale Combustion Calorimeter. The specimens were first kept at 100 °C for 5 min to remove adsorbed moisture, and then heated up to 700 °C at a heating rate of 1 °C/sec, in a stream of nitrogen flowing at 80 cm^3/min. The pyrolysis volatiles released from the thermal degradation of the sample into the nitrogen gas stream were mixed with a 20 cm^3/min stream of pure oxygen prior to entering a 1000 °C combustion furnace. Three samples weighing about 4.3 mg were tested for each system.

3.2.6 Analysis of Fabric Properties

Physical properties of the fabric were tested at USDA-SRRC using ASTM and AATCC (American Association of Textile Chemists and Colorists) Standards. ASTM D 3775 was used to determine the fabric count on the fabric sample, counting the number of yarns in the warp and fill directions at five different locations to determine the average number of yarns per inch. ASTM D 1424 was used to determine the fabric's resistance to tearing. This test was carried out using the Elmendorf falling pendulum apparatus (SDL Atlas, Stockport, UK). Two clamps secured the sample and a slit was cut down the center before a pendulum action attempted to tear the fabric. Control samples were tested five times and coated samples were tested three times due to insufficient material to allow for five test specimens. ASTM D 5035 was used to

determine the breaking force and percent of apparent elongation. A sample piece of fabric was placed in a constant-rate-of-extension tensile testing machine and a force was applied until the sample broke (Instron Corporation, Norwood, MA). As with the Elmendorf test, control samples were tested five times and coated samples were tested three times. To determine water-wicking ability, the AATCC Committee RA63 proposed test method for wicking was employed. A 25 mm × 175 mm strip of fabric was placed in a beaker with water, and the time it took the water to climb 2 cm vertically was measured. All fabrics were pre-conditioned at 21 °C and 65 % RH (according to ASTM D 1776) for 48 hours before testing.

3.3 Results and Discussion

3.3.1 Film Growth and Structure of BPEI/Laponite

The influence of the deposition mixture pH on the resulting film thickness was evaluated using ellipsometry. A series of films were prepared with varying BPEI solution pH, keeping the Laponite solution at its unadjusted pH of 10.1. Figure 3.1(a) shows that these films exhibit linear growth and Table 3.1 shows that films made with lower BPEI pH are thinner than those prepared at higher pH. Owing to its protonatable secondary and tertiary amine backbone and primary amine side chains, BPEI has a greater positive charge density at lower pH. It is for this reason that BPEI has stronger electrostatic adsorption with negatively charged substrates and clay, making it lay relatively flat and resulting in thinner films. A separate series of films was made, varying the pH of the Laponite solution and keeping the BPEI at its unadjusted pH of 10.3, to see

if similar variation in film growth would result. In this case, linear growth that varied with pH was again observed (Fig. 3.1(b)), but films are thicker at lower Laponite pH. In the system where Laponite is at pH 6, it may actually be forming a "house-of-cards" structure due to its edges being positively charged, which promotes edge-to-face associations.[205-206] The locally high clay concentration at the surface of the thin film could lead to gelation and ultimately to some type of collapsed house-of-cards structure that would explain the thicker deposition observed at pH 6 in Figure 3.1(b).

Table 3.1. Thickness per bilayer for various BPEI/Laponite recipes[202]

LbL system	nm per bilayer cycle
BPEI (pH 7)/Laponite	0.52
BPEI (pH 8)/Laponite	1.06
BPEI (pH 9)/Laponite	1.71
BPEI (pH 10)/Laponite	2.84
BPEI/Laponite	2.99
BPEI/Laponite (pH 6)	4.99
BPEI/Laponite (pH 8)	4.33
BPEI/Laponite (pH 10)	3.19

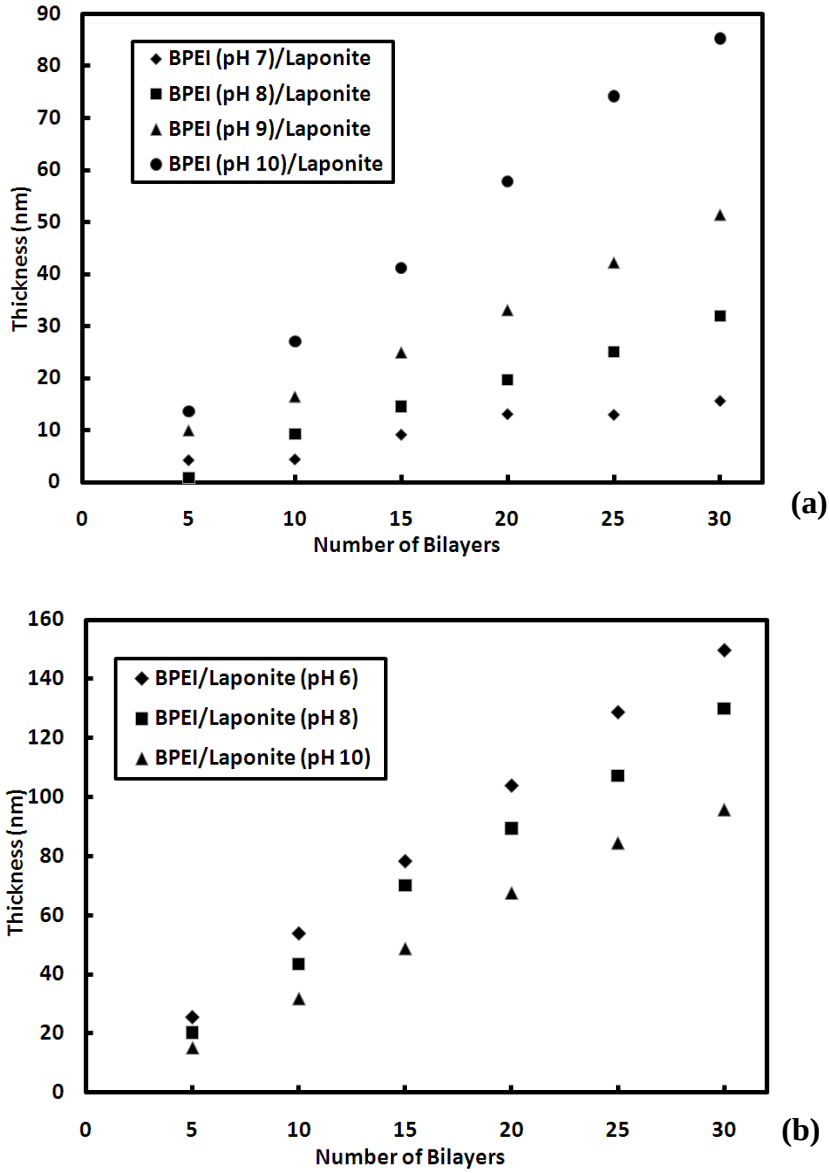

Figure 3.1. Film thickness as a function of the number of bilayers deposited for LbL assemblies made with varying BPEI (a) and Laponite (b) deposition mixture pH. Only one ingredient's pH was varied at a time, while the other was held at its unadjusted pH (10.3 for BPEI and 10.1 for Laponite).[202]

To further explore these structural mechanisms of film growth, another series of experiments was performed by adding salt into either the BPEI or Laponite solutions. Because of the charge screening effect of the salt,[207] the addition of increasing sodium chloride concentration to the BPEI deposition solutions (at pH 8) resulted in the formation of thicker films, as shown in Figure 3.2. In the case of unadjusted BPEI solution and Laponite suspensions (independent of pH) the thickness of the films is nearly unaffected by salt concentration. Compositional information was obtained by a quartz crystal microbalance, which measured the weight of each deposited layer. From the data shown in Figure 3.3 and Table 3.2, films of unadjusted BPEI and pH 6 Laponite appear to have the highest density and Laponite percentage, suggesting stacks of Laponite platelets were deposited on the substrate surface each coating cycle when the clay is at pH 6. When comparing the BPEI/Laponite (pH 6) with other BPEI/Laponite films at higher Laponite pH (see Table 3.1), the bilayers are not only thicker, but the weight percentage of Laponite is higher as well when using lower pH Laponite (see Table 3.2).

Table 3.2. Film density and composition for various BPEI/Laponite recipes[202]

LbL system	Density (g/cm^3)	BPEI wt. %	Laponite wt. %
BPEI (pH 8)/Laponite	1.42	31 ± 14	69 ± 14
BPEI/Laponite	1.61	38 ± 7	62 ± 20
BPEI/Laponite (pH 6)	1.91	17 ± 9	83 ± 7

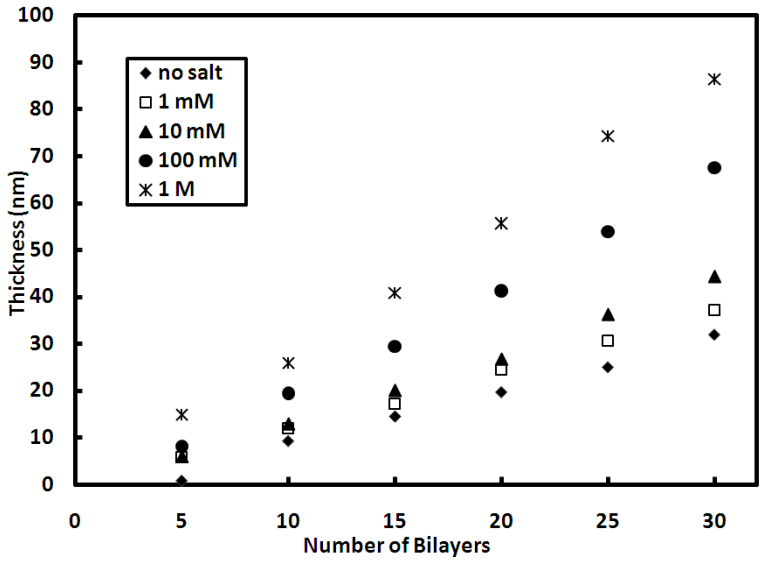

Figure 3.2. BPEI-Laponite film thickness as a function of bilayers deposited with varying NaCl concentration. The BPEI solution was maintained at pH 8 and Laponite pH was unadjusted.[202]

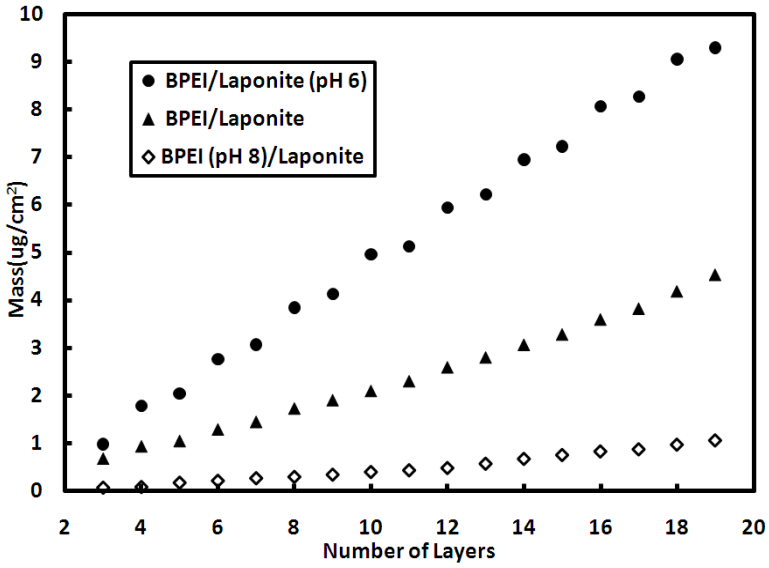

Figure 3.3. Film mass as a function of layers deposited for three different BPEI/Laponite systems. In all cases, BPEI is odd layers and Laponite is even. When no pH is specified for BPEI or Laponite, it means the unadjusted pH was used.[202]

Figure 3.4 shows TEM cross-sections of three sample films, made with different BPEI and Laponite pH conditions. These 30-bilayer films were deposited on polystyrene substrates to facilitate sectioning. The bilayers of the BPEI (pH 10)/Laponite film (Fig. 3.4(a)) are clearly thicker than the BPEI (pH 8)/Laponite film (Fig. 3.4(b)). The BPEI/Laponite (pH 6) film (Fig. 3.4(c)) appears to have a different cross-sectional microstructure from the other two films, which could be further evidence of somewhat collapsed edge-to-face associations (*i.e.*, house-of-cards). Several light-colored round or elliptical areas appear in the lateral view of this cross-section (pointed out by arrows), which correspond to the size of Laponite platelets tilted on their sides. In the same image (Fig. 3.4(c)), the outline of "standing" clay platelets on the film surface is clearly visible (topmost arrow), unlike what is observed in Figures 3.4(a) and (b). The thicknesses of films in these images correlate well to the ellipsometry data shown in Figure 3.1. All of the films appear wavy in the images, which may be caused by stress relaxation in the film during sectioning with a diamond knife and/or because of the tilted layers of clay.[208]

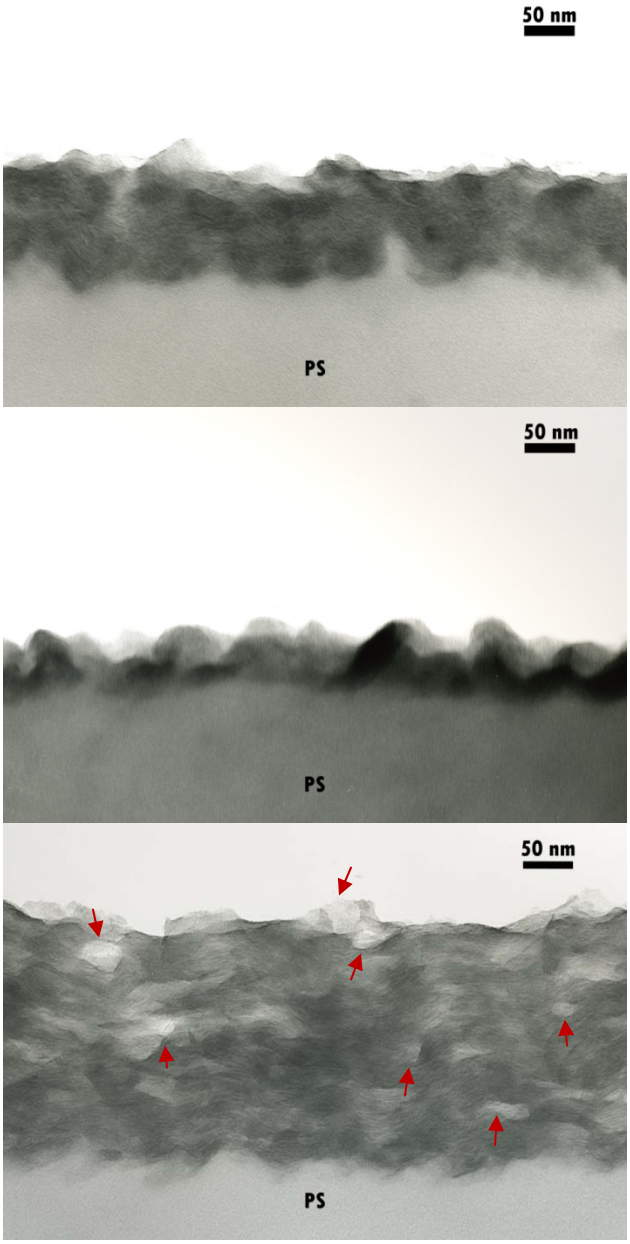

Figure 3.4. TEM cross-sectional images of 30 BL assemblies made with Laponite and BPEI at pH 10 (a) and pH 8 (b) and BPEI and Laponite at pH 6 (c).[202]

Tapping mode AFM was used to characterize the surfaces of 10 BL films because at this number of layers maximum roughness was reached in similar films (Laponite/PDDA).[193] Figure 3.5 shows height and phase images of a 10 BL BPEI (pH

7)/Laponite film. At lower magnification (Fig. 3.5(a) and (b)), the surface resembles a cobblestone path that is uniformly covered by clay platelets whose largest dimension is oriented parallel to the silicon wafer substrate. The size of the clay platelets looks uniform from these images and the surface texture is similar in all LbL films deposited with unadjusted Laponite (pH 10.1) and varying BPEI pH. A slightly different structure is observed on the surface of a film made with unadjusted BPEI (pH 10.3) and Laponite at pH 6, but surface roughness is similar for all films. The root-mean-square (rms) roughness of BPEI (pH 7)/Laponite is 2.5 nm, while it is 2.2 nm for BPEI (pH 10)/Laponite and 2.6 nm for BPEI/Laponite (pH 6) when using a 20 µm square area.

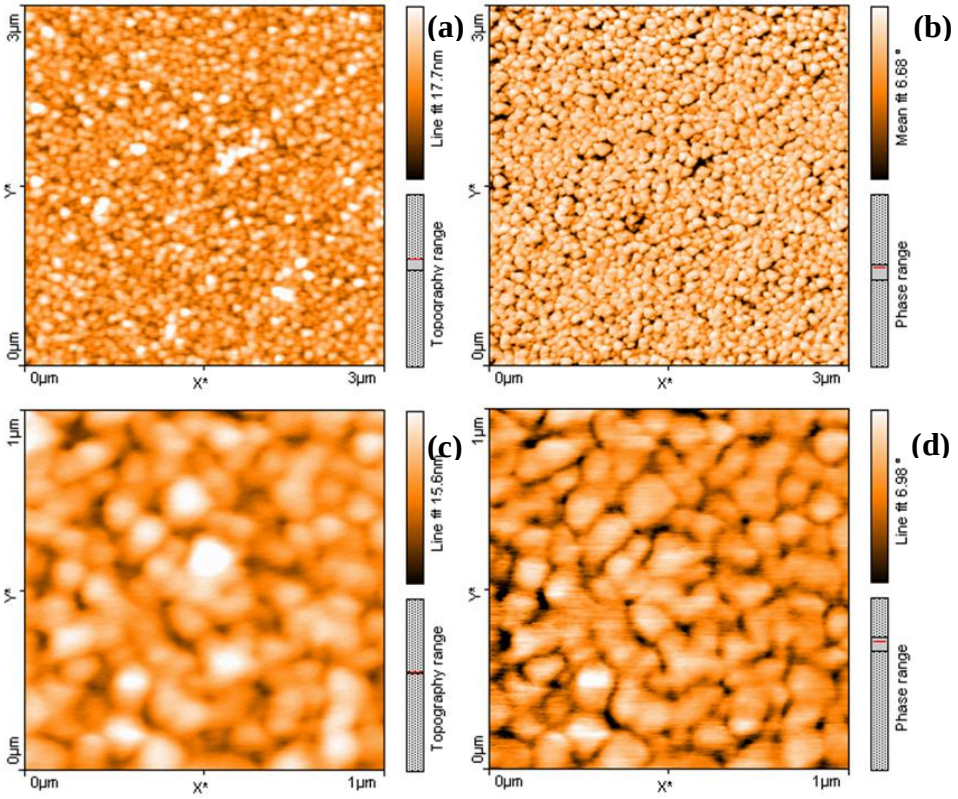

Figure 3.5. AFM height (a), (c) and phase (b), (d) surface images of a 10 BL BPEI (pH 7) /Laponite film. (a), (b) are under 3 µm scale and (c), (d) are under 1 µm scale.[202]

Figure 3.6 shows patterns from XRD performed on neat Laponite powder and four LbL films made with varying pH conditions. Neat clay powder shows the major characteristic peaks that are consistent with those reported in the literature.[198, 209] The low angle peak at 6.8° derives from a basal spacing of 13.0 Å, which is the periodic distance from platelet to platelet. Because the thickness of each platelet is 1 nm, the distance between platelets is 3 Å. In all four films, the low-angle peaks shift to ~ 6.3°, which means that the distance between platelets increases to about 4 Å. From these results, it appears that the clay platelets exhibit lamellar stacking,[210] with at least two layers of Laponite deposited per coating cycle. On the basis of AFM surface images, the films likely have ordering in the z direction, which agrees well with other studies of clay-based assemblies.[198, 208]

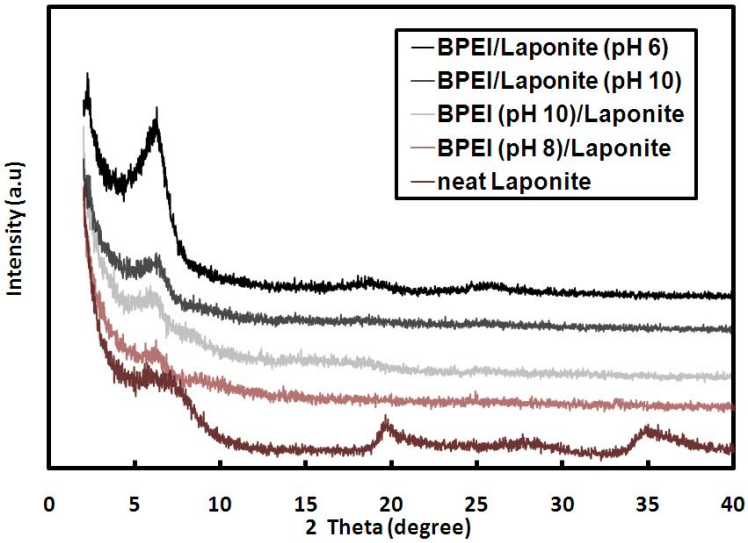

Figure 3.6. X-ray diffraction patterns for neat Laponite, and 30 BL films made by varying the pH of the BPEI and Laponite solutions.[202]

The BPEI/Laponite (pH 6) system exhibits the most pronounced low-angle peak (~6.3°) in Figure 3.6. The weight of each clay deposition, measured with QCM, suggests that each clay deposition is approximately 3.6 nm thick (assuming a planar packing density of 0.9), which translates to four stacked platelets. In the TEM image shown previously (Fig. 3.4(c)), it can be seen that this film is mostly arranged as lamellar layers, but the tilted clay platelets suggest a collapsed "house of cards" structure.[205-206] When the pH of Laponite suspensions is reduced with HCl, the H^+ ions also diminish the negative surface charge by attaching to the face of Laponite.[211] This combination of edge-to-face attractions and charge screening is believed to allow more Laponite to be adsorbed onto the assembly surface in each dipping cycle. This provides a possible explanation for the thicker growth observed for BPEI/Laponite (pH 6). None of the other systems studied exhibit such thick growth and evidence of tilted platelets.

3.3.2 Mechanical Behavior of BPEI/Laponite Assemblies

Hardness and reduced modulus of BPEI/Laponite assemblies were determined using nanoindentation, in which a force is applied to an indenter probe while continuously measuring the applied force (P) and the probe displacement (h). Figure 3.7(a) shows two example indents, one on a relatively thin film and the other on a thicker film. The peak load of indentation was 2 μN for all films, except BPEI (pH 8)/Laponite, which was 5 μN. The hardness (H) is defined as the ratio of the maximum load (P_{max}) to the projected contact area (A), shown in Eq. 3.1:

$$H = \frac{P_{\max}}{A} \tag{3.1}$$

The reduced modulus (E_r) is defined in Eq. 3.2, where S, the unloading stiffness, is defined by Eq. 3.3:

$$E_r = \frac{S\sqrt{\pi}}{2\sqrt{A}} \tag{3.2}$$

$$S = \frac{dP}{dh} \tag{3.3}$$

Figures 3.7(b) and (c) show these two mechanical properties for 40-BL films made with BPEI and Laponite at varying pH. The results indicate that the thinnest film (BPEI pH 8 and unadjusted Laponite) exhibits the highest reduced modulus which is proportional to stiffness (the initial slope of the unloading curve) and the same as elastic modulus to a first approximation.[212] This may be due to a substrate effect, since the film is only 40 nm thick and the indentation depth was more than 10 % of this value. However, examination of the load-displacement curves (Fig. 3.7(a)) reveals that this film is stiffer even during the initial loading segment, which indicates a higher modulus even before the onset of any substrate effect. The other three films have thicknesses above 100 nm and exhibit hardness of 0.5 ± 0.05 GPa with 10 % indentation depth, which is in agreement with those working with similar systems.[191]

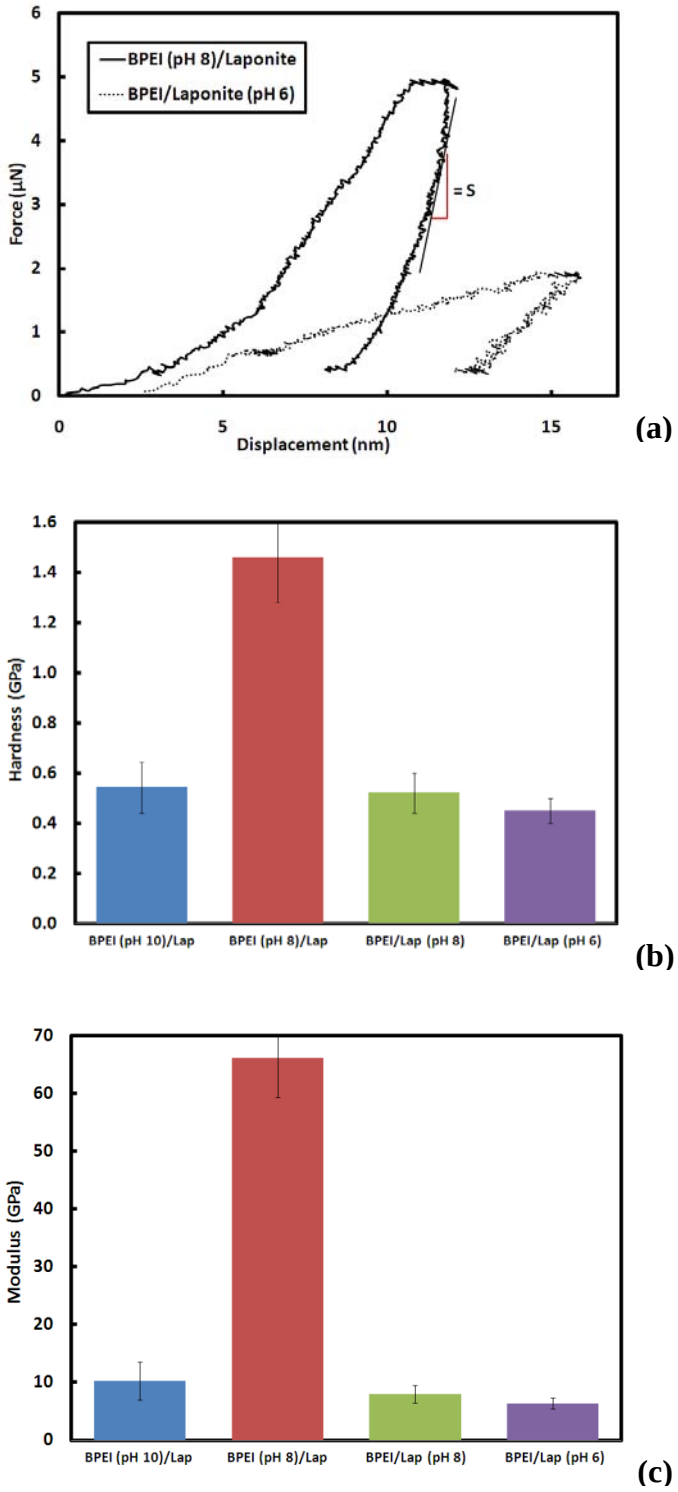

Figure 3.7. Load-displacement curves (a), and mechanical properties ((b) hardness and (c) elastic modulus) of 40 BL thin films.[202]

The reduced modulus is related to the modulus of elasticity (*E*) through Eq. 3.4:

$$\frac{1}{E_r} = \frac{(1-v_i^2)}{E_i} + \frac{(1-v_s^2)}{E_s} \tag{3.4}$$

where the subscript *i* corresponds to the indenter material, the subscript *s* refers to the indented sample material, and *v* is Poisson's ratio. For a diamond indenter probe, E_i is 1,140 GPa, which is a huge number compared to the substrate's modulus, so the reduced modulus of the film is very close to its modulus of elasticity. Even though the film made with unadjusted BPEI and Laponite at pH 6 has a greater concentration of clay (see Table 3.2), the hardness and modulus are lower than for the other three films. This is probably because it experiences less substrate effect when measuring the mechanical properties. Nevertheless, the modulus and the hardness values of the layer-by-layer thin films made with polymer and clay are relatively higher than those of pure polymer (*e.g.*, PDDA) films.[208] Because of the high transparency and good mechanical properties achieved in these nanocomposite thin films, this simple process could be used as a hard coating for plastic substrates, as an alternative to the sol-gel technique.[213-214]

3.3.3 Flame Resistance of BPEI/Laponite-Coated Fabric

Many researchers have shown that clay imparts flame resistance to bulk polymers.[7, 92, 215] Others have shown that polymer/clay LbL self-assembly can be applied on paper[183] and wood fibers.[180] PAH and Kaolin clay coatings on paper were shown to change the wettability of the paper from hydrophilic to hydrophobic.[183] PDDA and MMT coated wood fibers were observed to attain increased thermal stability relative to

the unmodified material tested by TGA.[180] At present, no literature shows LbL coating on cotton fabrics for the purpose of flame suppression. Fabric samples were coated with 10 BL of BPEI (pH 8)/Laponite and BPEI/Laponite (pH 6), which resulted in less than 2 % increase in fabric weight. At 500 °C, under an air atmosphere, the uncoated fabric left less than 0.9 wt% residue, as shown in Figure 3.8. The char weight percentages for the coated fabrics were much higher, and very close to each other (5 and 6 wt%) for the two different coatings. It seems that the clay coating delays the degradation of the cotton by providing a sheath-like ceramic barrier.

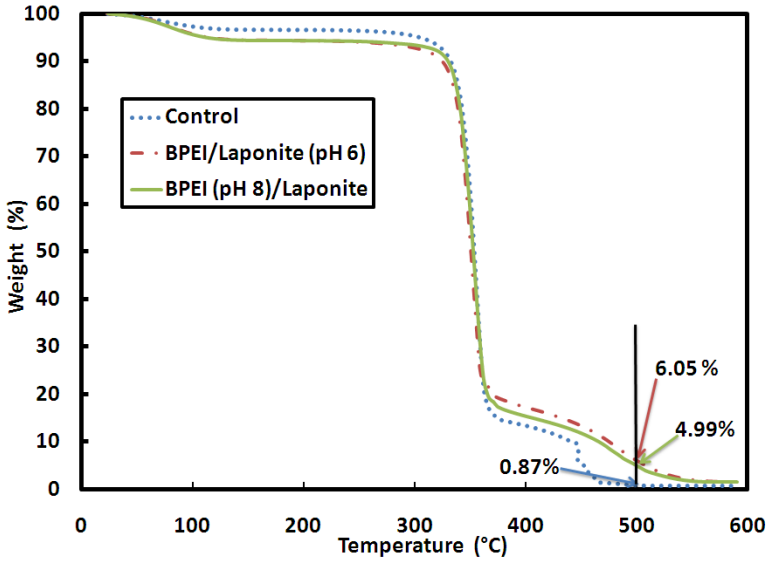

Figure 3.8. Weight loss as a function of temperature for cotton fabrics coated with 10 bilayers of BPEI/Laponite (pH 6) and BPEI (pH 8)/Laponite. These results were obtained using TGA at a heating rate of 20 °C/min.[202]

Equivalently coated fabrics were put through vertical flame testing (ASTM D6413). A more vigorous flame was observed on the control fabric compared to the

coated fabrics. Additionally, there were more afterglow on the control fabric. These three treatments showed similar ignition and after-flame times, but the afterglow times for coated fabrics were 8 to 10 seconds less than for the uncoated fabric. After burning, no control fabric was left on the sample holder, but the two coated fabrics left significant char, as shown in Figure 3.9. All the fabrics were examined by SEM, before and after flame testing. The control fabrics left only ashes after flame exposure, so the ashes were used as SEM samples in those cases. Under lower magnification the weave of the fabric can be clearly seen in Figure 3.10(a). After flame testing, the ash from the uncoated fabric (Fig. 3.10(b)) and the char from coated fabric (Fig. 3.10(c)) were examined under the same magnification. The weave structure of the char from coated fabrics is still relatively intact, but the threads of the char shrank after flame testing, leaving gaps between the threads.

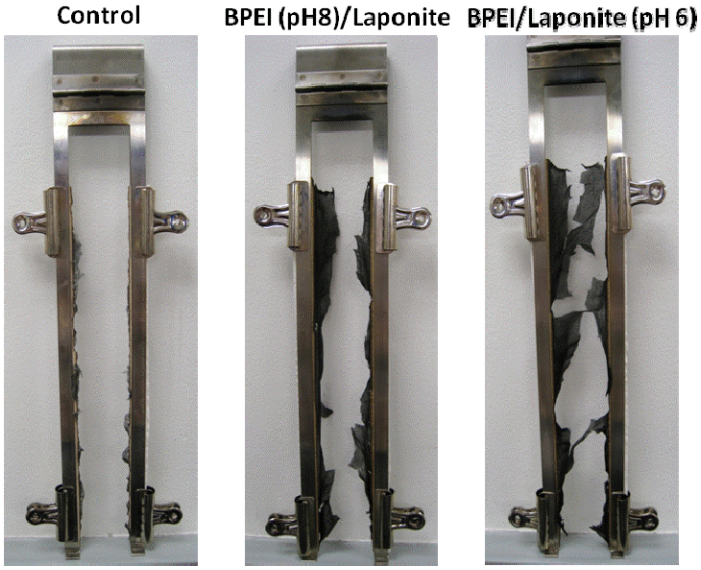

Figure 3.9. Images of uncoated and coated cotton fabrics following the vertical flame test. Coated fabric is 10 BL of a given recipe.[202]

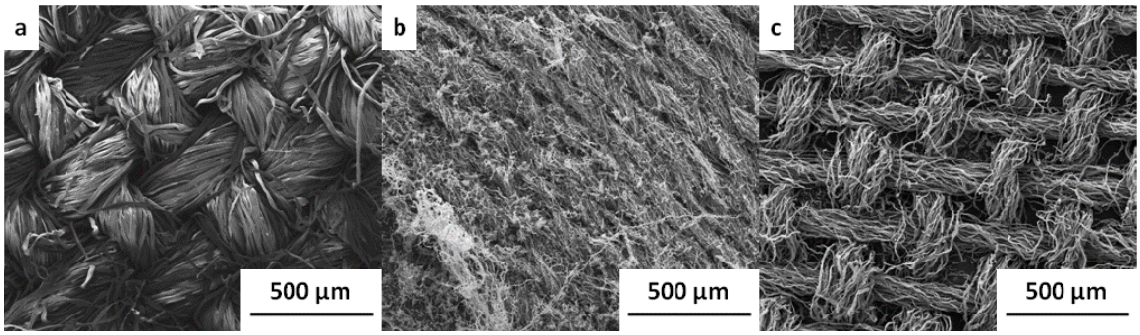

Figure 3.10. SEM images of virgin fabric before (a) and after (b) flame test; (c) coated fabric after flame test (BPEI (pH 8)/Laponite).[202]

Before the flame testing, the fiber surface in the control fabric (Fig. 3.11(a)) appears very clean and smooth compared to the coated fabrics (Fig. 3.11(b) and (c)). The aggregated Laponite particles can be seen on the fibers of the coated fabrics. Each fiber of the fabric was at least partially, if not completely, covered by the clay coating. After the flame testing, the char was again imaged. Because the control fabric was burned completely, its ashes were taken from the edge of the vertical flame sample holder for imaging. Broken pieces and holes in the fiber strands of the control fabric, caused by burning, can be seen very clearly in the SEM images (Fig. 3.11(d)), as well as some fibrous residues that are no longer the original fabric fibers. In the case of the char from the coated fabrics, a solid shield layer on the fibers can be seen clearly in Figures 3.11(e) and (f). It is possible that during burning at high temperature, the Laponite clay platelets sintered together, which could account for not seeing aggregated laponite or the edges of the platelets, but large continuous pieces of coating instead. There is no question that significant degradation occurs even in the coated fabric, but this work provides some

initial evidence that clay-based assemblies is an interesting alternative to current flame suppression technologies for fibers and fabrics.

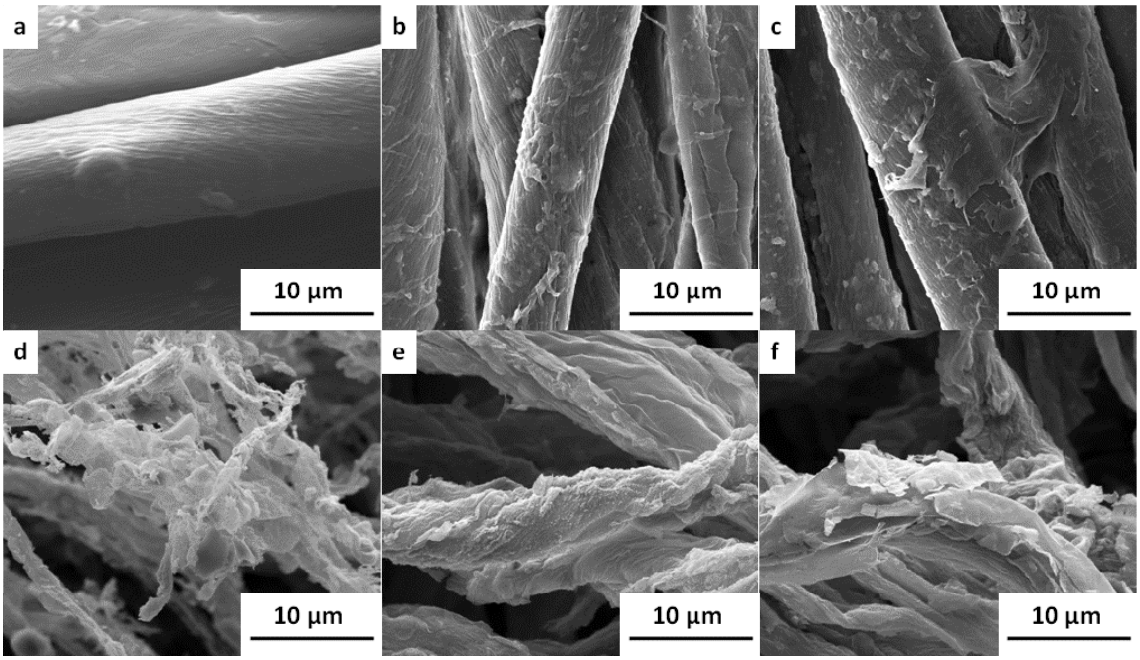

Figure 3.11. SEM images of fabrics before ((a)-(c)) and after flame test ((d)-(f)). (a) and (d) are uncoated fabrics, (b) and (e) are fabric coated with 10 BL of BPEI (pH 8)/Laponite, and (c) and (f) are fabric coated with 10 BL of BPEI/Laponite (pH 6).[202]

3.3.4 Film Growth and Structure of BPEI/MMT

Previous sections has shown that Laponite can impart some modest flame-retardance to cotton fabrics *via* LbL assembly.[202] In the present section, MMT is deposited with branched polyethylenimine (BPEI) to generate nanocomposite assemblies on cotton fibers. The thickness and weight composition of these films was tailored by changing the pH of the polymer solution and the concentration of the clay mixture. Four

different thin film recipes, BPEI pH 7 or 10, with MMT at 0.2 wt% or 1 wt%, were used to prepare the films whose growth is shown in Figure 3.12. All four systems grow linearly as a function of BPEI-MMT bilayers deposited. The film thicknesses are very similar for films made with the same pH BPEI solution, regardless of variation in clay concentration. Differences observed between high and low pH systems are due to the different degrees of charge density of the weak polyelectrolyte BPEI. When this polymer is highly charged, the polymer chains adopt a flat conformation due to self-repulsion of like charges along its backbone, whereas at low charge density, the polymer has a more coiled and bulky conformation due to intra-chain H-bonding.[25] In order to better understand this growth process, a quartz crystal microbalance was used to measure the weight increase associated with the deposition of each individual layer.

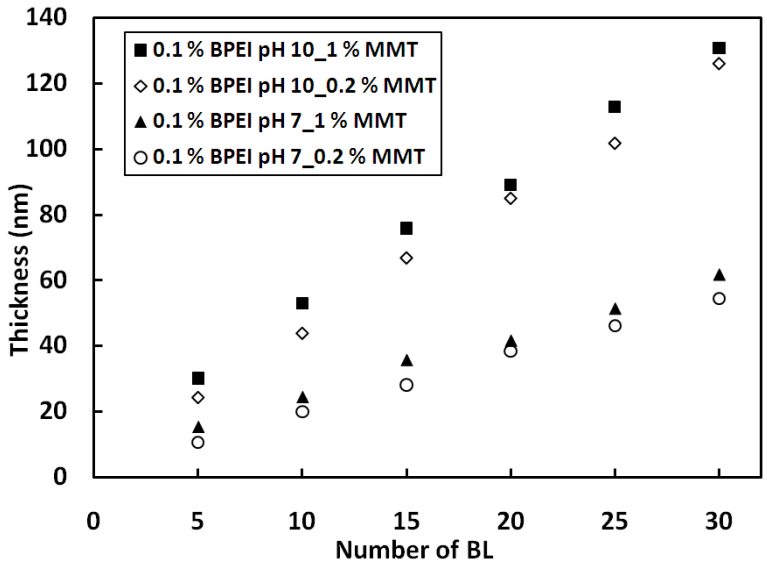

Figure 3.12. Film thickness as a function of the number of bilayers deposited, for a series of LbL assemblies made with varying pH of the BPEI solution and concentration of the MMT mixture. MMT was used at its unadjusted pH of 9.8.[216]

Figure 3.13 shows the QCM data for the four different recipes described above. There is not much difference observed in mass per layer of films made with pH 7 BPEI and the two different concentrations of MMT suspensions (0.2 and 1 wt%), but the films made with pH 10 BPEI and two different concentrations of MMT show a significant difference in mass. The amount of BPEI deposited for each layer is similar between the films made with the same pH, but BPEI at pH 7 deposits less in each layer than BPEI pH 10 (about one-third the amount). The films made with 1 wt% MMT suspension and BPEI at different pH values have higher clay loadings (MMT/BPEI ratio) than films made with 0.2 wt% MMT suspension. In all four recipes, film thickness seem to be influenced primarily by the pH of the BPEI solution and only modestly by the concentration of clay. However, film weight is a different story. As mentioned above, when BPEI has a higher charge density (at low pH), it lies flatter on the charged substrate due to intra-chain self-repulsion, and the clay platelets can only lay parallel to the substrate, covering the topmost surface. In this case, films made with a 1 wt% MMT mixture would achieve better coverage per deposition than films made with 0.2 wt% MMT, resulting in similar thicknesses and weights for the two films. On the other hand, when BPEI has a lower charge density (at pH 10), it is more coiled and entangled than in its high charge density state, this results in thicker, rougher layer deposition that would conceivably allow for more clay platelets to deposit due to the greater surface area of this relatively coarse (on the nanoscale) surface. In this scenario, a higher concentration of MMT (1 wt%) could result in more loading of the BPEI surface during each deposition step than the more dilute mixture (0.2 wt% MMT).

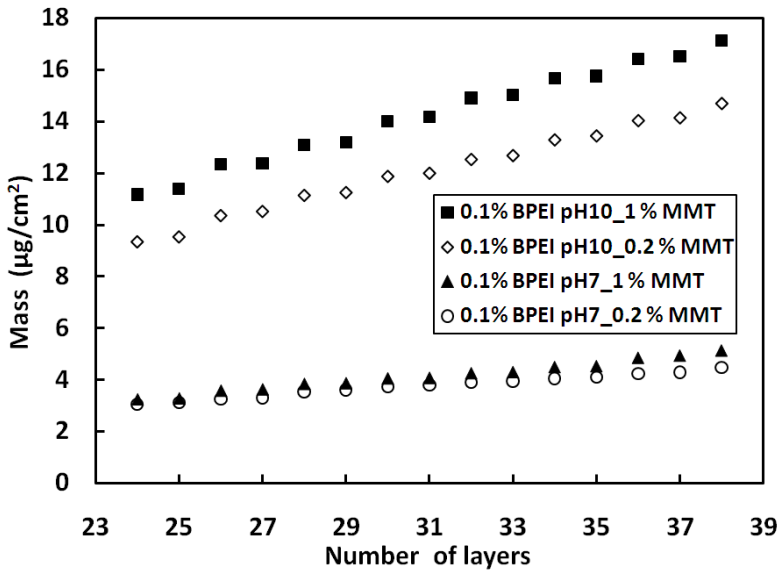

Figure 3.13. Film mass as a function of individually deposited clay and polymer layers for four different BPEI/MMT systems. In all cases, odd layers are BPEI and even layers are MMT.[216]

Tapping mode AFM was used to characterize the surfaces of 30 BL MMT-composite thin films made with high and low pH BPEI. The root-mean-square (rms) roughness (using a 20 µm square area) for the BPEI pH 7/1 wt% MMT film is 38 nm (Fig. 3.14(a) and (b)), while it is 62 nm for the BPEI pH 10/1 wt% MMT film (Fig. 3.14(c) and (d)), suggesting that the surface is covered by clay platelets whose largest dimension is oriented parallel to the surface of the silicon substrate. Because of the different morphology of BPEI at high and low charge densities, the surface is rougher for films made with pH 10 BPEI that has little charge. Figure 3.14(e)[217] shows a TEM cross-section of a 40 BL film made with BPEI pH 10/0.2 wt% MMT, to provide some idea of structure through the thickness of these films. This film was deposited on a polystyrene substrate to facilitate sectioning. The individual layered clay can be seen

very clearly, as well as the places where the clay platelets meet. The film appears wavy in the images, which was likely caused by stress relaxation in the film during sectioning.[208] Even so, the nano brick wall structure of these films is very evident. It is this unique nanostructure that is believed to provide flame resistance to cotton fabric.

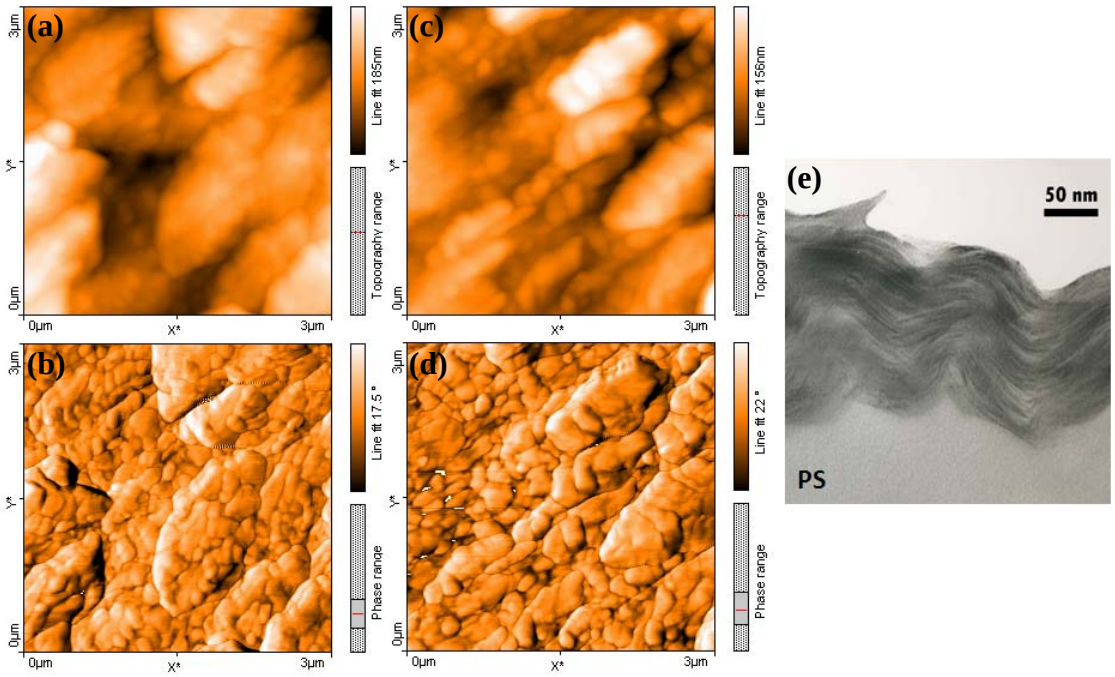

Figure 3.14. AFM height (a) and phase (b) surface images of a 30 BL BPEI pH 10/1 wt% MMT film; height (c) and phase (d) images of a 30 BL BPEI pH 7/1 wt% MMT film; and TEM cross-section (e) of a 40 BL assembly made with BPEI pH 10/0.2 wt% MMT.[216]

3.3.5 Flame Resistance of BPEI/MMT-Coated Fabric

Cotton fabric was coated with 5 and 20 BL of BPEI/MMT, using the four different recipes described in the previous section describing thin film growth. The coating weight was determined by weighing 12 × 15 in. samples of fabric before and

after coating. All samples were weighed only after oven-drying at 80 °C for 2 hours to remove moisture. Weight added to the fabric by each coating system is shown in Table 3.3 as a percentage of the uncoated weight. The weight gain from coating on fabric does not correlate well to the weight gain measured by QCM for the films assembled on a quartz crystal. At 5 BL, fabric coated using BPEI at pH 10 is heavier than fabric coated using pH 7 BPEI, but at 20 BL the fabric weight gain was greater with pH 7 BPEI. This may be linked to differences in adhesion and substrate geometry. Figure 3.15 shows two coatings that were prepared using a 1 wt% MMT mixture with BPEI at high and low pH. All of the individual cotton fibers are easily discerned for the 20 BL coating made with BPEI at pH 10 (Fig. 3.15(a)). The same coating applied using BPEI at pH 7 (Fig. 3.15(b)) appears to have pulled away from the fiber to some extent during the deposition process, which allowed it to bridge multiple fibers. It is likely that coating draped between fibers provided additional surface area for deposition, which resulted in grater add-on percent at 20 BL.

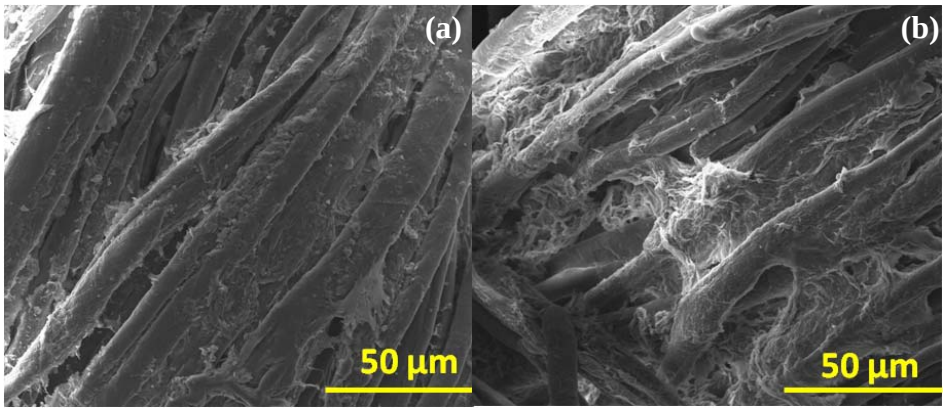

Figure 3.15. SEM images of cotton fabric coated with 20 BL of BPEI/MMT. These coatings were made using BPEI at pH 10 (a) and 7 (b). Both coatings were prepared with a 1 wt% MMT deposition mixture.[216]

Figure 3.16 shows TGA results for each of four coating recipes at 5 (Fig. 3.16(a)) and 20 BL (Fig. 3.16(b)). At 500 °C, under an air atmosphere, the uncoated control fabric left less than 1.8 wt% residue. With the addition of 2 wt% for a 5 BL coating and 4 wt% for a 20 BL coating, residue weight percentages for the coated fabrics are one order of magnitude higher than the control. The residue amounts for the control fabric and each coated fabric are summarized in Table 3.3. At the final stage of the testing (around 600 °C), there was essentially no char left from the control fabric, but there was a significant amount of residue left from 20 BL-coated fabrics. The mass of the residue from a coated fabric clearly demonstrates that there is preservation of cotton during burning, because some residues are greater than the mass of the coating itself (see add-on % in Table 3.3). The amount of charred cotton in the residue is higher than the mass difference between residue and the coating by itself (in all cases), because at least a fraction of the BPEI in the coating is degraded during heating (pure BPEI completely decomposes below 650 °C). It should be noted that there is a direct correlation between added coating weight (Table 3.3) and residue generated in the TGA. Additionally, the fiber bridging and heavier coverage by the pH 7 BPEI system at 20 BL (Fig. 3.15) results in 10 % greater coating weight, but 67 % greater char at 600 °C.

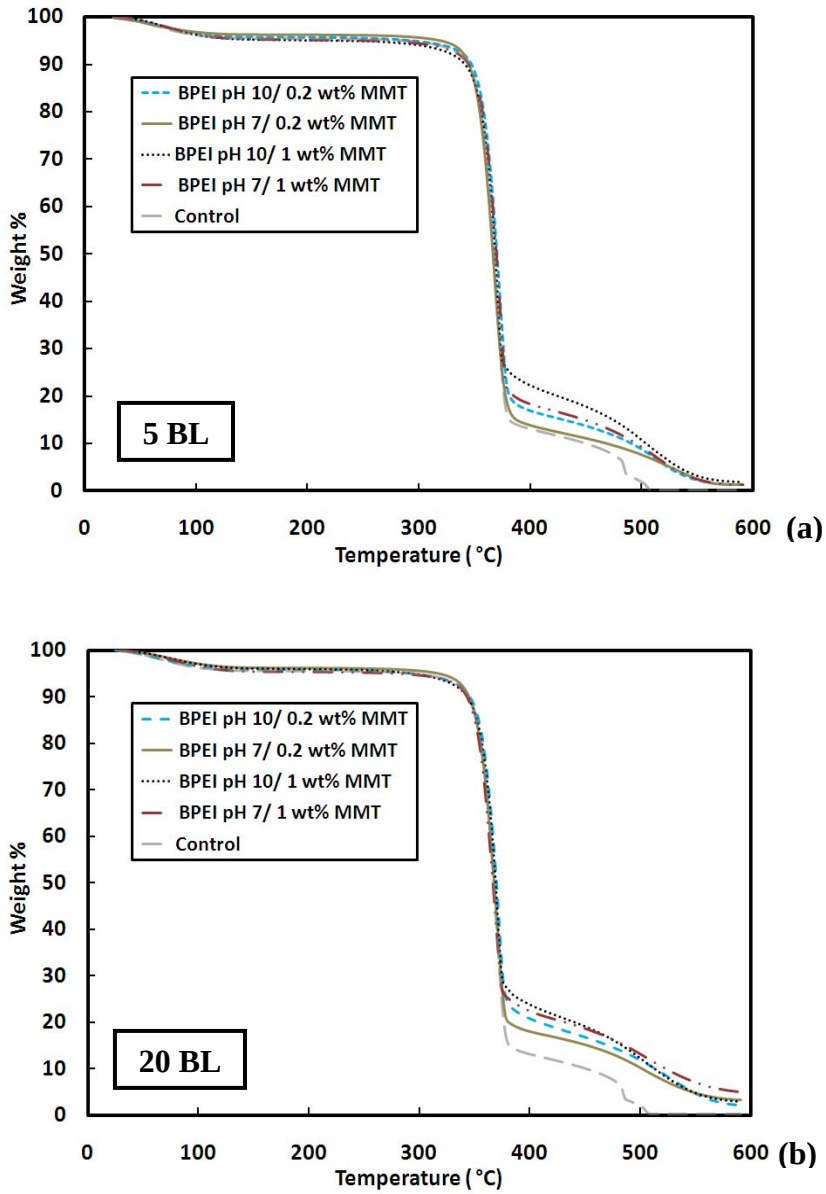

Figure 3.16. Weight loss as a function of temperature for cotton fabrics coated with 5 BL (a) and 20 BL (b) of 0.1 wt% BPEI (pH 10 and 7) with 0.2 and 1 wt% MMT. These results were obtained using TGA at a heating rate of 20 °C/min under an air atmosphere.[216]

Table 3.3. Weight added by coating fabrics, and residue amounts after heat treatment[216]

	Add-on (%)		500°C residue (%)		600°C residue (%)	
Sample	5 BL	20 BL	5 BL	20 BL	5 BL	20 BL
Control			1.77[b]		0.30[b]	
BPEI pH10/0.2% MMT	2.05	2.31	9.12	11.70	1.29	2.09
BPEI pH 7 /0.2% MMT	0.97	2.89	7.00	10.39	1.17	3.28
BPEI pH10/ 1 % MMT	2.23	4.06	11.26	12.16	1.70	2.82
BPEI pH 7/ 1 % MMT	1.82	4.41	9.33	13.02	1.47	4.72

a: Residue values obtained from TGA testing under air atmosphere.
b: The residue weight percent of uncoated fabric.

An equivalent set of coated fabric samples was put through vertical flame testing (ASTM D6413). Time to ignition did not increase upon coating the fabric, but a brighter and more vigorous flame was observed on the control fabric compared to the coated fabrics, as shown in Figure 3.17 at 5 seconds after ignition. The flame on the coated fabric was not very vigorous. Additionally, more glow was seen on the control fabric after the flame was removed. The control and eight different coated fabrics showed similar after-flame times (*i.e.*, time fire observed on samples after direct flame removed), but the afterglow times for coated fabrics were 9 seconds less than for the uncoated fabric. After burning, no control fabric was left on the sample holder, but all four 20 BL-coated fabrics left significant residues, as shown in Figure 3.18. The residues from 20 BL-coated fabrics are heavier and have preserved the fabric structure better than the residues from fabrics coated with only 5 BL, although even these thinner coating provide significant char.

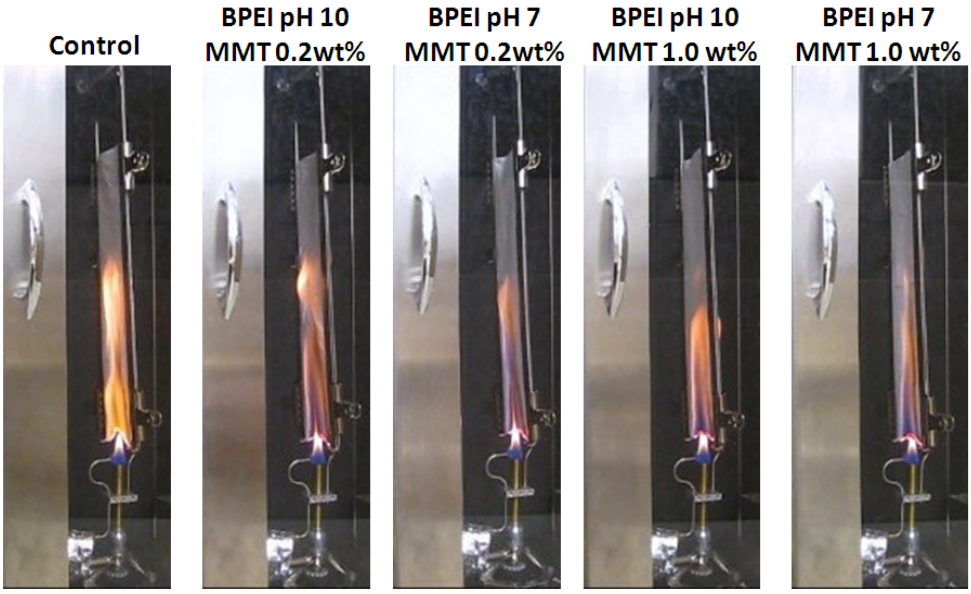

Figure 3.17. Images of vertical flame testing of the uncoated and coated cotton fabrics 5 seconds after ignition. The coated fabrics are 20 BL of a given recipe.[216]

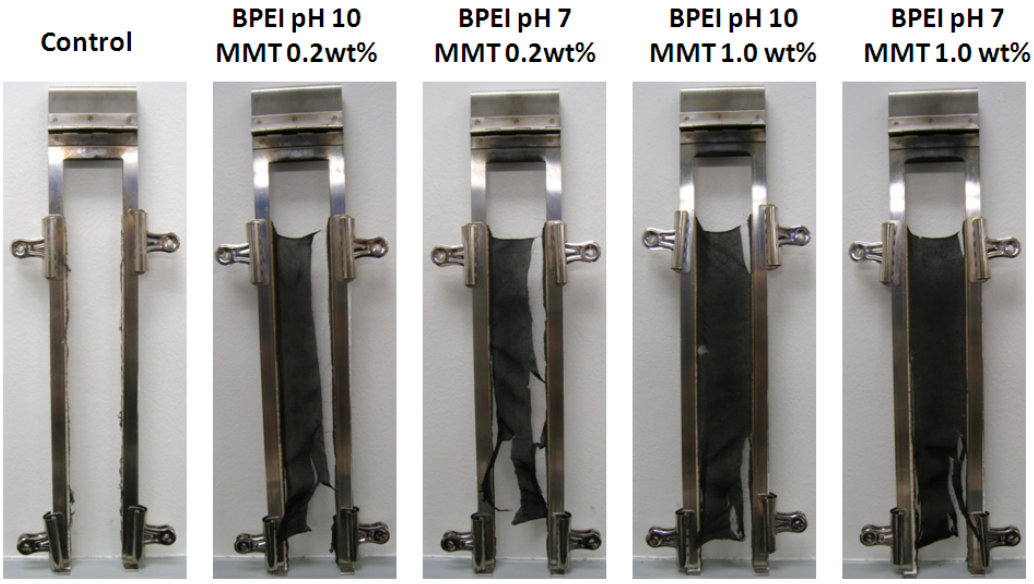

Figure 3.18. Images of uncoated and 20 BL coated cotton fabrics following the vertical flame test.[216]

All fabrics were imaged by scanning electron microscopy, before and after flame testing, to evaluate the surface morphology and fabric structure. The control fabric left only ash after flame exposure, so these ashes were used for imaging, whereas coated fabric images are more representative from the center of the charred remains. In Figures 3.19(a) and (b), the uncoated and 5 BL (BPEI pH 10/0.2 wt% MMT)-coated fabrics are shown prior to the flame test. The fiber surface in the control fabric appears very clean and smooth compared to the coated fabrics. Small MMT aggregates can be seen on the fibers of the coated fabrics that are likely the result of inefficient rinsing of fabric between layers. Each fiber of the fabric is at least partially, if not completely, covered by the clay coating. After flame testing, the ash from the uncoated fabric and the residue from coated fabric were imaged under the same magnification. Figure 3.19(c) very clearly shows that the ashes of the uncoated cotton fabric no longer have the same fabric structure and shape of the original fibers. Broken pieces and holes in the fiber strands illustrate the complete destruction that occurs during burning of uncoated cotton. It is surprising that with only 5 BL, the fabric structure is maintained and the fibers are relatively intact (Fig. 3.19(d)). It is possible that during burning at high temperature, the MMT platelets fuse together to some extent, which could account for not seeing aggregated MMT or the edges of the platelets after burning, but rather large continuous pieces of coating instead.

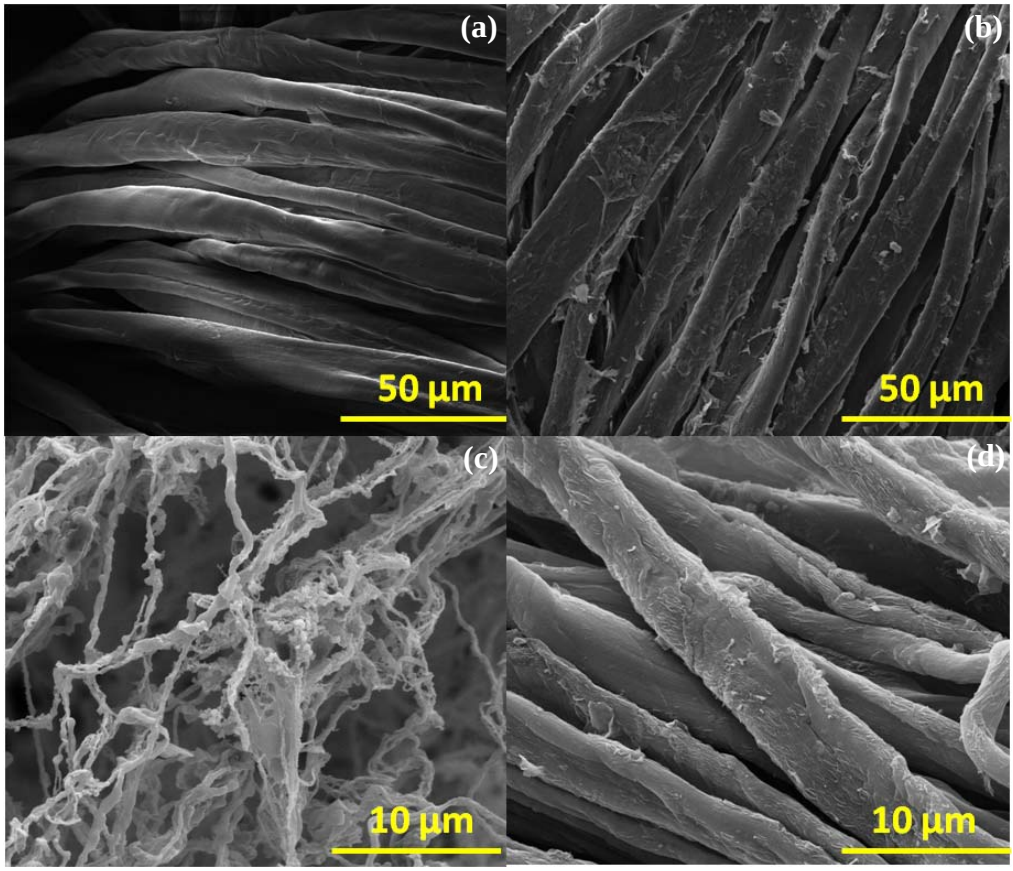

Figure 3.19. SEM images of uncoated fabric before (a) and after (c) the vertical flame test. 5 BL-coated fabric (BPEI pH 10/0.2 wt% MMT) before (b) and after (d) flame test is also shown.[216]

Figure 3.20(a) shows a low magnification image of the fabric before burning, coated with 5 BL of BPEI pH 7/1 wt% MMT. The dimensions of the weave structure in uncoated and coated fabrics are identical, which means that the LbL coating process does not alter the fabric dimensions. After burning, ash remaining from the uncoated fabric does not show the weave structure anymore (Fig. 3.20(b)), but the residue from coated fabrics retain the weave structure, especially with a 20 BL coating of BPEI pH 7/1 wt% MMT (Fig. 3.20(d)). Even the width of individual yarns is similar to the width

before burning for this sample. The 5 BL (BPEI pH 7/1 wt% MMT)-coated fabric also retained its weave structure (Fig. 3.20(c)), although the threads shrank after flame testing, leaving gaps between the yarns. Interestingly, despite using the same concentration of clay deposition mixture (1 wt% MMT), the weave structure of the residue from 20 BL-coated fabric made using pH 10 BPEI (Fig. 3.20(e)) has larger gaps between yarns as compared to the fabric coated (20 BL) using pH 7 BPEI. This is a somewhat expected result due to the smaller add-on percentage of the BPEI pH 10 coating, as well as to the fiber bridging, achieved by the coating when highly charged pH 7 BPEI is used (see Table 3.3 and Fig. 3.15), which may have provided greater barrier to fibers deeper within the fabric.

The XRD pattern in Figure 3.21 provides additional evidence of coating on the fabric. The low-angle peak at 7.8° for neat MMT clay derives from a basal spacing of 11.4 Å, which is the periodic distance from platelet to platelet. On the fabric coated with BPEI pH 7/1 wt% MMT, the peak is shifted to 6.4°, suggesting that even on the non-flat fiber surface the clay can be deposited in an orderly manner. The basal spacing is increased to 13.7 Å because of intercalation with BPEI. After vertical flame testing, the residue from coated fabric was also scanned by XRD, which resulted in a decrease from 13.7 to 12.7 Å. This result suggests that the intercalated BPEI is decomposed or ablated during the burning process, resulting in a reduction of the basal spacing of MMT. The positions of the low-angle MMT peak (data not shown) of fabric coated with BPEI pH 10/1 wt% MMT (before and after flame test) show no significant difference between the two recipes.

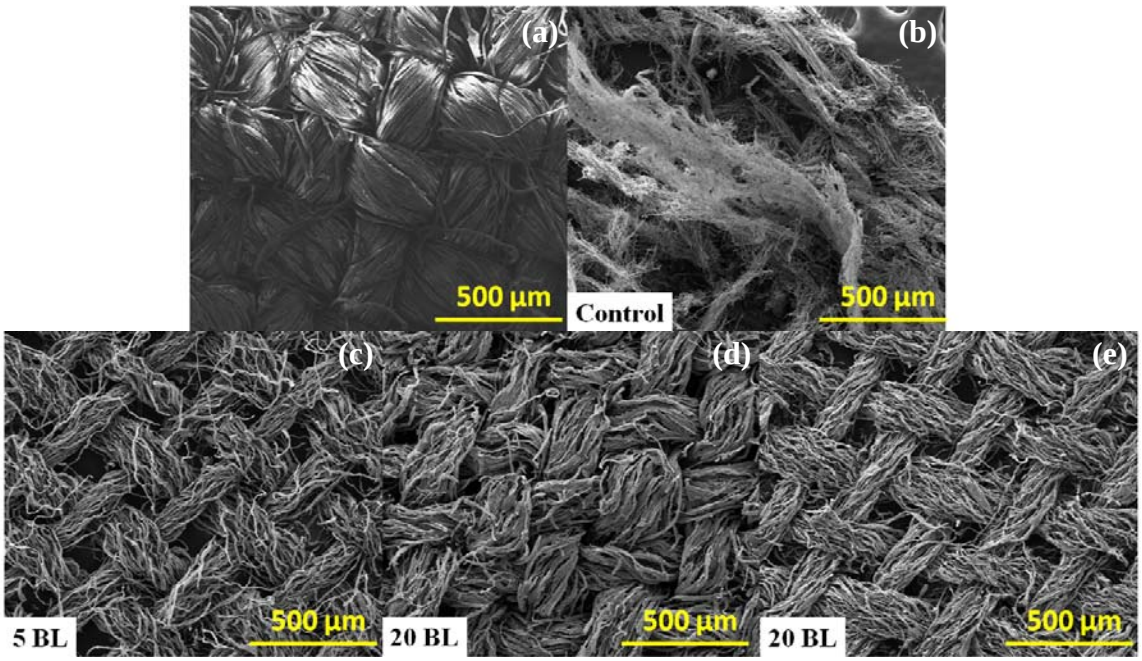

Figure 3.20. Low magnification SEM images highlighting the weave structure of fabrics before and after burning: coated fabric before burning (a), ash from control fabric after burning (b), residues from fabric coated with 5 (c) and 20 BL (d) of BPEI pH 7/1 wt% MMT, and residue from fabric coated with 20 BL of BPEI pH 10/1 wt% MMT (e).[216]

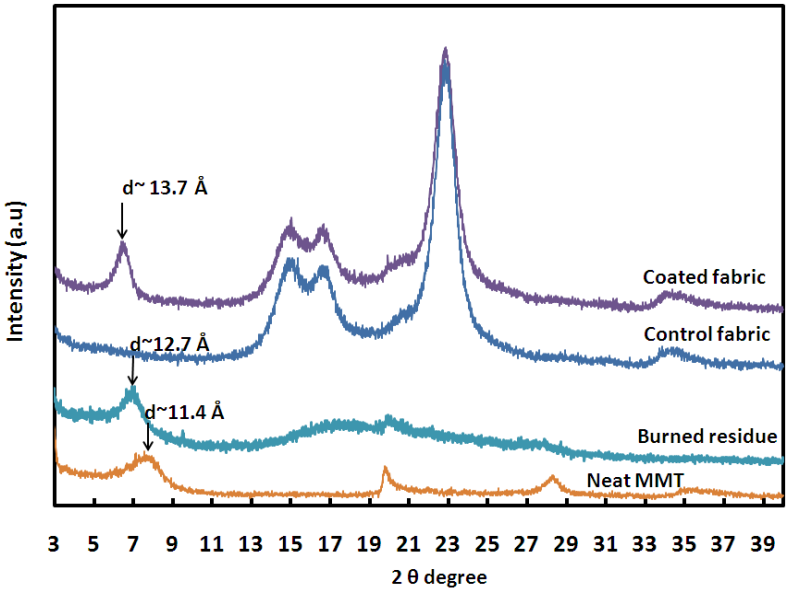

Figure 3.21. X-ray diffraction patterns for neat MMT, 20 BL BPEI pH 7/1 wt% MMT coated fabric, before and after burning, and the control fabric.[216]

Another tool for assessing the fire behavior of small (mg) samples is the microscale combustion calorimeter (MCC).[218-219] Key parameters coming from the MCC test include temperature at maximum heat release rate (Tp), specific heat release rate (HRR in W/g), and total heat release (THR in kJ/g). Residue is calculated by weighing the sample before and after the test. A derived quantity, the heat release capacity (HRC in J/g K) is obtained by dividing the maximum value of the specific heat release rate by the heating rate during the test. HRC is a molecular level flammability parameter that is a good predictor of flame resistance and fire behavior when only research quantities are available for testing. Reproducibility of the test for homogeneous samples is about ± 8 %.[220]

MCC data for the coated fabric samples are summarized in Table 3.4. All residues from coated fabrics tested at 700 °C under nitrogen atmosphere are higher than those from uncoated fabric. The residue does not come only from the coating (see add-on % in Table 3.3), but rather the fabric itself was somewhat preserved (1 – 5 wt%) when coated with various recipes. These results suggest that clay surrounds each fiber and acts as a protective barrier capable of promoting char formation during the pyrolysis of the fabric. An increase in charring induces a decrease in the amount and rate of combustible volatile release, resulting in lower flammability (as evidenced by lower THR and HRC values in the MCC). The maximum reduction in THR (20 %) and HRC (15 %), as compared to the control, is observed in the fabric coated with 5 BL of BPEI pH10/1 wt% MMT. Increasing the number of bilayers up to 20 for the same sample does not appear to produce any significant variation in the MCC data. This suggests that a 5

BL coating may be sufficient for generating an effective fire barrier on the textile. An increase in Tp is also observed in all coated fabrics, which is likely due to the formation of a low permeability barrier that delays the release of combustible volatiles.

Table 3.4. Microscale combustion calorimeter results for various coated fabrics[216]

Sample	Residue (%)	HRC (J/g K)	THR (kJ/g)	Tp (°C)
Control	2.88 ± 0.40	273.67 ± 25.38	11.63 ± 0.21	369 ± 0.58
BPEI pH 10/ 0.2% MMT				
5 BL	6.38 ± 1.50	254.33 ± 25.01	11.23 ± 0.25	374 ± 0.58
20 BL	7.48 ? 0.50	250.33 ? 14.50	11.10 ? 0.36	376 ? 2.65
BPEI pH 7/ 0.2% MMT				
5 BL	6.75 ± 0.60	260.33 ± 4.04	11.17 ± 0.40	376 ± 2.00
20 BL	6.74 ? 0.20	286.33 ? 8.51	11.90 ? 0.36	369 ? 0.58
BPEI pH10/ 1 % MMT				
5 BL	10.52 ± 0.30	220.00 ± 6.08	9.87 ± 0.31	382 ± 0.58
20 BL	10.49 ? 0.50	221.30 ? 7.57	10.23 ? 0.06	380 ? 0.58
BPEI pH 7/ 1 % MMT				
5 BL	8.37 ± 0.50	251.30 ± 10.02	10.73 ± 0.25	379 ± 1.00
20 BL	10.54 ? 0.30	240.30 ? 11.37	10.70 ? 0.50	377 ? 2.65

3.3.6 Physical Properties of Fabric

There is no difference in appearance between coated and uncoated fabric. Even tactile assessment of the fabric (by touch of hand) is the same for all coated and uncoated samples tested. In many cases the addition of a flame retardant results in loss of strength or the degradation of other fabric properties (*e.g.*, moisture wicking), so it is important to know if this coating technology alters these properties. Fabric count, tear

and tensile strength, and wicking behavior of coated fabrics were evaluated in comparison with control fabric.

Fabric count was determined by following the ASTM D 3775 standard method. Yarn number in the warp and fill directions of the fabric was counted on a 25 × 25 mm area. Five randomly selected areas from each coated fabric were used to determine the average fabric count. These counts are summarized in Table 3.5, where the yarn numbers of 5 BL-coated fabrics in both directions are shown to be only 1.2 % different from the control fabric. For the 20 BL-coated fabrics, the yarn number is less than 2.5 % different in warp direction, while in fill direction there is less than a 5 % difference. These results demonstrate that the coating of polymer and clay layers on the fabric did not significantly alter its physical structure. Wet processing of cotton fabric with traditional textile finishes often causes shrinkage and compaction in the yarns, resulting in more yarns per inch and affecting the comparison of physical properties of the treated fabrics to control materials.[221]

Table 3.5. Fabric counts of uncoated and coated fabrics[216]

Sample	BL number	Warp	Fill
Control		79	78
BPEI pH10/0.2% MMT	5	78	79
	20	81	81
BPEI pH 7 /0.2% MMT	5	78	78
	20	80	82
BPEI pH10/ 1 % MMT	5	80	78
	20	78	79
BPEI pH 7/ 1 % MMT	5	79	79
	20	77	79

The Elmendorf tearing test, which uses a falling pendulum to determine the amount of force required to tear the fabric (ASTM D 1424), was used to evaluate tear strength. A strip tensile strength test was used to determine the maximum force that can be applied to a material (sampled as a strip) until it fractures (ASTM D 5035). Additionally, the strip test measures the apparent elongation of the fabric. The Elmendorf and tensile tests showed similar results, which are summarized in Table 3.6. The warp direction for the coated fabrics exhibited improvement in both tearing and breaking strength when compared to the control fabric, while the fill direction showed a general decrease in strength. The elongation results had slight directionality as well. The warp direction showed a decrease in elongation, while the fill direction showed an increase. All of these properties are within 10 % of the uncoated fabric, so the data do not reveal a clear connection between coating and strength properties. The nature of these results suggest that they are not based on a change in fiber structure due to the coating, but rather are within the range of strength and elongation for the uncoated fabrics. In other words, the coating neither greatly improved nor harmed the fabric's mechanical strength. This is an improvement relative to traditional textile finishing, decrease the tensile strength of cotton fabric.[222]

Table 3.6. Tearing force and tensile breaking force of uncoated and coated fabrics[216]

Sample	BL number	Tearing Force (lbs)		Breaking Force (lbs)		Elongation (%)	
		Warp	Fill	Warp	Fill	Warp	Fill
Control		2.11	2.02	66.30	69.34	19.5	30.7
BPEI pH10/0.2% MMT	5	2.26	1.99	72.92	68.09	15.7	38.5
	20	2.25	2.02	67.23	63.66	16.9	36.4
BPEI pH 7 /0.2% MMT	5	2.24	2.12	80.33	65.88	14.7	36.8
	20	2.22	2.05	75.29	66.13	14.7	36.3
BPEI pH10/ 1 % MMT	5	2.21	1.86	80.11	61.54	12.1	30.1
	20	2.25	1.80	78.58	73.50	13.5	31.2
BPEI pH 7/ 1 % MMT	5	2.29	2.01	71.35	66.43	12.8	31.1
	20	2.04	1.87	68.76	63.23	14.5	30.8

The AATCC Committee RA63 proposed test method for wicking was used to test the transfer of water through the various fabric samples. Most standard fabrics absorb water through capillary action, using the gaps between warp and fill yarns as small capillaries, causing them to absorb a comparatively large amount of water. The wicking test measures the time it takes water to travel up a piece of fabric in an Erlenmeyer flask or beaker. Shorter wicking times (*i.e.*, faster movement of water up the test strip) indicate better wicking ability. The wicking distance is 20 mm and wicking rates were calculated by dividing the wicking distances by the average wicking times. Wicking rates in the warp and fill directions of each fabric are summarized in Table 3.7. For all coated fabrics, both warp and fill wicking rates are much slower (by a factor of 2-3) than the control fabric, indicating that their ability to absorb and transport water is not as great as the control. This is not so surprising, considering the outermost clay layer has been analyzed using *ab initio* molecular dynamics, where it was concluded that its tetrahedral surface (*i.e.*, the oxygen plane, which is the widest dimension in MMT

surface) can be considered hydrophobic.[223] In addition, static contact angle results were 72° for a coating of BPEI pH 7/1 wt% MMT on a Si wafer, and 74° for BPEI pH 10/1 wt% MMT, suggesting that the MMT-covered surface is more hydrophobic since both contact angles are larger than the 38° measured for a bare Si wafer. Among the four different types of fabric coatings studied here, the ones involving pH 7 BPEI have slower wicking rates than those made using pH 10, which suggests that it is harder for water to be transported through pH 7 BPEI coated fabrics. This behavior might be caused by the MMT platelets lying parallel to the fiber surface during deposition, with highly charged BPEI at pH 7 packing the platelets especially tightly. Such an arrangement of clay platelets, which are slightly hydrophobic, provide excellent coverage and sealing of fiber surfaces, thus interfering with the moisture transport both along and through the fiber. This is an area of ongoing research and improved wicking (if desired) could presumably be accomplished by applying a few bilayers of highly hydrophilic polymers.

Table 3.7. Vertical wicking rate of fabrics[216]

Sample	BL number	Wicking Rate (mm/s)	
		Warp	Fill
Control		2.50	2.61
BPEI pH10/0.2% MMT	5	1.25	0.91
	20	1.22	1.00
BPEI pH 7 /0.2% MMT	5	0.72	0.48
	20	0.82	0.67
BPEI pH10/ 1 % MMT	5	2.00	0.79
	20	1.22	0.97
BPEI pH 7/ 1 % MMT	5	0.81	0.44
	20	0.86	0.61

3.4 Conclusions

Growth, structure, and mechanical behavior of LbL thin films, composed of the weak polyelectrolyte BPEI and Laponite clay, were studied. Film thickness per bilayer can be tuned from 0.5 to 5 nm by altering pH of the aqueous deposition solutions. The thickest films are achieved with unadjusted BPEI (pH 10.3) and pH 6 Laponite. AFM images show very uniform film surfaces and a highly-ordered polymer/clay assembly in all of the BPEI/Laponite systems. Tilted clay platelets can be seen in TEM cross-section images of the film made with unadjusted BPEI and pH 6 Laponite, which could be a collapsed house-of-cards structure that consists of edge-to-face assocations. Nonetheless, XRD shows that the gallery spacing in the lamellar structure is the same for films made using different BPEI and Laponite pH values. At 40 BL, these films have a hardness of 0.5 GPa and reduced modulus of 6 to 10 GPa, depending on recipe. This type of thin film system may be useful for ion (charge) transport[198] and protective layers (*e.g.*, hard coating or flame resistance). These assemblies can be directly applied to cotton fabric and results in significant improvement in thermal stability. SEM images show that LbL coating three-dimensionally coats the surface of each individual thread of the fabric and provides some flame suppression.

When Laponite is replaced with montmorillonite, films assembled with high or low pH BPEI, and 1 or 0.2 wt% clay suspensions, all showed linear growth as a function of the number of BL deposited. Higher BPEI pH resulted in much thicker assemblies due to lower charge density. With respect to clay, using a higher concentration resulted in slightly thicker films. Flame-retardant properties of 5 and 20 BL coatings on cotton

fabric were tested with TGA, vertical flame testing, and microscale combustion calorimetry. A 7 to 13 % residue was left over from coated fabric after heat treatment at 500 °C under an air atmosphere, whereas the control fabric completely combusted. This level of charring is significant, because the coating contributed only 1 to 4 wt% to the fabric (depending on recipe and number of layers) prior to burning. During actual burning in the vertical flame test, afterglow time was significantly reduced for the coated fabrics. The weave structure of the fabric, as observed in SEM images, was well preserved relatively to the chars from coated fabrics, whereas the scant ashes from the control fabric showed little structure. SEM also revealed that each individual yarn was protected by a sheath-like coating. Additionally, MCC data revealed lower heat release for coated fabrics, suggesting that fewer combustible volatiles were generated. The physical properties of the fabrics did not show great differences between control and coated, suggesting that the coating does not adversely affect the desirable properties of the fabric itself. The simplicity of the LbL process provides a convenient method for imparting flame resistance to fabric using relatively benign ingredients. This concept could be further developed to impart flame retardant behavior to clothing and other materials for fire safety applications (*e.g.*, soft furnishings).

CHAPTER IV

GROWTH AND FIRE PROTECTION BEHAVIOR OF POSS-BASED MULTILAYER THIN FILMS[‡]

4.1 Introduction

Polyhedral oligomeric silsesquioxane (POSS) is a well-defined cluster with an inorganic core (Si_8O_{12}) surrounded by eight organic groups, which can reinforce polymer chain segments and control chain motions by maximizing the surface area and interaction with polymers in composites.[102-103] POSS does not suffer from the increased processing viscosity typically associated with using other inorganic fillers.[224-225] This ease of uniformly dispersing POSS, using simple blending into polymers (without further modification), has caused it to be investigated as a filler for polymer reinforcement and thermal property enhancement.[104, 107] During burning in air, the organic groups on POSS cages can undergo homolytic Si–C bond cleavage (~ 300 – 350 °C), resulting in the fusion of the POSS cages and the formation of a thermally- and oxidatively-stable silicon-oxycarbide "blackglass" surface ("Si–O–C ceramified char") created from the initial $(RSiO_{1.5})_n$ composition.[226] The formation of this thin layer provides a physical char barrier against combustion, preventing the diffusion of oxygen into the underlying material (and also limiting heat transfer).[227] Several POSS-containing

[‡] Reprinted with permission from "Growth and fire protection behavior of POSS-based multilayer thin films" by Yu-Chin Li, Sarah Mannen, Jessica Schulz, and Jaime C. Grunlan, *J. Mater. Chem.* **2011**, 2*1*, 3060-3069. © Royal Society of Chemistry 2011.

polymer composites have been studied and they all showed improved combustion properties and greater char yields relative to unfilled polymers.[105, 107, 228] When polymers are in the form of fibers, flame retardants are conventionally applied during polymerization, or by spinning, and coating. Polypropylene (PP)-POSS multifilament yarn was made *via* a melt spinning process and knitted into fabrics, which showed that POSS could improve the thermal stability of PP by increasing the time to ignition (TTI).[123] A polyurethane (PU)-POSS system was coated onto polyester and cotton fabrics, with a thickness of 36 μm, and both showed reduced heat release rate (HRR) and longer TTI.[108]

This chapter describes the incorporation of two types of POSS, with positively-charged amino side chains and with negatively-charged oxide ions, into LbL assemblies to provide flame resistance to cotton fabric. Others have explored the layer-by-layer growth of similar types of POSS, but only a single type was paired with either polymers[229-230] or colloidal nanoparticles[181, 231] OctaAmmonium POSS® (denoted as (+)POSS) and OctaTMA POSS® (denoted as (–)POSS) were used to build thin films composed entirely of POSS nanocages. Another $(RSiO_{1.5})_n$ chemical, aminopropyl silsesquioxane oligomer (AP), was also used to assemble films with (–)POSS. The thickness and the mass composition of the two different films were characterized before applying them to cotton fabric to evaluate their thermal stabilities. Vertical flame testing, microscale combustion calorimetry, and a methenamine pill test were performed to evaluate the fire behavior of coated cotton. The best recipe is 20 BL of AP (pH 10)/(–)POSS (pH 10), which reduces the total heat release by 23 %, and peak heat

release rate (pHRR) by 20 %, relative to uncoated cotton fabric. The coated fabrics were imaged with scanning electron microscopy (SEM) before and after flame testing. After flame testing, the residues are shown to maintain fiber shape and fabric weave structure. Fourier transform infrared spectroscopy (FTIR) was used to confirm the presence of POSS on the fibers. This work demonstrates that effective flame retardant coatings can be deposited on fabrics using layer-by-layer assembly of Si-containing molecules exclusively. With growing concern over toxicity of brominated flame retardants, this Si-based coating provides an environmentally-friendly alternative.

4.2 Experimential

4.2.1 Chemical Reagents and Substrates

Aminopropyl silsesquioxane oligomer (AP, 23 wt% in water, Gelest, Inc. Morrisville, PA), octa(3-ammoniumpropyl) octasilsesquioxane octachloride (OctaAmmonium POSS®, (+)POSS) and octakis(tetramethylammonium) pentacyclo-[9.5.1.1^{3,9}.1^{5,15}.1^{7,13}] octasiloxane 1,3,5,7,9,11,13,15-octakis(cyloxide)hydrate (OctaTMA POSS®, (–)POSS) (both from Hybrid Plastics®, Hattiesburg, MS) (see structure in Fig. 4.1), NaOH and HCl (both from Aldrich, Milwaukee, WI) were obtained commercially and used without further purification. Silicon wafers (University Wafer, South Boston, MA) and polished Ti/Au crystals with a resonance frequency of 5 MHz (Maxtek, Inc. Cypress, CA) were used for film characterization. Desized, scoured and bleached plain-woven cotton fabric was supplied by the United States Department of Agriculture (USDA) Southern Regional Research Center (SRRC, New Orleans, LA).

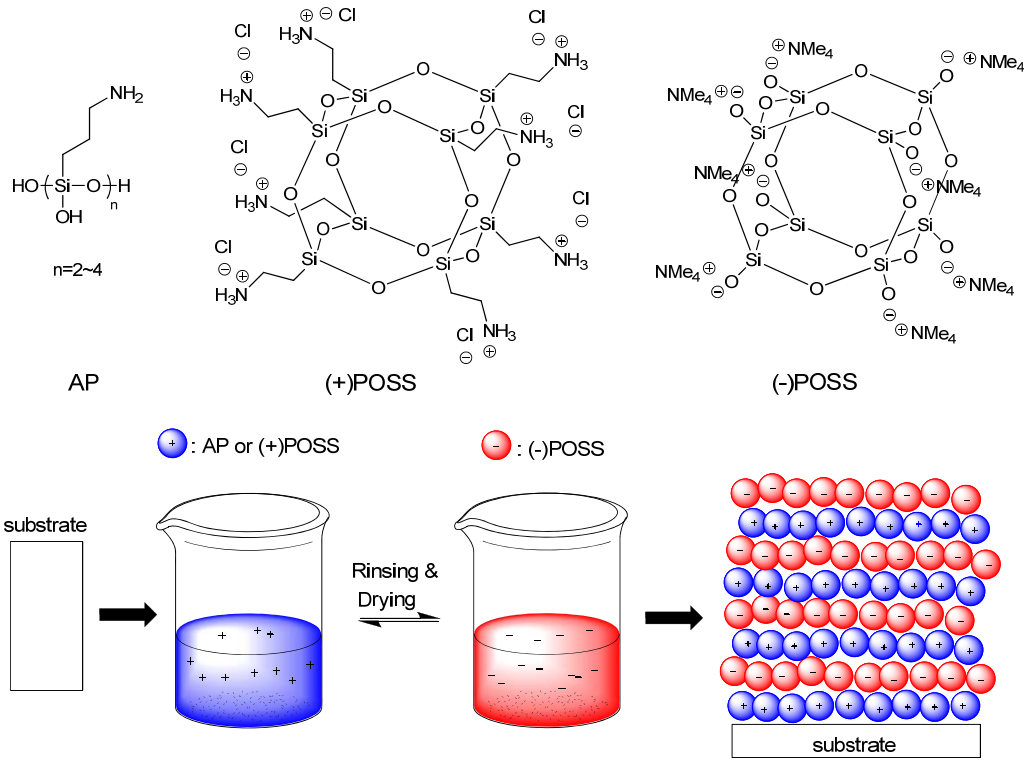

Figure 4.1. Chemical structures of deposition materials and schematic of the LbL deposition process used to prepare Si-based assemblies. Steps 1 – 4 are repeated until the desired number of bilayers is deposited.[232]

4.2.2 Layer-by-Layer Deposition

1 wt% AP pH 10, 10 mM (+)POSS pH 7.5, and 10 mM (–)POSS pH 10 were prepared as the deposition solutions. All films were assembled on a given substrate using the procedure shown in Figure 4.1 and as described in Section 3.2.3.

4.2.3 Film Growth Characterization

The film growth characterization procedure is the same as described in Section 3.2.4.

4.2.4 Thermal Stability, Flammability, Combustibility and Ignition Testing of Fabric

All dried fabrics were stored in dessicator prior to testing and all tests were conducted in triplicate to obtain the reported averages. The thermal stability of uncoated and coated fabrics was measured with a Q50 Thermogravimetric Analyzer (TA Instruments, New Castle, DE). Each sample was approximately 10 mg and was tested in both an air and nitrogen atmosphere, from room temperature to 600 °C, with a heating rate of 20 °C/min. Vertical flame testing was performed on 3 × 12 in. sections of uncoated and coated fabrics according to ASTM D6413. An Automatic Vertical Flammability Cabinet, model VC-2 (Govmark, Farmingdale, NY), was used to conduct this testing. Microscale combustibility experiments were conducted with a Govmark MCC-1 Microscale Combustion Calorimeter, according to ASTM D7309. The sample size was around 15 mg and samples were tested with a 1 °C/sec heating rate under nitrogen from 200 to 600 °C. The pyrolysis volatiles released from the thermal degradation of the sample are pushed into a 900 °C combustion furnace where they are mixed with oxygen. The timed methenamine burning tablet (Vesta Pharmaceutical Inc, Indianapolis, IN), used to simulate a small scale ignition test, was burned for 130 s under controlled conditions. The fabric size used for this test in this study is 4 × 6 in.

4.2.5 Analysis of Fabric

Surface images of control and coated fabric, as well as afterburn residues (after direct exposure to flame), were acquired with a Quanta 600 field-emission scanning electron microscope (FE-SEM, FEI Company, Hillsboro, OR). Energy-Dispersive X-ray

(EDX) analysis was conducted with an Oxford system microanalyzer attached to the FE-SEM. An Alpha FT-IR (Bruker Optics Inc., Billerica, MA), with platinum ATR module, was used to characterize the coated fabrics and afterburn residues.

4.3 Results and Discussion

4.3.1 Growth and Structure of Si-Based Assemblies

1 wt% AP in deionized water has an unadjusted pH of 10.7. In order to have more protonated amine groups (*i.e.*, higher charge density) the solution was adjusted to pH 10 by adding 1 M HCl. For POSS solutions, in order to have the same amount of POSS molecules in both solutions, and also keep them similar to the concentration of the AP solution, 10 mM (+)POSS and (–)POSS solutions were prepared. Growth of these POSS-POSS assemblies was evaluated at several pH values. The unadjusted pH of (+) and (–)POSS are 3.2 and 11.6, respectively, but films did not grow under these conditions. By adjusting the pH of (+)POSS to 7.5 and (–)POSS to 10, a film grew linearly as a function of the number of bilayers deposited. The diameter of the POSS cage is ~ 6 Å, so one bilayer of POSS may be expected to be around 1.4 nm. This corresponds with the thickness measured for the 30 BL POSS-only film shown in Figure 4.2, which is 41.4 nm. The AP solution was adjusted to pH 10 to match (–)POSS. The growth of AP and (–)POSS was also examined as a function of BL deposited and this film also grew linearly, with a 30 BL film achieving a thickness of 89 nm.

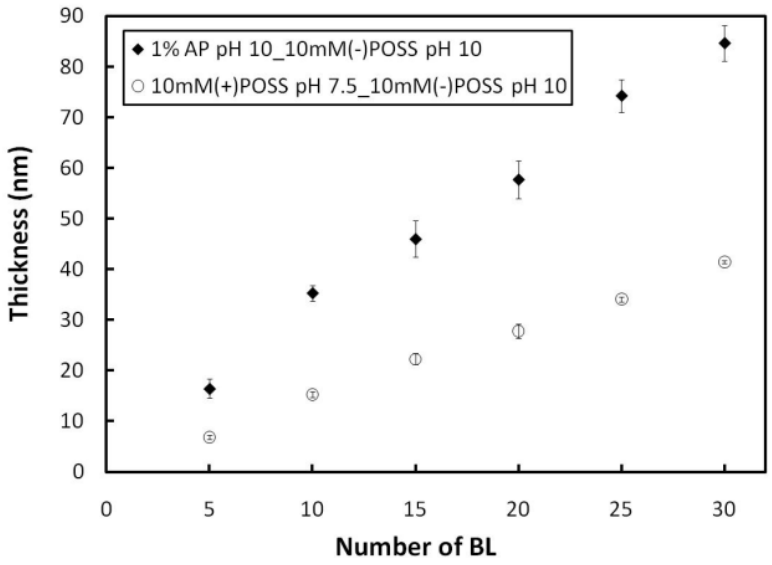

Figure 4.2. Film thickness as a function of the number of bilayers deposited. Films were assembled from aqueous solutions with 1 wt% AP at pH 10 or 10 mM (+)POSS at pH 7.5, paired with 10 mM (–)POSS at pH 10.[232]

Films were weighed during deposition using a QCM. When measured after each deposition step (Fig. 4.3), linear mass growth of the two films was revealed, just like the ellipsometric thickness trend (Fig. 4.2). A 30 BL AP/(–)POSS film has a mass of 5.77 μg/cm^2, while it is 2.58 μg/cm^2 for a (+)POSS/(–)POSS film. These differences are due to both film thickness and density. The density of the films is mass per unit area divided by thickness. The density of the AP-film is 0.65 g/cm^3 and the (+)POSS-film is 0.62 g/cm^3. AP is 46 wt% in AP/(–)POSS film and (+)POSS is 44 wt% in (+)POSS/(–)POSS film. An AP/(–)POSS film is thicker and heavier than a (+)POSS/(–)POSS film due to the AP molecules depositing more efficiently in each dipping cycle than (+)POSS. AP molecules are smaller (one quarter the molecular weight) and have less charge than (+)POSS. Hydrogen bonding among amino and hydroxyl groups on neighboring AP

molecules likely form efficiently packed, stable AP aggregates, preventing them from being rinsed away between deposition steps.

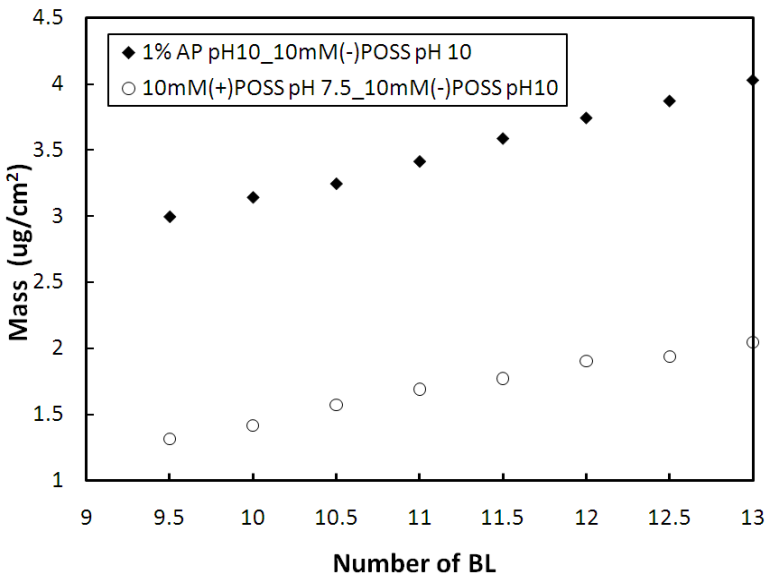

Figure 4.3. Accumulated film mass as a function of deposited layers for the two 10 mM (–)POSS (pH 10)-based films.[232]

Tapping mode AFM was used to characterize the surfaces of 30 BL AP/(–)POSS and (+)POSS/(–)POSS films. Figures 4.4(a) and (b) show height and phase images of the AP-film, while Figures 4.4(c) and (d) are height and phase images of the (+)POSS-film. A granular surface can be seen in both films, and this clustering/aggregation of POSS species has been observed by others.[233-234] It is interesting to note that the diameter of the clusters in the AP-film are larger than those in the (+)POSS-film, which may be further evidence of more AP molecules depositing on the film surface during each deposition step, resulting in more aggregation. The root-mean-square (rms) area roughness (using a

20 µm square area) for the AP-film is 9.3 nm, while it is 3.6 nm for the (+)POSS-film. In terms of roughness as a percentage of film thickness, the AP-film, which is 10.5 %, is slightly rougher than the (+)POSS-film at 8.7 %. This roughness likely contributes to the relatively high contact angle for the AP-film (91°) compared to the smoother (+)POSS-film (56.2°). Both of these films are more hydrophobic than the bare silicon wafer, which has a contact angle of 38.8°.

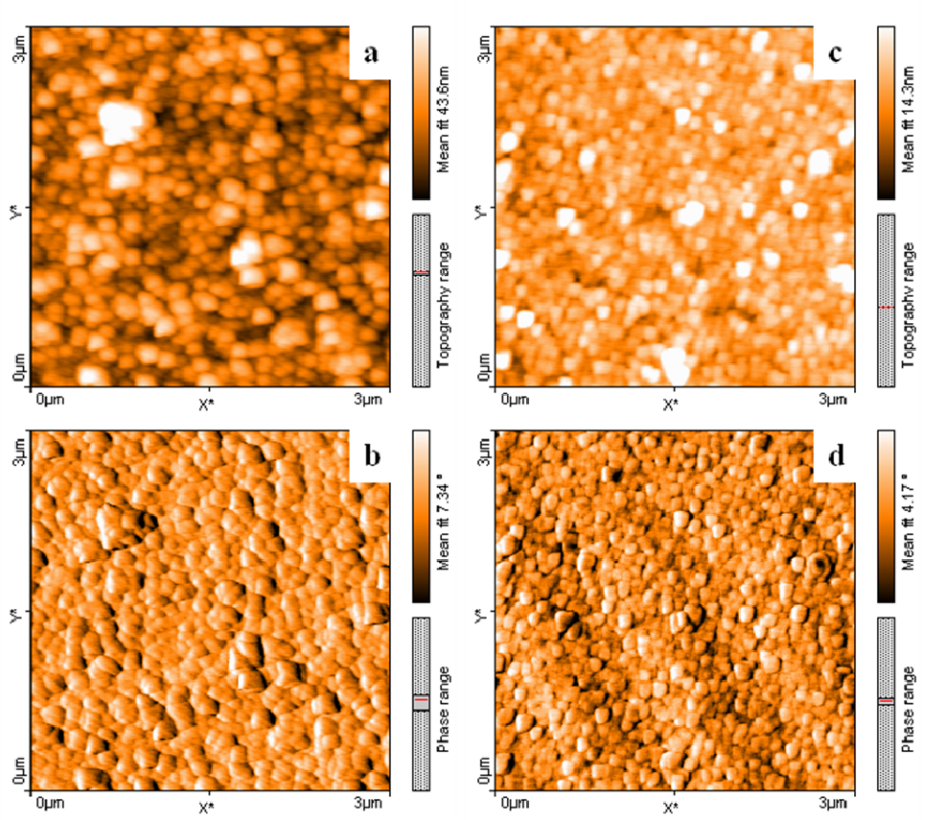

Figure 4.4. AFM height (a) and phase (b) surface images of a 30 BL AP/(–) POSS film. Height (c) and phase (d) images of a 30 BL (+)POSS/(–) POSS film are also shown.[232]

4.3.2 Thermal Properties of Coated Fabric

The AP/(–)POSS and (+)POSS/(–)POSS coatings characterized in the previous section were applied to cotton fabric. The as-received fabric is pure cellulosic fibers (starches, waxes and proteins were removed from the raw cotton fabric). Hydroxyl groups on cellulose have an isoelectric point of pH 2.5 – 3, which means that during the coating process, as long as the pH values of the dipping solutions are higher than 3, the zeta potential of the cellulose is negative (*i.e.*, it carries negative surface charge).[235] The coating weight was measured after the fabrics were dried in the oven (80 °C for 2 h) and cooled down to room temperature. The thermal properties of 5, 10, 20, and 30 BL-coated fabrics were examined by TGA, under both air and nitrogen atmospheres, with a heating rate of 20 °C/min. The mass % of the residue is plotted as a function of temperature in Figure 4.5. Figures 4.5(a) and (b) show AP-fabrics and (+)POSS-fabrics under air atmosphere, respectively. The uncoated control fabric begins to degrade around 350 °C and full degradation is reached near 500 °C. All coated fabrics have degradation curves similar to the control, but they show higher mass at 380 °C, and this mass gradually decreases all the way to 600 °C. This is in contrast to the control, which has a second abrupt mass drop before 500 °C that results in complete loss of residue.

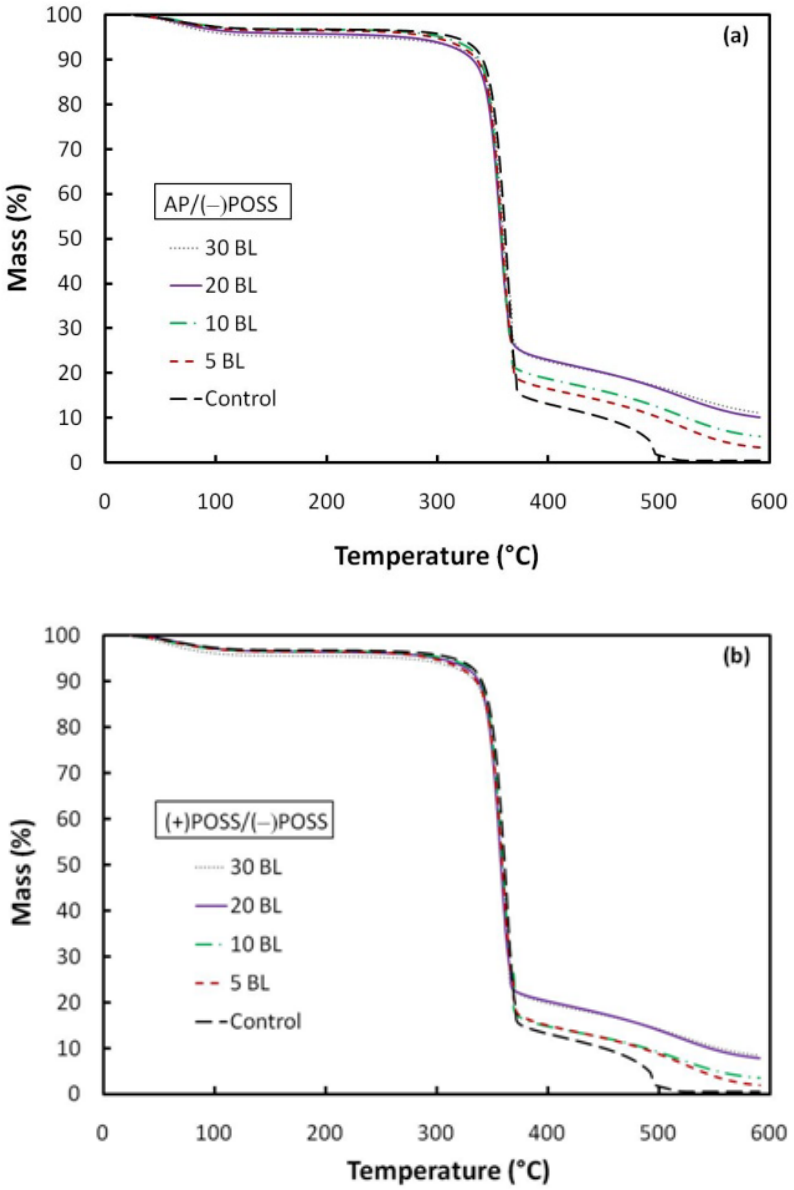

Figure 4.5. Weight loss as a function of temperature for cotton fabrics coated with 5, 10, 20 and 30 BL of AP/(–)POSS (a) and (+)POSS/(–)POSS (b). Control refers to the uncoated cotton fabric.[232]

The final residues of each coated fabric at 600 °C are directly related to the coating weight added. Residues increase with the number of bilayers added. In Table 4.1, the weight add-on is the percentage added by the coating to the original fabric weight. For both coating systems, the weight gain increased as the coating BL numbers increased, but not linearly, probably due to the complex geometry of the fabric surface, which does not allow more coating layered on fibers when the space between fibers are filled. The temperatures at 50 % mass for all the fabrics are very close to one another, under both air and nitrogen. From Table 4.1 and Figure 4.5, 20 and 30 BL of AP- and (+)POSS-coated fabrics have very similar residue weight left at 500 and 600 °C under both atmospheres, suggesting that the effective thickness limit on the fabric was reached. Thickness is believed to be somewhat limited by the tight spacing between individual cotton fibers that results in reduced deposition and some flaking off of the coating due to inter-fiber rubbing. Moreover, the 5 and 10 BL (+)POSS-coated fabrics have very similar curves on the plot and similar coating weight gain as well, suggesting that the first 10 BL were not very stable (*i.e.*, did not adhere to the fabrics very well) because of the small size of the molecules, which means relative few charged groups per molecule. It is not surprising that all the final residues are less than the coating wt%, because both AP and (+) POSS have organic side chains that easily volatilize at high temperatures. Both pure chemicals were run under the same TGA conditions in air, and AP had 59 wt% left and (+)POSS had 50 wt% left at 600 °C.

Table 4.1. Thermogravimetric analysis of control and eight different coated fabrics[232]

		air			N_2		
systems	**add-on (%)**	**Temp. at 50 % mass**	**mass % at 500°C**	**mass % at 600°C**	**Temp. at 50 % mass**	**mass % at 500°C**	**mass % at 600°C**
Control	-	361.35	1.71	0.54	371.88	7.67	2.74
AP/(–)POSS							
5 BL	3.87	357.66	10.05	3.29	369.18	10.67	8.76
10 BL	7.48	358.05	12.67	6.01	370.16	12.77	8.86
20 BL	13.83	357.17	16.57	10.22	372.45	17.71	15.24
30 BL	14.2	359.66	16.84	10.91	371.16	18.54	15.08
(+)POSS/(–)POSS							
5 BL	4.63	359.22	8.36	1.88	369.64	9.7	6.91
10 BL	5.5	359.23	9.32	3.49	367.31	10.65	7.38
20 BL	7.42	357.32	10.02	7.89	368.38	14.74	11.59
30 BL	10.05	358.39	14.11	8.11	368.63	15.91	12.18

Fabrics coated with 5, 10 and 20 BL (30 BL not shown due to the limitations described above) of the AP and (+)POSS-based assemblies were subjected to vertical flame testing (ASTM D6413). Times to ignition for the control and all coated fabrics are very similar, within 0.5 s of one another, which is within error. After-flame time for all coated fabrics is 1 to 3 s longer than control. All burning processes were video-recorded and the images shown were captured from the videos at the same time. Differences of flame size can be distinguished, between the control and two different coated fabrics, as shown in Figure 4.6. Six seconds after ignition, the size of the flame for the two 10 BL AP- and (+)POSS-coated fabrics is clearly smaller (in both vertical and horizontal directions), and less bright, than the flame on the control fabric. In addition, more glow was observed on the control fabric after the flame was removed. The afterglow times for 8 different coated fabrics were 8 to 9 s less than the uncoated fabric, which was 10 s. In

other words, once the flame on the control fabric died out, there was still glow along the edges of the residue. In the case of the coated fabrics, the glow disappeared in less than 2 s once the flame disappeared. Horizontal burn testing (ASTM D5132) revealed similar flame speed with or without a coating, although coated fabrics again displayed a diminished flame size. After burning, there was practically no char left from the control fabric, but all coated fabrics left significant residue, as shown in Figure 4.7(a) and (b). In general, more bilayers on a fabric left more residue and char was darker after flame testing. Char weight was found to increase as the number of bilayers increased from 5 to 20.

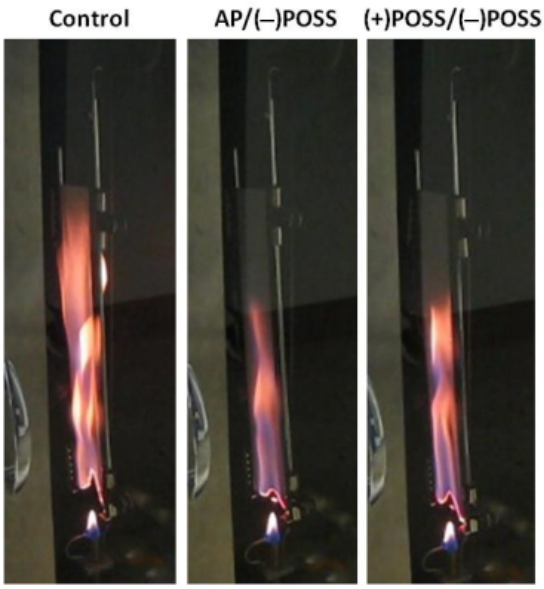

Figure 4.6. Images of vertical flame testing of the uncoated and coated cotton fabrics 6 seconds after ignition. The coated fabrics are 10 BL of a given recipe.[232]

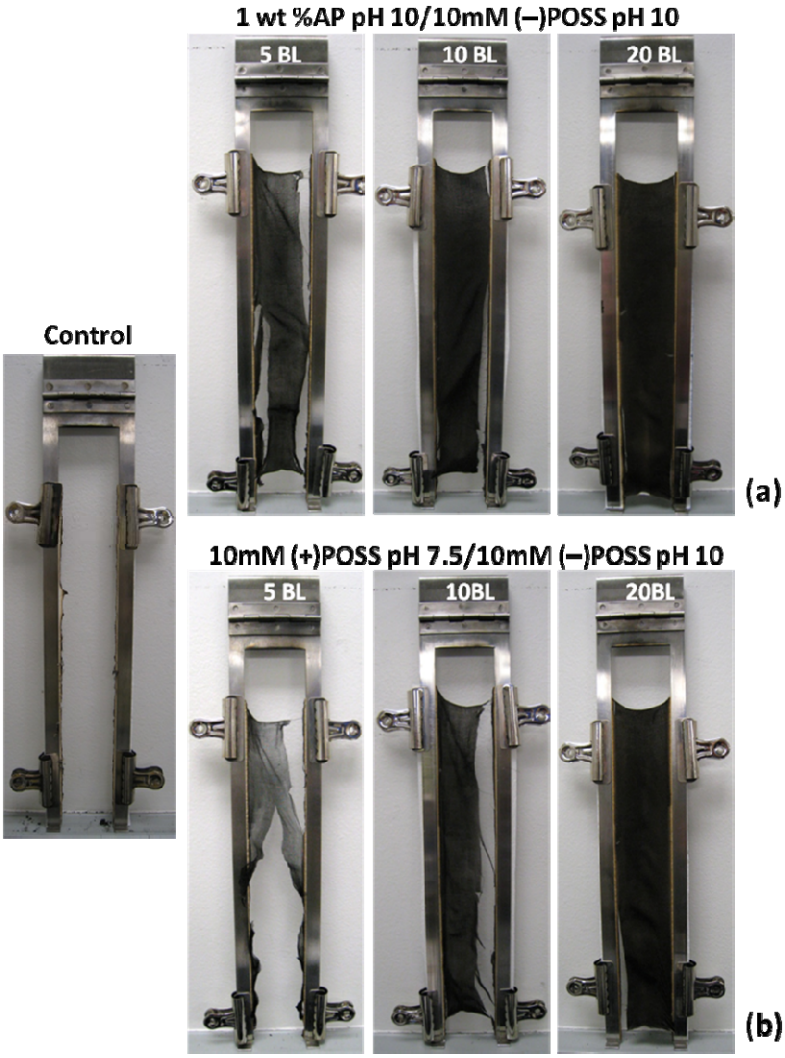

Figure 4.7. Images of control, 5, 10, and 20 BL-coated cotton fabrics following the vertical flame test. Residues of fabrics coated with AP/(–)POSS (a), and (+)POSS/(–)POSS (b), are shown.[232]

Microscale combustion calorimeter is also used for assessing flammability. MCC data for the fabric samples are summarized in Table 4.2. Char from all coated fabrics is higher than that from uncoated fabric, with char yield increasing with more bilayers on the fabric. Greater char yield was accompanied by the lower total HR and pkHRR. The maximum reduction in total HR (23 %) and HRR peak (20 %), as compared to the

control, are observed for the fabric coated with 20 BL of AP/(–)POSS. From the (+)POSS/(–)POSS coated fabrics, the best performance is also the 20 BL-coated fabric, which shows a 17 % reduction in total HR and 11 % in reduction in pkHRR.

Table 4.2. Microscale combustion calorimetry results for various coated fabrics[232]

Sample	char yield (wt%)	HRR peak Value (W/g)	HRR peak Temp(°C)	Total HR (kJ/g)
control	4.98±0.03	285±2	380.67±0.58	12.83±0.06
AP/(–)POSS				
5 BL	7.47±0.11	296±4	373.33±0.58	12.07±0.06
10 BL	9.87±0.2	274.33±10.41	374.67±1.15	11.67±0.12
20 BL	14.13±0.25	227.33±5.86	377±2	9.9±0.2
(+)POSS/(–)POSS				
5 BL	6.02±0.08	268±18	374.33±2.31	11.53±0.15
10 BL	6.95±0.06	292.33±8.08	372±1	12.33±0.06
20 BL	12.23±0.05	253.33±6.11	376.67±1.53	10.6±0.1

In an effort to better observe the ignition characteristics of these coated fabrics, a pill test was performed. This test, which is much less severe than the vertical flame test, subjects textiles to a small source of glow, similar to a lighted cigarette.[236] The pill was placed in the center of the fabric and burned for 130 s. Two different 10 BL-coated fabrics were tested, along with the control. The control fabric caught fire after the fabric started charring and was burned completely by the end of the test, as shown in Figure 4.8(a). In contrast, the coated fabrics (Fig. 4.8(b) and (c)) did not catch fire, but only smoldered and charred around the tablet. The charred area gradually increased during the process but once the pill stopped burning and charring also stopped. The size of the char for AP-coated fabric was 7 × 20 mm and it was 7 × 53 mm for (+)POSS-coated fabric.

Figure 4.8. Pill test images of post-burn control fabric (a), 10 BL AP/(–) POSS coated fabric (b), and 10 BL of (+)POSS/(–)POSS coated fabric (c).[232]

4.3.3 Characterization of Burned Fabric

Fabrics coated with 5, 10 and 20 BL of AP/(–)POSS and (+)POSS/(–)POSS were imaged by SEM prior to burning. Images of 30 BL-coated fabrics were omitted due to the similar coating weight and thermal behavior compared to fabric coated with 20 BL. The amount of AP/(–)POSS coating can be distinguished (top row in Fig. 4.9), where 5 BL-coated fibers are covered with a thin layer of the coating and some particulate-like aggregates. More aggregates can be seen on 10 BL-coated fibers and a very thick layer of coating is on top of each fiber surface with 20 BL. At 20 BL, aggregates can even be seen in between the fibers, which helps explain the similar behavior for 30 BL-coated fabrics, because the spaces between fibers are filled with the coatings, (akin to reaching saturation). The weave structures of fabrics after burning were also examined (bottom row of Fig. 4.9). The 10 nm thickness and 3.8 wt% of coating from 5 BL AP/(–)POSS were enough to preserve the weave structure of fabric, although significant fiber shrinkage is observed. For 10 and 20 BL, the degree of shrinkage decreased with increasing bilayers.

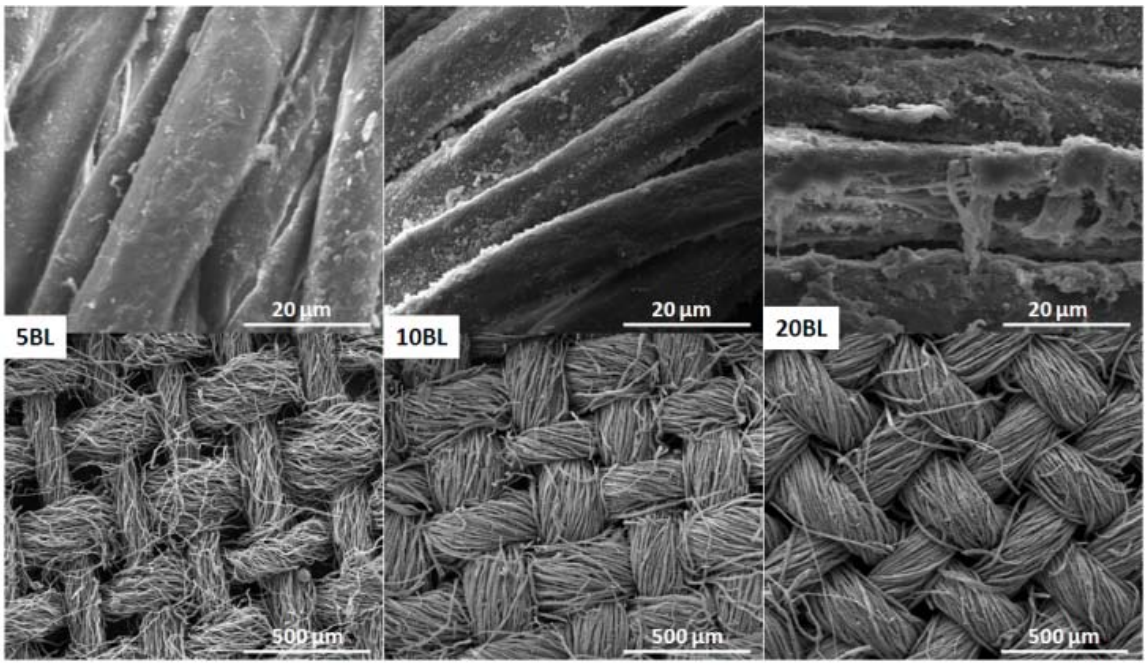

Figure 4.9. SEM images of 5, 10 and 20 BL of AP/(–)POSS coated fabrics. The top row images are coated fabrics before flame testing, while bottom row images show the weave structure of residues after burning the coated fabrics in the vertical flame test.[232]

The 20 BL residues in particular appear to have preserved the three-dimensional structure of the fabric weave. Unlike the 10 BL residue, where despite preserving the weave, they are flatter. In the case of (+)POSS/(–)POSS coated fabrics (top row images of Fig. 4.10), the coating amount also increased with increasing bilayers, but compared to the AP-coated fibers in Figure 4.9, the amount of (+)POSS/(–)POSS coating appears to be much less. This reduced level of coating resulted in looser weave structures after burning (bottom row of Fig. 4.10) compared to the AP-coated residues coated with the same number of bilayers.

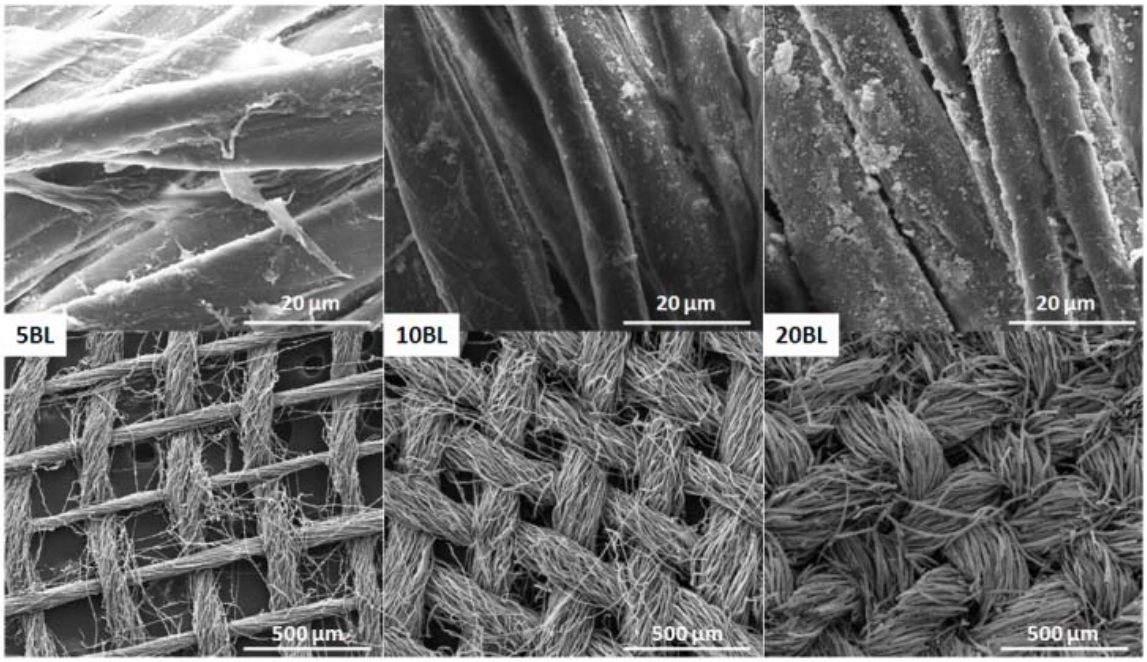

Figure 4.10. SEM images of 5, 10 and 20 BL of (+)POSS/(–)POSS pH 10 coated fabrics. The top row images are coated fabrics before flame testing, while bottom row images show the weave structure of residues after burning the coated fabrics in the vertical flame test.[232]

During vertical flame testing, the spot on the coated fabrics that first caught fire and started the burning process had a glow that persisted for several seconds. With the exception of this spot, the flame and glow stopped immediately once the triangular main flame passed through. The flame moved upward continuously and left residue the size of the original sample. At the end of the burning, the residue is dark brown, except for the initial ignition spot, which is white. This white-colored char is seen in all coated fabrics, except 5 BL of (+)POSS/(–)POSS, and its area increases with the number of bilayers deposited. In contrast, the control fabric has no char at all. As the main flame passed through, the control was completely consumed, leaving persistent glow at the edges of the sample holder. Figure 4.11(a) is the 20 BL AP/(–)POSS coated fabric after burning.

The white spot was imaged under SEM, which shows some broken fibers that are hollow (Fig. 4.11(b)). Under higher magnification (Fig. 4.11(c)), the hollow tube is clearly visible, with a diameter of 10 µm that is similar to the diameter of individual fibers before burning. The Si-based oligomers and nanocages may have gone through bond breaking and re-formed a network-like structure to create a continuous ceramic tube that was hollowed out after the cellulosic core (*i.e.*, cotton fiber) was completely burned out. The surface of the hollow tube was subjected to EDX analysis (Fig. 4.11(d)) and showed very strong Si and O peaks, suggesting an amorphous silica structure,[229] with some trace carbon left from the cellulose.

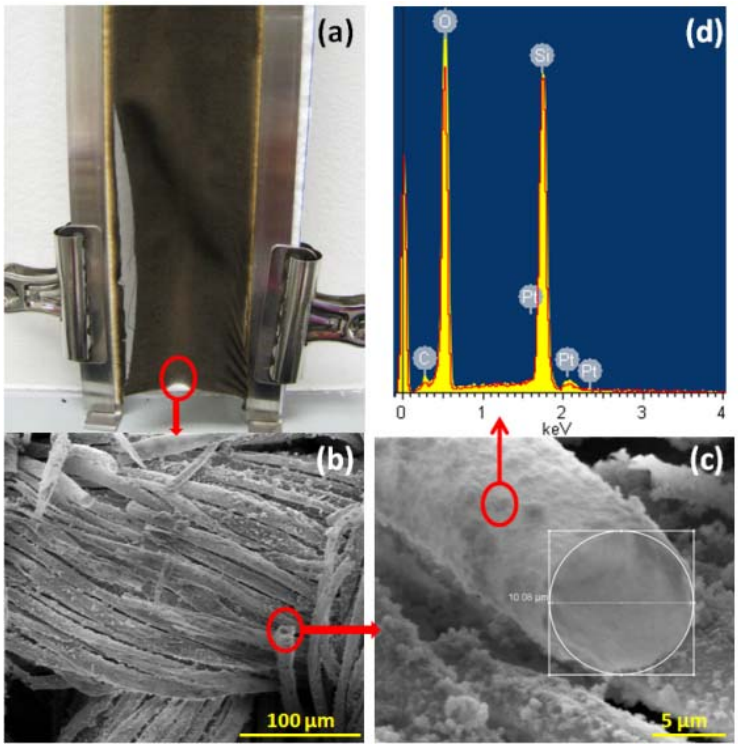

Figure 4.11. Residue of 20 BL of AP/(–)POSS coated fabric after vertical flame testing (a), SEM image of the white char (b), higher magnification SEM image of the hollow siliceous fiber tube (c), and EDX analysis of the hollow tube (d).[232]

The FTIR spectrum of uncoated cotton fabric exhibits an O–H stretching absorption around 3300 cm^{-1}. As the number of deposited bilayers increases, these absorbance peaks (of uncoated fabric) decrease due to shielding from the AP/(–)POSS, as shown in Figure 4.12(a). No major absorbance peaks from the coating are observed in the spectrum except a small peak at 795 cm^{-1} that is from Si–C bonds on AP, but it is only seen at higher bilayers. The same situation is observed for (+)POSS/(–)POSS coated fabrics. After vertical flame testing, the residues of coated fabrics were also examined with FTIR. Characteristic absorbance peaks of cellulose (from 2500 to 3500 cm^{-1}) are missing from the char of the coated fabrics, as shown in Figure 4.12(b). Very strong absorption is seen at 1050 cm^{-1}, from Si–O–Si asymmetric stretching. This peak is believed to be caused by stretching from the network structure rather than stretching from the POSS cages, which occurs at ~ 1110 cm^{-1}.[228] This would explain the ceramic tube shown in Figure 4.11(c). Another unique absorption peak on the char is at 805 cm^{-1}, which is from Si–O–Si symmetric stretching. Similar spectra are found with (+)POSS/(–)POSS coated fabrics and chars.

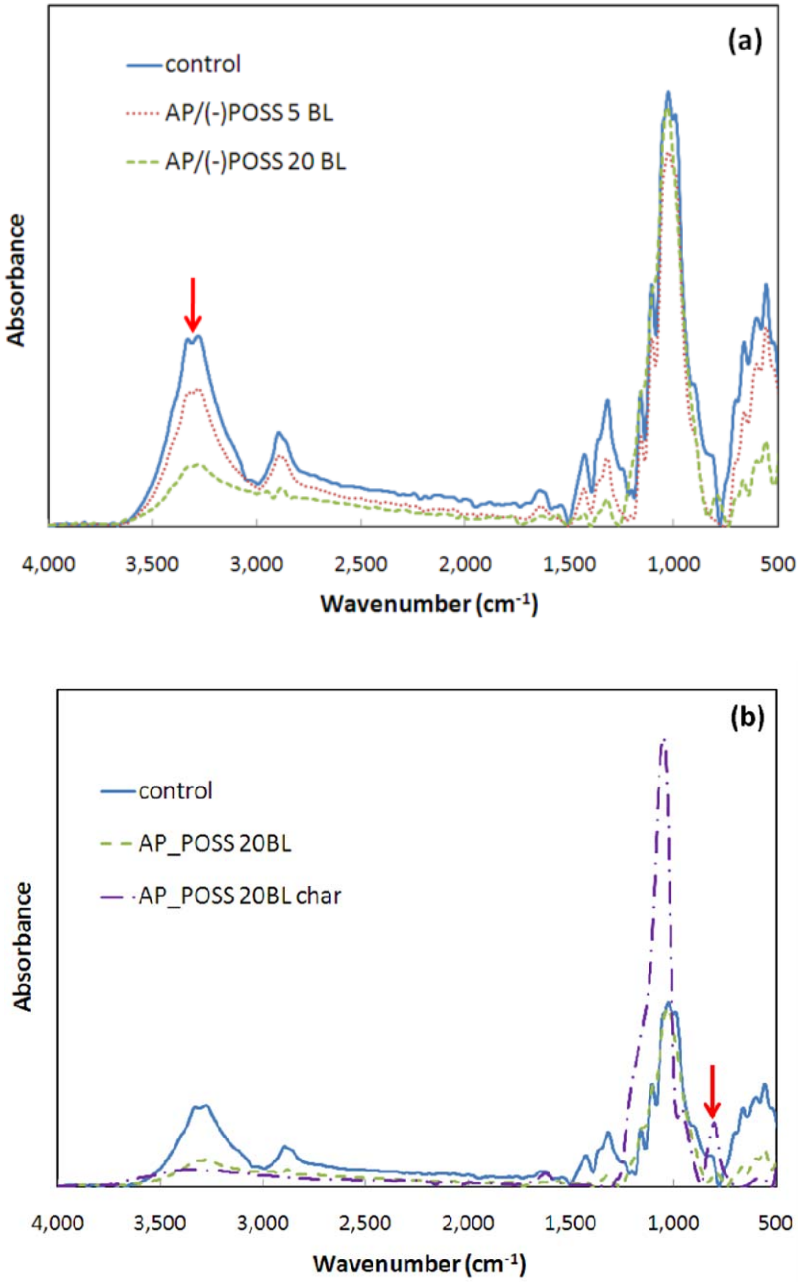

Figure 4.12. FTIR spectrum of control and AP/(–)POSS coated fabrics, at 5 and 20 BL (a). Spectrum comparison of AP/(–)POSS 20 BL coated fabric, and char.[232]

4.4 Conclusions

Layer-by-layer assemblies of Si-oligomer and charged POSS were successfully grown on flat substrates and on cotton fabric, growing linearly as a function of bilayers deposited. AP/(–)POSS assemblies deposit thicker and heavier layers than (+)POSS/(–)POSS assemblies, possibly due to hydrogen bonding among the AP oligomer's side chains. Fabrics coated with these two recipes showed greatly reduced afterglow times during vertical burn testing and the weave structures on their residues are highly preserved compared to the uncoated fabric. The fabric coated with 20 BL of 1 wt% AP pH 10/10 mM (–)POSS pH 10 exhibits the greatest reduction in total heat release (23 % compared to the control) and peak of heat release rate (20 %), as measured by microscale combustion calorimetry. Additionally, coated fabrics show good performance in the methenamine pill test, which mimics a small scale fire (*e.g.*, from a smoldering cigarette). If furnishing textiles are flame retardant, there is a reduced chance for a large-scale fire to progress from a small-scale fire source, which ultimately saves lives and property. In addition to their flame retardant behavior, these Si-based thin films may be useful for other applications, such as low dielectric constant for lowering signal delay, due to their nanoporous structure.[233-234] It is also possible that inorganic micro-tubes could be produced using this technique of burning out the polymeric core, which may be easier than using the more traditional etching of an inorganic template.[237-240]

CHAPTER V

INTUMESCENT LAYER-BY-LAYER COATINGS ON COTTON FABRIC

5.1 Introduction

There are two different pyrolysis routes for cotton (*i.e.*, cellulose). At high temperature (>300 °C), it breaks down to various small molecules (such as aldehydes, ketones, and alcohols), which are highly volatile and flammable.[241] Cellulose can also decompose below 300 °C, under dehydration,[45] which will generate carbonaceous char and water, and much less heat.[242] One of the most effective ways to make cotton more fire resistant is to use a flame retardant which makes the pyrolysis of cotton occur at a lower temperature, which will result in less heat evolved, fewer flammable volatiles produced, and promotion of char formation. Intumescent systems suppress flammability through a condensed-phase mechanism, by interrupting the self-sustained combustion of polymer at an earlier stage.[243-244] The intumescence process results from a combination of charring and foaming at the surface of the burning polymer. The resulting foamed cellular charred layer, whose density decreases as a function of temperature, protects the underlying material from the action of the heat flux or the flame.[245] This charred layer acts as a physical barrier that slows down heat and mass transfer between the gas and condensed phases. Traditional intumescent flame retardants contain four key components: a source of carbon (or *carbon donor*), a source of acid (or *acid donor*), a source of gas (or *blowing agent*) and a binder to keep all the components suspended in a liquid dispersion and form a solid film on a surface.[246]

In this chapter, poly(sodium phosphate) (PSP) acts as the acid source and is negatively-charged in water. Poly(allyl amine) (PAAm) is positively-charged in water, because of the amine functional groups, and is used as the blowing agent. Thin films made with these two chemicals using LbL assembly can be directly deposited onto cotton fabric, which eliminates the need for a binder. Cellulose itself functions as the carbon source,[247] creating a complete intumescent system. These intumescent thin films were tailored by varying the concentration of PSP and PAAm, and using them in combination with clay (in an effort to get a synergistic effect). In TGA testing, all coated fabric show a reduced degradation temperature, but there is significant residue left at 600 °C. Vertical flame testing shows coated fabric to be highly preserved, with no ignition occurring in some cases (*i.e.*, the fabric did not burn). Postburn analysis of coated fabric shows a cellular (foamed) layer with SEM imaging. Cone calorimetry shows that peak heat release rate (pHRR) and total heat release (THR) are reduced to one-third of the measurement from control (uncoated) fabric, with only 4 wt% added to the original fabric weight. This study marks the first intumescent flame retardant created using layer-by-layer assembly, which dramatically reduces the flammability of cotton.

5.2 Experimental

5.2.1 Chemical Reagents and Substrates

Poly(allyl amine) (PAAm) (Mw 15,000, 15 wt% in water. Polysciences, Inc., Warrington, PA), poly(sodium phosphate) (PSP) (sodium hexametaphosphate, crystalline, +80 mesh, 96 %, Aldrich, Milwaukee, WI), (see both structures in Fig. 5.1),

BPEI and MMT (as described in Section 3.2.1), NaOH and HCl (both from Aldrich) were obtained commercially and used without further purification. Silicon wafers (University Wafer, South Boston, MA) and polished Ti/Au crystals with a resonance frequency of 5 MHz (Maxtek, Inc. Cypress, CA) were used as substrates for characterization of film growth. Desized, scoured and bleached plain-woven cotton fabric was supplied by the United States Department of Agriculture (USDA) Southern Regional Research Center (SRRC, New Orleans, LA).

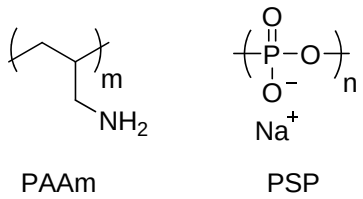

Figure 5.1. Structures of PAAm and PSP.

5.2.2 Layer-by-Layer Deposition

0.1 and 0.5 wt% PAAm pH 7, 0.2 and 1 wt% PSP pH 7, 1 wt% BPEI pH 10, and 1 wt% MMT were used as aqueous deposition solutions. 1 wt% BPEI pH 10 was used as the first deposition solution for all assemblies. All films were assembled on a given substrate using the procedure described in Section 3.2.3. For the fabric coating, in order to get higher negative surface charge,[235] the fabric was soaked in pH 10 deionized water for 5 minutes before deposition.

5.2.3 Film Growth and Fabric Characterization

Film growth characterization is described in Section 3.2.4. Surface images of coated fabric, as well as of the char (after direct exposure to flame), were acquired with a Quanta 600 FE-SEM (FEI Company, Hillsboro, OR).

5.2.4 Thermal Stability, Flammability and Combustibility Testing of Fabric

TGA, vertical flame testing, and microscale combustion calorimetry were used as described in Section 4.2.4. Horizontal flame testing was performed on 4 × 12 in. sections of uncoated and coated fabrics according to ASTM D 5132. An automatic horizontal flammability cabinet (HC-2 model, Govmark, Farmingdale, NY) was used to conduct this testing. Cone Calorimeter experiments were conducted on a FTT Dual Cone Calorimeter with a 35 kW/m^2 heat and an exhaust flow of 24 L/s, using the standardized cone calorimeter procedure (ASTM E 1354). All samples were mounted vertically as per a modified cone calorimeter standard (ASTM E 1740) and the sample size is 4 × 4 in.

5.3 Results and Discussion

5.3.1 Film Growth and Characterization

Low and high concentration deposition solutions were prepared. 0.1 wt% PAAm, which has a pH of 10.6, was lowered to pH 7 to increase the charge density. Based on the molecular weight of monomer repeat units, 0.1 wt% PAAm is 20 mM. In order to use the same concentration of the PSP, 0.2 wt% was used. 0.2 wt% PSP has a pH of 7.2, which was adjusted to pH 7 to match the pH of the cationic (PAAm) solution. The high

concentration solutions contained 0.5 wt% PAAm or 1 wt% PSP. The pH of high concentration PAAm and PSP solutions were adjusted from 11 and 6.9, respectively, to 7. BPEI is substituted for the first layer to improve adhesion to the substrate.[248] For example, $(PAAm/PSP)_{40}$ is actually (BPEI/PSP),$(PAAm/PSP)_{39}$, meaning the first bilayer is composed of BPEI and PSP, and the following 39 bilayers are comprised of PAAm and PSP. One other system is also examined, 10 BL of 1 wt% BPEI pH 10/1 wt% MMT, followed by 20 BL of 0.5 wt% PAAm/1 wt% PSP, to examine the growth and barrier of a combined system. Clay layers are expected to provide a physical barrier to protect the fabric. To prevent the loss of this barrier effect after PSP layers have expanded after heating, it is underneath the intumescent layers.

As shown in Figure 5.2, the low concentration system grows much thinner. When polyelectrolyte deposition solutions are at high concentration, the growth is much thicker and more linear from 10 to 40 BL. A similar growth trend was found with assemblies of PAH/PSP at higher concentration, although that system used a spray method and different ionic strength.[248] As for the combined clay/intumescent system, the first 10 BL of BPEI/MMT grow linearly, as described in Chapter III, and the following 20 BL of high concentration PAAm/PSP matches the growth in the absence of clay, but with a 10 BL offset. It is clear that polyelectrolyte concentration influences growth, but different surface morphology (Si wafer or clay layer) of the substrate has little influence.

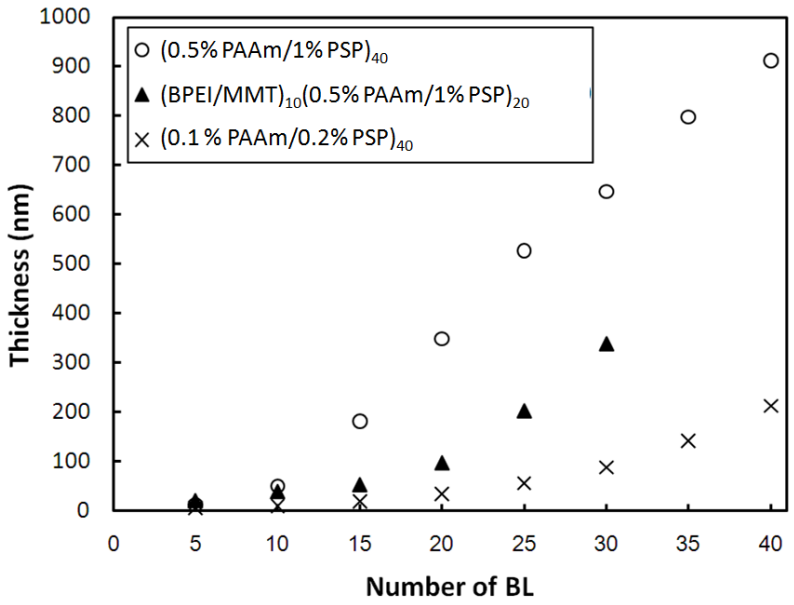

Figure 5.2 Film thickness as a function of the number of bilayers deposited. Films were assembled with low and high concentration of PAAm pH 7and PSP pH 7, and a film made with 10 BL of BPEI pH 10 and MMT plus 20 BL of high concentration PAAm/PSP.

Figure 5.3 shows the weight growth of the films made with high concentration PAAm/PSP and the combined system. The growth trend of these two films is similar to the thickness growth trend (Fig. 5.2). PAAm/PSP has a more linear mass increment compared to the combined system, which has a linear trend up to 10 BL, and then it grew somewhat exponentially when PAAm/PSP started depositing. In its initial exponential growth stage (from 0 to 10 BL), the neat PAAm/PSP system contains 34.7 wt% PAAm and 65.3 wt% PSP. Beyond 10 BL this system exhibits very linear growth (from 10 to 30 BL), with 40.1 wt% PAAm and 59.9 wt% PSP. As for the combined system, the first 10 BL contains 12. 3 wt% BPEI and 87.7 wt% MMT, and from 10 to 20 BL (the initial exponential growth of high concentration PAAm/PSP), 31.4 wt% PAAm

and 68.6 wt% PSP was found, very similar to the other film at the start of its growth. These results further confirm the minimal influence of substrate composition on LbL film growth.

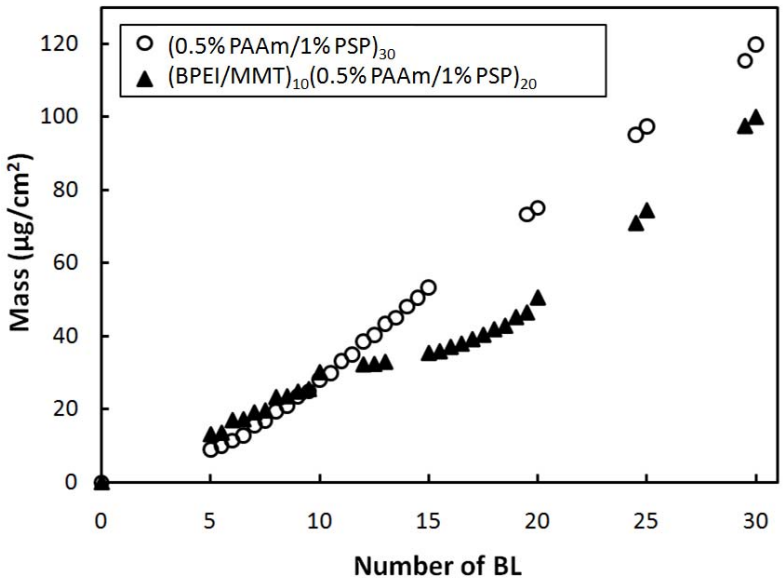

Figure 5.3 Accumulated film mass as a function of deposited layers for the high concentration PAAm pH 7/PSP pH 7 system and with 10 BL of BPEI pH 10/MMT combined with 20 BL of high concentration PAAm/PSP.

5.3.2 Thermal Stability of Coated Fabric

Fabrics coated with 10, 20, 30 and 40 BL of low and high concentration PAAm/PSP, and the combined systems of 10 BL of BPEI/MMT with 0, 10, 20 and 30 BL of high concentration PAAm/PSP, were prepared. Thermal properties of coated fabrics were measured by TGA under an air atmosphere with a heating rate of 20 °C/min. The mass % of the residue is plotted as a function of temperature in Figure 5.4.

10, 20 and 30 BL of low and high concentration PAAm/PSP show a lower degradation temperature compared to the control fabric (Fig. 5.4(a) and (b)). PSP-coated fabrics decomposed near 320 °C, 30 °C lower than the control, and this degradation also finished nearly 40 °C earlier, at around 340 °C. Beyond this significant mass loss, the degradation curves became smoother compared to the control, leading to a higher residual weight at the end of the test. The mass % increased as the number of BL increased. The final mass was 2 to 4 % higher than the coating weight % added on the fabric, as shown in Table 5.1, suggesting the fabric itself was preserved to some extent.

The high concentration PSP-coated fabric produced a much greater residue because of the higher coating weight on the fabric. The coating weight of the low concentration PSP-coated fabric slightly increased as the coating BL increased, while the high concentration PSP-coated fabric has a larger weight gain difference every 10 BL (from 10 to 30 BL) deposited on the fabric. These results are similar to the thickness trend observed in Figure 5.2. As for the 40 BL high PSP-coated fabric, the weight gain is not increased as expected. It is likely that tighter gaps between fibers limited film deposition beyond 30 BL, which also diminished the improvement in thermal stability. As for the combined systems, an individual 10 BL of BPEI/MMT coated fabric was used as a base of comparison. As shown in Figure 5.4(c), the 10 BL BPEI/MMT coated fabric has a slightly higher degradation temperature than the control fabric, suggesting the clay layers provide a physical barrier. After the large mass loss, the 10 BL MMT-coated fabric has a higher residual mass from 400 to 570 °C compared to the control, but only 2.8 wt% mass is left from this fabric at the end of the test, similar to the coating mass %

(Table 5.1). 10, 20 and 30 BL of high concentration PSP, on top of 10 BL BPEI/MMT all show lower degradation temperature, with degradation finishing earlier than the control and 10 BL MMT-coated fabric. Only the combined 20 BL-coated fabric has a residue weight greater than the original coating weight. The thermal stability of fabric did not improve by adding 10 BL of clay layers underneath the PSP layers and the residues are primarily equivalent to the coating itself, probably because the polyphosphates were blocked by MMT, which prevents phosphorylation to occur on hydroxyls of cellulose.

Table 5.1. Thermogravimetric analysis of control and coated fabrics

Sample	% Mass added	Temp. at 75% mass	Mass % at 500 °C	Final mass %
Control	0	354.18	1.73	0.29
$(0.1\%\ PAAm/0.2\%\ PSP)_{10}$	2.27	324.93	19.22	3.52
$(0.1\%\ PAAm/0.2\%\ PSP)_{20}$	3.49	325.66	21.86	5.40
$(0.1\%\ PAAm/0.2\%\ PSP)_{30}$	4.38	326.66	25.02	8.31
$(0.5\%\ PAAm/1\%\ PSP)_{10}$	4.71	323.4	23.13	6.46
$(0.5\%\ PAAm/1\%\ PSP)_{20}$	11.69	330.93	29.71	14.30
$(0.5\%\ PAAm/1\%\ PSP)_{30}$	21.34	329.99	36.62	24.17
$(0.5\%\ PAAm/1\%\ PSP)_{40}$	29.19	333.56	40.57	29.45
$(1\%\ BPEI/1\%\ MMT)_{10}$	2.08	362.85	15.38	2.83
$(BPEI/MMT)_{10}(0.5\%\ PAAm/1\%\ PSP)_{10}$	9.08	328.47	25.67	9.70
$(BPEI/MMT)_{10}(0.5\%\ PAAm/1\%\ PSP)_{20}$	16.87	335.16	31.65	14.43
$(BPEI/MMT)_{10}(0.5\%\ PAAm/1\%\ PSP)_{30}$	29.43	334.45	36.78	24.47

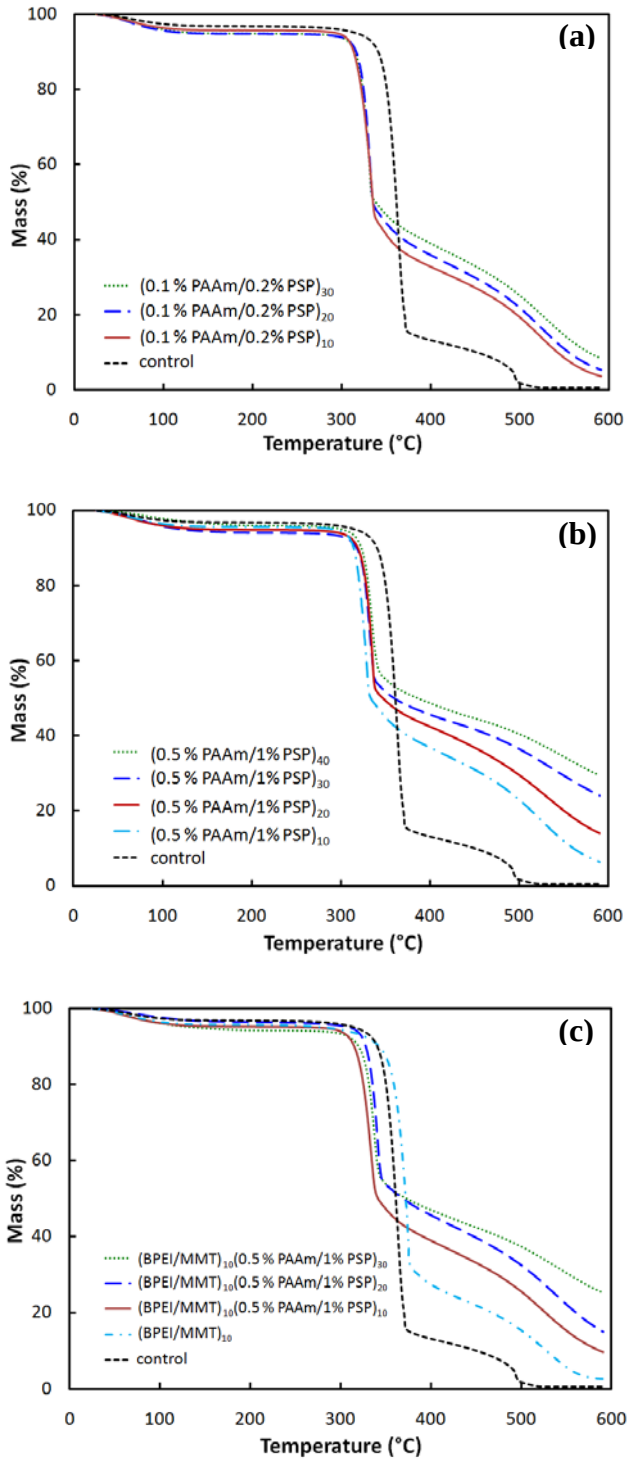

Figure 5.4. Weight loss as a function of temperature for fabric coated with different bilayers of low (a) and high (b) concentration PAAm/PSP, and BPEI/MMT)$_{10}$(PAAm/PSP)$_{10n}$ (c).

5.3.3 Flame Testing of Coated Fabric

Three different assembly recipes were coated on cotton fabric for vertical flame testing (VFT). The uncoated control fabric was completely consumed by the direct flame, as shown in Chapters III and IV (Figs. 3.18 and 4.7). For the low concentration PSP-coated fabrics, even with only a 10 BL coating (coating weight 2.3 % with respect to the fabric weight), the residue was preserved as a complete piece, without shrinking or disappearing (Fig. 5.5(a)). With more bilayers, the char weight % increased after burning, as shown in Table 5.2. Char weight is 7 to 9 times greater than the coating weight added on the fabric, meaning the cotton itself is truly preserved and the residue is not just coming from the coating. During the burning, flame color and size on the coated fabric was less bright and smaller than the flame on the control fabric. After-flame time also decreased and there was no afterglow at all. For the high concentration PSP-coated fabrics, a 10 BL-fabric burned completely and with a complete residue. When the BL number increased, the unburned part on the fabric increased, as shown in Figure 5.5(b). In one trial out of three, the flame extinguished on the 30 BL-fabric, so it was not burned all the way through. Unfortunately, a 40 BL coating only extinguishes one out of six samples, but all the flame testing measurements are similar to the 30 BL samples. As for the combined system, the 10 BL MMT-coated fabric did not preserve the whole piece of char after burning, but by adding another 10 BL PSP-coating, the char was more complete and the residue increased from 7 to 25 wt%. When adding 20 or 30 BL of PSP coating on top of the 10 BL MMT coating, the amount of residue and unburned part

increased. There was some molten residue on top of the dark char that makes the afterburn fabric look more grayish in some places, as shown in Figure 5.5(c).

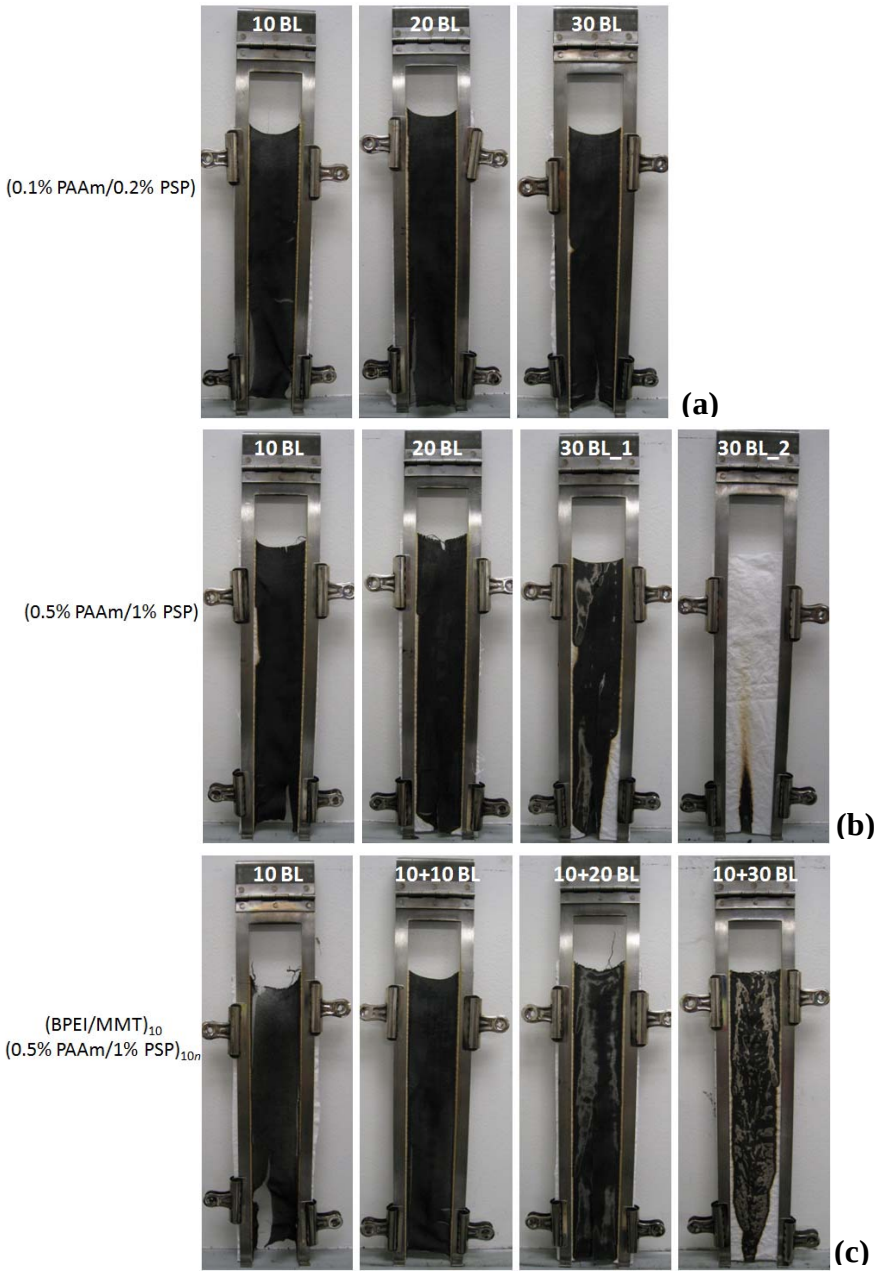

Figure 5.5. Images of coated fabrics following vertical flame testing. Residue of fabrics coated with low (a) and high (b) concentration PAAm/PSP, and the combined system (c) are shown.

Table 5.2. Measurement of coated fabrics from vertical flame testing

Sample	% Mass added	After-Flame time (s)	Afterglow time (s)	Residue (%)
Control	0	11.3	17.8	0
$(0.1\%\ PAAm/0.2\%\ PSP)_{10}$	2.27	2.8	1.4	18.26
$(0.1\%\ PAAm/0.2\%\ PSP)_{20}$	3.49	6.2	0	27.48
$(0.1\%\ PAAm/0.2\%\ PSP)_{30}$	4.38	3.8	0	29.69
$(0.5\%\ PAAm/1\%\ PSP)_{10}$	4.71	5.7	0	33.36
$(0.5\%\ PAAm/1\%\ PSP)_{20}$	11.69	6.1	0	36.81
$(0.5\%\ PAAm/1\%\ PSP)_{30}$	21.34	6.7	0	53.99
$(1\%BPEI\ pH10/1\%MMT)_{10}$	2.08	7.8	1.52	7.12
$(BPEI/MMT)_{10}(0.5\%\ PAAm/1\%\ PSP)_{10}$	9.08	4.3	0	25.04
$(BPEI/MMT)_{10}(0.5\%\ PAAm/1\%\ PSP)_{20}$	16.87	5.8	0	34.39
$(BPEI/MMT)_{10}(0.5\%\ PAAm/1\%\ PSP)_{30}$	29.43	8.4	0	48.03

Horizontal flame testing (HFT) was used to measure the burning rate of fabric. The burning of all fabrics was recorded and the time for the flame to travel between two scribed lines on the sample holder was measured. Table 5.3 shows the burning rate of each fabric, along with total burning time. Fabric coated with low concentration PAAm/PSP exhibits a higher burning rate than the control, along with the fabric coated with 10 BL of the other two systems (high concentration PAAm/PSP and combined system). When fabric coated with 20 BL (or more) of high concentration PAAm/PSP, with or without 10 BL MMT underneath, the rate became slower, and the flame size is much smaller compared to the control (Fig. 5.6). There is no char left from the control fabric after HFT (Fig. 5.6(d)), and the residues from all coated fabrics look similar to the residues from VFT. For example, the char from the high BL number of high concentration PAAm/PSP and combined system (Fig. 5.6(e) and (f)) show the lighter color char and molten residue and the dark char.

Table 5.3. Burning rate of control and coated fabrics from horizontal flame testing

Sample	Time (s)	Rate (mm/min)
Control	75.12	203.7
$(0.1\%\ PAAm/0.2\%\ PSP)_{10}$	44.6	343.0
$(0.1\%\ PAAm/0.2\%\ PSP)_{30}$	64.4	237.6
$(0.5\%\ PAAm/1\%\ PSP)_{10}$	66.5	230.1
$(0.5\%\ PAAm/1\%\ PSP)_{30}$	93.23	164.1
$(1\%\ BPEI/1\%\ MMT)_{10}$	65.3	234.3
$(BPEI/MMT)_{10}(0.5\%\ PAAm/1\%\ PSP)_{10}$	56.87	269.0
$(BPEI/MMT)_{10}(0.5\%\ PAAm/1\%\ PSP)_{30}$	96.93	157.8

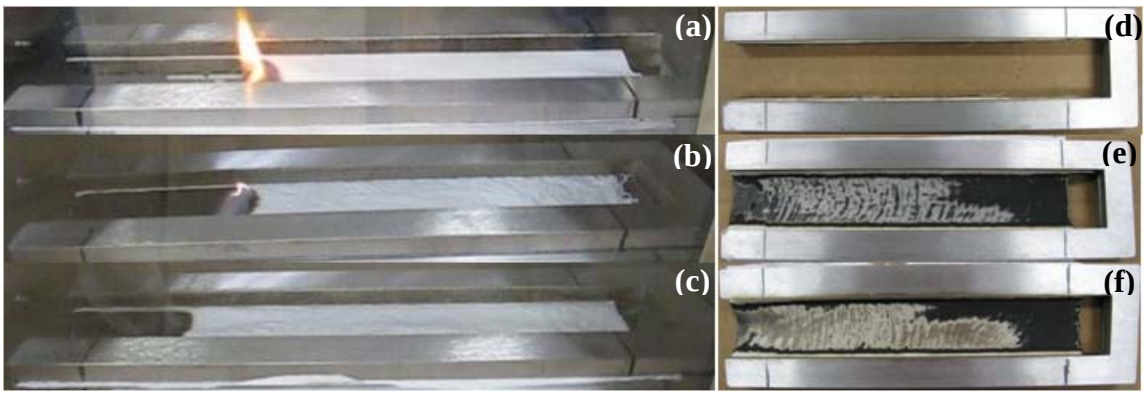

Figure 5.6. Images of in progress horizontal flame testing of control (a), 20 BL of high concentration PSP-coated (b), and $(BPEI/MMT)_{10}(PAAm/PSP)_{20}$ coated (c) fabric. These images were taken 30 seconds after the flame passed the first scribed line. Post-test images of the control (d), 30 BL of high concentration PSP-coated (e), and $(BPEI/MMT)_{10}(PAAm/PSP)_{30}$ coated (f) fabric are also shown.

Figure 5.7 shows fabric and afterburn residues imaged with SEM. The weave structures of all coated fabric before and after flame testing did not change much. Additionally, these coatings do not alter the weave structure of the control fabric. No shrinkage of the cotton thread was observed after burning, although the surface of the 30

BL fabric looks rougher than the 10 BL due to the thicker coating. Since there was no char left from the control fabric after burning, there is no weave image shown here. At higher magnification, the coating on the fibers can be more clearly distinguished with regard to the number of bilayers. The control fiber has a smooth surface (Fig. 5.8(a)). As for the high concentration PSP-coated fabric, the fiber structure and shape of 10 BL fabric (Fig. 5.8(b)) are similar to the control, but when the BL number increases to 20 (Fig. 5.8(c)), some fibers appear linked with each other. When the number of bilayers reaches 30 and beyond (Fig. 5.8(d) and (e)), the gaps between fibers are gradually disappears and the fibers look thicker.

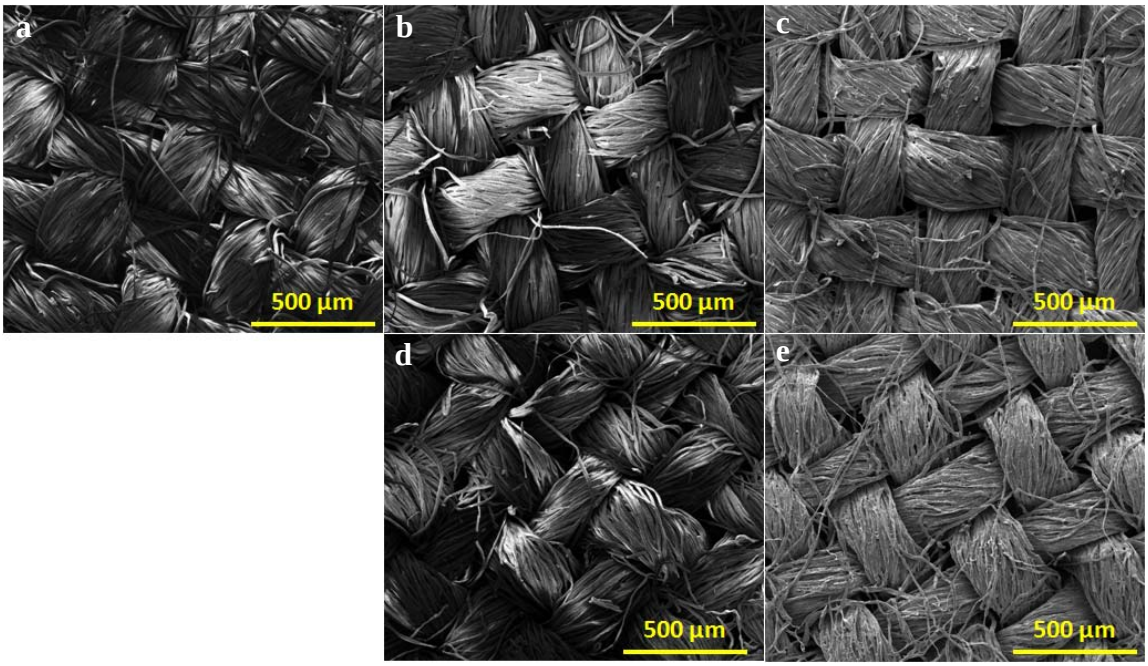

Figure 5.7. Weave structure of control fabric (a), 10 (b) and 30 (c) BL of high concentration PSP-coated fabric, before burning, and the residue of 10 (d) and 30 (e) BL fabric after burning.

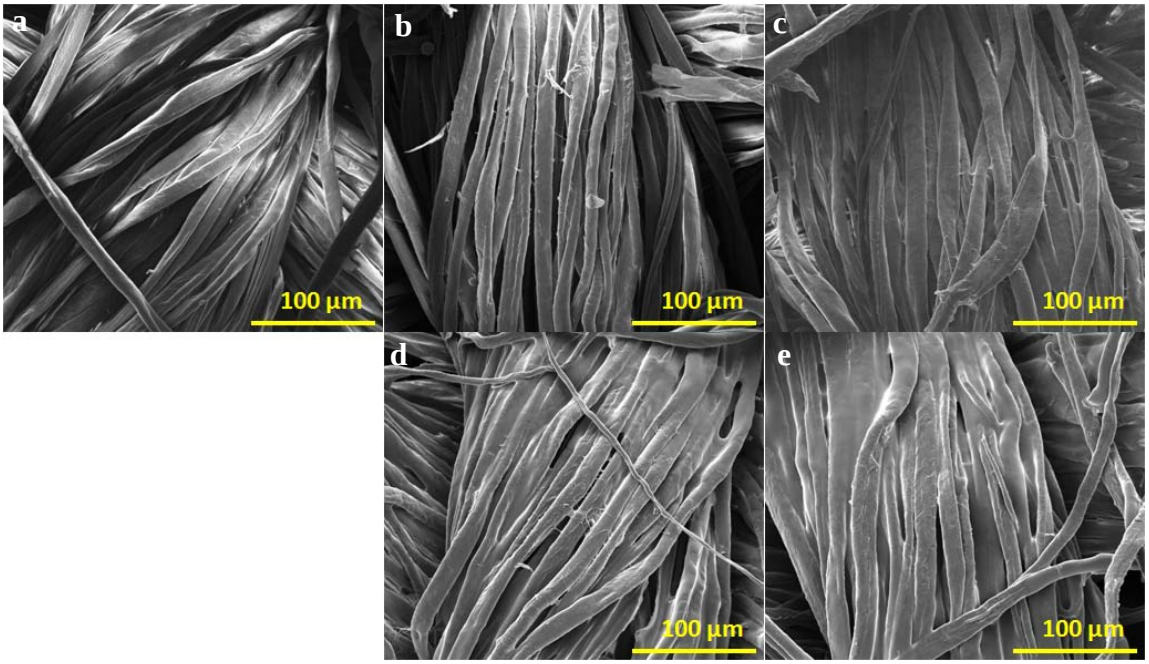

Figure 5.8. SEM images of control fabric (a) and fabric coated with 10 (b), 20 (c), 30 (d), and 40 (e) BL of high concentration PSP before burning.

A closer look at the coated fabrics after burning reveals evidence of intumescent behavior. Four different thicknesses of high PSP-coated fabric have dark char after burning (Fig. 5.5(b)), but starting from 20 BL, the area of lighter color residue increases with the BL number. The dark residues from these coated fabrics are shown in Figure 5.9. Most of the fibers in 10 and 20 BL fabric maintain their integrity after burning, with a few fibers unwound, and the coatings still link fibers together (Fig. 5.9(a) and (b)). When the number of bilayers reaches 30 and 40, the afterburn images look different. There are bubbles coming out of the gap between fibers (Fig. 5.9(c)), which is likely the coating in between the fibers that has swelled and expanded due to the intumescent effect.

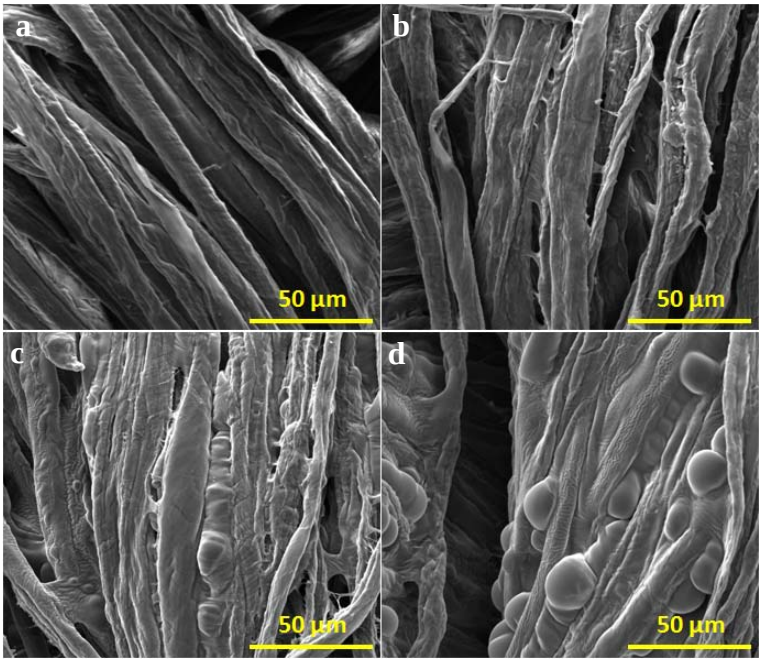

Figure 5.9. SEM images of 10 (a), 20 (b), 30 (c) and 40 (d) BL of high concentration PSP-coated fabric after burning.

The light-color char on 20 to 40 BL fabrics is different than the dark char. The bubbles observed on the fibers of 20 BL coated residues (Fig. 5.10(a)) seem less dense (more transparent) than the bubbles in between fibers shown in Figure 5.9. With 30 BL, the white color char is increased, and it surrounds the shiny char, which is caused by numerous bubbles that flattened out to a glassy, foamed surface on top of the fabric, as shown in Figure 5.10(b). At 40 BL, the residue on the fabric surface after burning is much more dense. This char has both a shiny and a molten part, which is from a relatively thicker layer of foamed surface, as shown in Figure 5.10(c). Underneath the foamed layer, the fibers are still intact and the swelled coating (bubbles) can be clearly seen. These images demonstrate the intumescent action of these thin coatings that protects the fibers by forming a swollen foamed layer.

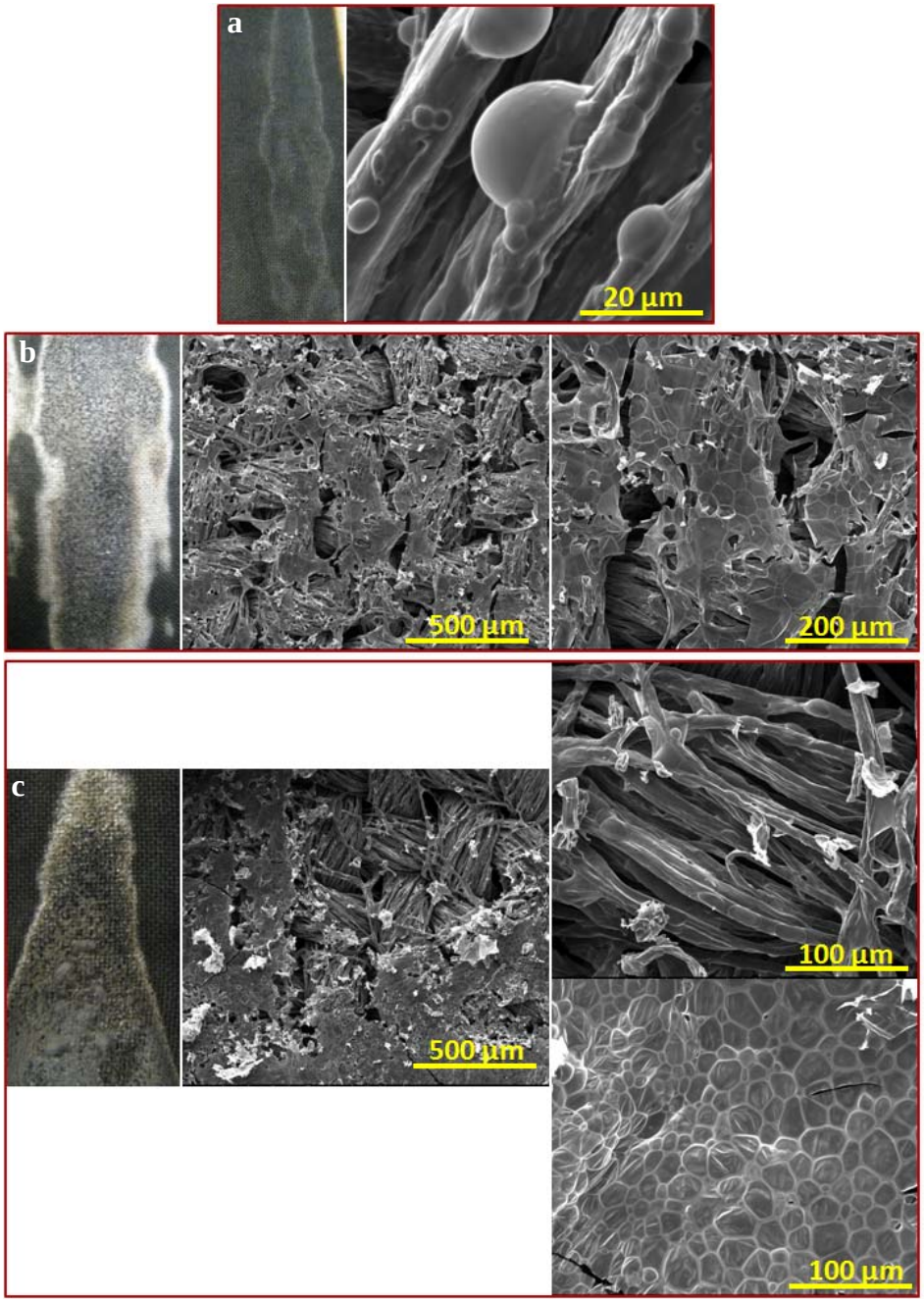

Figure 5.10. Digital and SEM images of 20 (a), 30 (b), and 40 (c) BL high concentration PSP-coated fabric after burning.

5.3.4 Calorimetry of Coated Fabric

Control, 10 and 30 BL of high concentration PSP-coated fabrics were tested with the microscale cone calorimeter at 1 °C/sec heating rate under nitrogen, using method A of ASTM D7309 (pyrolysis under nitrogen). Control and 10BL-coated fabric were tested from 200 to 500 °C and 30BL-coated fabric was tested up to 600 °C. Each sample was run in triplicate to evaluate reproducibility of the flammability measurements. Typical results from the MCC focus on heat release measurements and the results that were recorded from each of the materials are shown in Table 5.4. The main differences are in the total heat release and char yields, but there is some notable reduction in peak HRR as well. Going from the control to the 10BL, the char yield goes up significantly and the total HR drops. Peak HRR drops as well, going from ~250 W/g down to 160-180 W/g. The peak HRR occurs at a lower temperature than that of the control sample, suggesting a decrease in thermal stability for the whole system, which was also observed in TGA testing (see Fig.5.4). This decreased thermal stability is from the low temperature reactions that occur with the intumescent coating to keep heat release low. With the 30 BL sample, a slight increase (not significant) in peak HRR value, and a secondary peak forming at elevated temperature, are observed (Fig. 5.11). It is believed that this second peak is the additional char forming from the extra 20 BL of coating in this sample and this additional char burns off as a small HRR event around 450 °C. This second peak is not seen at all in the 10 BL sample, which suggests 10 BL is more optimal than 30 BL. The lower temperature of the peak HRR event may indicate that the 10 BL sample will

ignite sooner than the control, but that is not clear from the cone calorimeter data. The seemingly decreased thermal stability may not really be a problem in practice.

Table 5.4. Microscale combustion calorimetry measurement for high PSP-coated fabric

Sample	Char % Yield	HRR Peak(s) Value (W/g)	HRR Peak Temp (°C)	Total HR (kJ/g)
Control	9.59±0.61	252.94±8.18	399.68±1.25	11.77±0.23
10BL	33.32±0.13	177.46±9.90	336.87±0.12	4.1±0.1
30BL	32.3±0.34	185.33±6.66, 25.33±0.58	342±1.15, 452±2.65	5.8±0.1

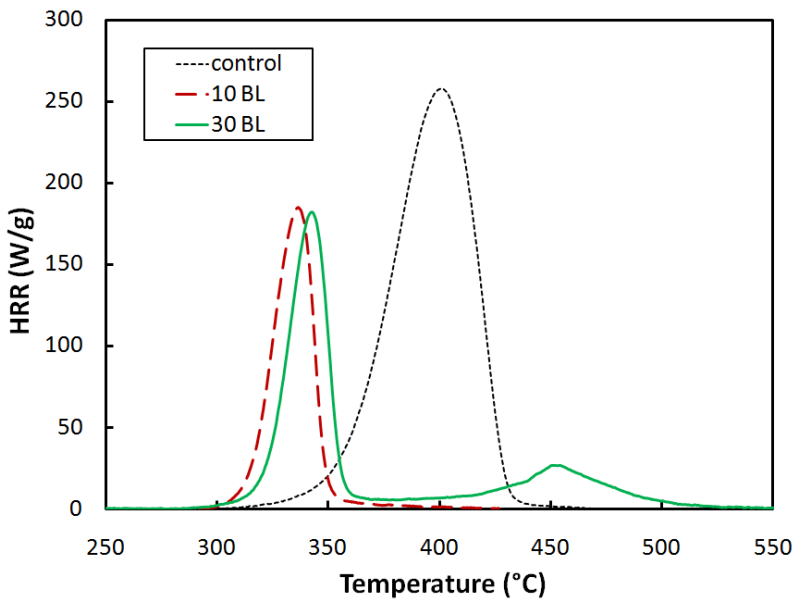

Figure 5.11. Heat release rate as a function of temperature for control, 10 and 30 BL of high concentration PSP-coated cotton fabric.

The same three fabric samples in Table 5.4 were tested with a FTT Dual Cone Calorimeter at a 35 kW/m^2 heat, with an exhaust flow of 24 L/s, using the standardized cone calorimeter procedure (ASTM E 1354). Data collected from all samples is believed to have an error of ±10% and were calculated using a specimen surface area of 88.4 cm^2. All samples were tested in triplicate as per the ASTM E1354 standard. The only data which may have an error greater than 10% would be the mass loss, which is tied to the load cell measurements. The cone calorimeter load cell is really only accurate to the closest gram, so there is considerably more error for samples this light in weight. The summary of data collected from the cone calorimeter tests are summarized in Table 5.5. Overall the samples exhibit low flammability, which is expected with samples containing very little flammable mass (due to their light weight). Coated fabric yielded erratic fire behavior, with some of the samples not igniting at all. When the sample did not ignite, the smoke released increases. This is to be expected, as mass is still pyrolyzing off the surface of the sample, but since it does not burn (no flaming combustion) smoke is generated instead. As can be seen with the data for the samples which showed this type of behavior (10 and 30 BL), if the sample ignites, smoke is low (gases are burned up cleanly) and if it does not ignite, smoke is greater. When smoke is higher, heat release is lower, because the sample did not ignite. Even with the samples that ignited there appears to be some scatter in the data, so additional work may be needed to determine if the fabric is homogeneously coated with the LbL system, or if these materials just show erratic ignition behavior at this heat flux.

Table 5.5. Cone calorimeter data of control, 10 and 30 BL of high PSP-coated fabric

Sample	Time to ignition (s)	Peak HRR (kW/m^2)	Time to Peak HRR (s)	Average HRR (kW/m^2)	Weight % Loss (%)	THR (MJ/m^2)	Total smoke Release (m^2/m^2)
Control-1	44	61	62	29	76.9	1.4	5
Control-2	48	74	64	40	76.9	1.5	2
Control-3	42	66	60	33	76.9	1.3	2
Average	45	67	62	34	76.9	1.4	3
10BL-1	6	39	19	7	22.9	0.4	2
10BL-2	no ign.	10	76	5	61.5	0.6	23
10BL-3	45	29	55	14	38.8	0.2	3
Average	n/a	26	50	9	41.1	0.4	9
30BL-1	9	32	22	8	33.1	0.4	4
30BL-2	no ign.	11	99	5	46.4	0.6	25
30BL-3	42	21	52	12	33.1	0.2	3
Average	n/a	21	58	8	37.5	0.4	11

Flammability behavior for the control fabric was relatively reproducible (Fig. 5.12(a)). All three samples had a delayed ignition and gave off a small blue flame with yellow tips. Some burning embers were noted at the edges of the samples right before the sample extinguished. The final chars were very fragile and mostly burned through, and the char did not stick to the aluminum foil. Unlike the control samples, all three 10 BL samples burned differently. This can be seen in the erratic heat release data (Fig.5.12(b)). Despite some anomalous results, the HRR is quite low for this fabric, and so some of the erratic data can be attributed to instrument noise due to the HRR being near the detection limits of the instrument. The observed fire behaviors are different for each of the samples, with the first sample igniting quickly and then extinguishing quickly. The second sample did not ignite at all, but a small flash was observed, and white smoke was given off from the sample. When the fabric stopped smoking, the test

was stopped (~120 seconds). As for the third sample, it was slow to ignite, and then burned with a small light blue flame before going out quickly. All of the final chars were intact, but some soot stuck to the aluminum foil. 30 BL samples also showed erratic burning behavior and HRR, and again since the HRR was low, it is within the noise of the instrument (Fig. 5.12(c)). The first sample ignited quickly with a light blue flame that had yellow tips and extinguished quickly as well. A second sample did not ignite at all, nor was any flashing observed. The third sample was slow to ignite, then burned with a light blue flame and extinguished quite quickly after the delayed ignition. All of the samples showed significant levels of durable char formation.

It is clear that the use of intumescent LbL coatings greatly lowers the flammability of cotton fabric, but it is not clear what the coatings achieve in regard to ignition behavior. As was shown here, the use of LbL coatings gives very erratic ignition (or in some cases, no ignition at all) under a 35 kW/m^2 heat flux. It is possible that the heat flux was not hot enough to sustain ignition or the LbL coating is not uniform on the fabric surface. Even with this erratic ignition behavior, when the samples ignite, the heat release is not very high. These results demonstrate that this coating is providing a flame retardant effect and yielding durable char structures that cannot easily burn through or disintegrate upon burning.

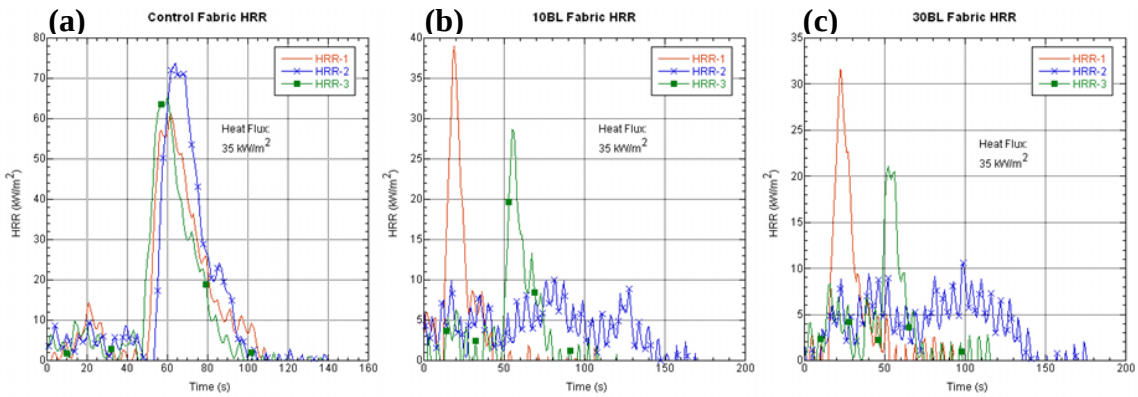

Figure 5.12. Heat release rate as a function of time of control (a), 10 BL (b), and 30 BL (c) of high PSP-coated fabrics.

5.4 Conclusions

Layer-by-layer assemblies of PAAm and PSP were successfully grown on various substrates, including cotton fabric. Growth of these films can be tuned by varying the concentration of the polyelectrolytes. Adding 10 BL of 1 wt%BPEI pH 10/1 wt% MMT underneath did not change the growth trends. By applying these thin coatings on fabric, afterglow is eliminated and after-flame time is reduced in flame testing. Fabric coated with 0.5 wt% PAAm pH 7/1 wt% PSP pH 7 left areas of unburned fabric after vertical flame testing. Weave structure and fiber integrity of fabric after burning are well preserved. SEM imaging revealed a cellular, foamed layer on top of the coated fabric, which is from the intumescent behavior. When the amount of coating reached a critical point (30 BL of PAAm/PSP), the flame extinguished on the fabric during the flame testing. From microscale calorimetry data, peak heat release rate and total heat release of fabric shows a 30 % and 65 % reduction compared to the control fabric, with only 4.7

wt% coating added to fabric. This work demonstrates the first intumescent layer-by-layer coating and the result is better than previously studied clay-based assemblies. More work is needed to produce coatings that completely prevent ignition and also to make these films more mechanically flexible.

CHAPTER VI

CONCLUSIONS AND FUTURE WORK

The ultimate goal of this dissertation research was to create a nanocoating system that would be compatible with any type of substrate (with proper surface pre-treatment) and extinguish flame on the coated substrate. By incorporating flame retardant materials into layer-by-layer assemblies, anti-flammable nanocoatings were deposited on complex substrates, such as cotton fabric, to impart anti-flammability. This work lays the foundation for using these types of thin film assemblies to make a variety of complex substrates (foam, fabric, etc.) flame resistant.

6.1 Polyelectrolyte/Clay Thin Film Assemblies

Thin films of BPEI and clay (Laponite and MMT) were prepared using layer-by-layer assembly. Film thickness and composition were tailored by altering the pH and concentration of the deposition mixtures. BPEI at pH 10 produced the thickest film, while 1 wt% MMT give the highest clay loading. In all films, the clay platelets are uniformly deposited and look analogous to a cobblestone path, on their surface (Fig. 3.5), and a nano brick wall, from a highly magnified side view (Fig. 3.14). Several 40 BL Laponite films, with thicknesses of 100 nm or more, exhibit elastic moduli ranging from 7 to 10 GPa and hardness around 0.5 GPa, suggesting that these transparent thin films could be useful as hard coatings for plastic substrates. When these coatings are deposited on cotton fabric, each individual fiber is uniformly coated and the fabric has

significantly more char left after burning than the uncoated fabric. Postburn residues of coated fabric reveal that the weave structure and fiber shape were preserved. The BPEI pH 7/1 wt% MMT recipe was most effective. Microscale combustion calorimeter testing showed that all coated fabrics exhibited reduced total heat release relative to an uncoated control. Fiber count and strength of uncoated and coated fabric are similar. These results demonstrate that LbL assembly is a relatively simple method for imparting flame-retardant behavior to cotton fabric.

6.2 POSS-Based Multilayer Thin Film Assemblies

Fully siliceous layer-by-layer assembled thin films, using polyhedral oligomeric silsesquioxanes (POSS) as building blocks, were successfully deposited on various substrates, including cotton fabric. Water-soluble OctaAmmonium POSS ((+)POSS) and OctaTMA POSS ((-)POSS) were used as cationic and anionic components for thin film deposition from water. Aminopropyl silsesquioxane oligomer (AP) was also used as an alternative cationic species. The thickness of the AP/(–)POSS and (+)POSS/(–)POSS films are shown to increase linearly with bilayers deposited. Thermogravimetric analysis (TGA), vertical flame testing (VFT), microscale combustion calorimetry (MCC) and pill testing were performed on cotton fabric coated with 5 – 20 bilayers of a given recipe. All coated fabrics showed improved preservation (*i.e.*, greater residue following heating to 600 °C) and resistance to degradation from direct flame. With less than 8 wt% added to the total fabric weight, more than 12 wt% char remained following MCC for the cotton coated with 20 bilayers (+)POSS/(–)POSS. Furthermore, afterglow time was reduced

and the fabric weave structure and shape of the individual fibers were highly preserved following VFT. It is expected that this environmentally-friendly coating could be used to impart flame retardant behavior to a variety of fabrics, for protective clothing and soft furnishings, and other complex substrates like foam.

6.3 Intumescent Layer-by-Layer Assemblies

Intumescent assemblies were successfully created with PAAm and PSP as the positively- and negatively-charged electrolytes, respectively. These films can be tailored by changing the concentration of the polyelectrolytes in the aqueous deposition solutions. Application of this system to cotton lowers the thermal stability of the fabric, but leads to a significant amount of char left at the end of the TGA under an air atmosphere. After-flame time was reduced and no afterglow was observed for all coated fabrics during vertical flame testing. Fabric coated with 0.5 wt% PAAm pH 7/1 wt% PSP pH 7 left unburned fabric after burning, which increased with increasing the number of PAAm/PSP bilayers deposited. Weave structure and fiber integrity were well preserved following VFT, and foamed layers (resulting from intumescent effect during heating) were observed under SEM imaging. From MCC data, peak heat release rate and total heat release were reduced by 30 % and 65 %, respectively, compared to the control fabric. This work demonstrates the first intumescent layer-by-layer coating on fabric and further research is expected to produce nanocoatings that completely prevent ignition of fabric exposed to fire.

6.4 Future Research Plan

From the results in Chapter V, it is known that increasing the concentration of deposition solutions will increase the coating weight on the substrate. Greater coating weight has typically led to a significant amount of char formation. Phosphorus-based materials used in LbL assembly can chemically react with cellulose and potentially result in a self-extinguishing treatment. There is still room to improve this current intumescent system by exploring other ingredients. Durability of these flame retardant coatings on fabric is another issue to be investigated. Additionally, this technique will eventually need to scale up to become commercially viable. These three areas of future work are described in more detail below.

6.4.1 Improved, Softer Intumescent Coatings

The easiest way to improve intumescent nanocoating effectiveness would be to increase the concentration of PAAm and PSP solutions (1 and 2 wt%, or 2 and 4 wt%, respectively, and so on), which will be able to decrease the BL number and perhaps the stiffness of the fabric as well. Direct contact between phosphate and cellulose could be achieved by immersing cotton fabric into deionized water with pH lower than 2 (the isoelectric point of cellulose is around 2.5),[235] followed by a phosphate solution as the first deposition. Polyvinyl alcohol (PVOH) is a good candidate for an additional carbon source that contains hydroxyls, which will be phosphorylated as well and increase the intumescent behavior. PVOH could be incorporated as part of a trilayer, PSP/PVOH/PAAm (or in reversed order, depending on the surface charge of the

substrate), with electrostatic attraction and hydrogen bonding as the driving force.[249] Other small molecules, such as sugar alcohols (*e.g.*, sorbitol and mannitol), and pentaerythritol (as shown in Fig. 6.1 and Table 6.1), are also hydroxyl-rich. These small –OH rich molecules can substitute for, or be used together with, PVOH. It has been shown that small molecules can be incorporated into LbL assemblies by adding them into the polyelectrolyte mixtures.[34] BPEI can substitute for PAAm, as they are both N–rich polymers. Additionally, diammonium phosphate can be added into PVOH to substitute for the PSP layer (or enhance it). Other acid sources can also be examined, for example, water-soluble polyborate.[250-251]

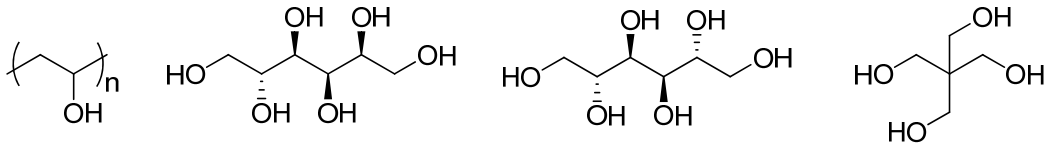

PVOH Sorbitol Mannitol Pentaerythritol

Figure 6.1. Structures of hydroxyl-rich molecules.

Table 6.1. Potential ingredients for intumescent systems[252]

(a) Acid source	(b) Carbonization agent
Inorganic acid source	Starch
Phosphoric	Dextrins
Sulfuric	Sorbitol, mannitol
Boric	Pentaerythritol, monomer, dimer, trimer
Ammonium salts	Phenol-formaledhyde resins
Phosphates, polyphosphates	Methylol melamine
Borates, polyborates	Char former polymers (PA-6, PA-6/clay nanocomposite PU, PC,...)
Sulfates	
Halides	
Phosphates of amine or amide	**(c) Blowing agents**
Products of reaction of urea or guanidyl urea with phosphoric acids	Urea
Melamine phosphate	Urea-formaldehyde resins
Prodcut of reaction of ammonia with P_2O_5	Dicyandiamide
	Melamine
Organophosphorus compounds	
Tricresyl phosphate	
Alkyl phosphates	
Haloalkyl phosphates	

Adding clay layers underneath the intumescent layers resulted in smoldering rather than burning in HFT (Section 5.3.3). Building upon this idea, further synergy may be achieved by putting clay layers amongst the intumescent layers. For example, adding 1 BL of MMT/PAAm after every 5 trilayers (TL) of PSP/PVOH/PAAm could really improve efficacy. There are a lot of variations and combinations that are possible for these intumescent coatings. An additional advantage of using clay is that the fabric will likely be softer due to some disruption of the relatively stiff PAAm/PSP system. Some replacement of PAAm and /or PSP, with small N-rich and/or P-rich molecules, could also improve coating softness/flexibility.

6.4.2 Improvement of Nanocoating Durability

When coating fabric, especially for clothing, washability becomes a significant issue (*i.e.*, the coating must survive repeated washings). Crosslinking of these polyelectrolyte multilayers, following deposition, is the most straightforward method to make these nanocoatings more robust. Crosslinking could happen between PSP and cellulose by curing the fabric at a temperature above 130 °C, which will drive off water. This phosphorylation can also happen between phosphates and other –OH rich molecules. A crosslinking agent, such as glutaraldehyde, can react with amines from PAAm to from N=C bonds (Schiff base),[253] and with hydroxide to form acetal bridges (Fig. 6.2).[165] Different crosslinking methods would be evaluated when the chemistry of coating system changes. Testing the durability of these flame retardant coatings is accomplished through subjecting treated fabric to numerous laundering washing/drying cycles, according to American Association of Textile Chemists and Colorists (AATCC) Method 124.[254]

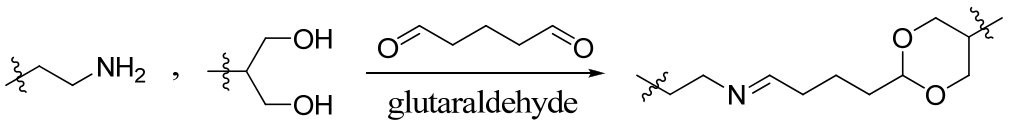

Figure 6.2. Covalent bonds formed between glutaraldehyde and amine or hydroxide groups.

6.4.3 Commercial Scale Production

The LbL assembly technique can be easily scaled up for industrial purposes. Ali Mehrabi and Jay Akhave, from Avery Dennison (Pasadena, CA), described a continuous process for manufacturing electrostatically self-assembled polymer coatings (U.S. Patent Application 2004/0157047 A1, abandoned). A schematic of this roll-to-roll process and a pilot unit are shown in Figure 6.3. A roll of fabric could be used in this type of process, much like the plastic film shown here, but rollers could be used to squeeze out the water instead of using air dryers. This immersion process can be replaced by spraying,[255] which could speed up this process and improve uniformity of the coating. Spraying may be the more commercially viable option for high speed deposition. Removal of the rinsing and/or drying steps may also be possible to further simplify processing and reduce cost. The whole area of large-scale processing of LbL coatings is a rich area waiting to be studied.

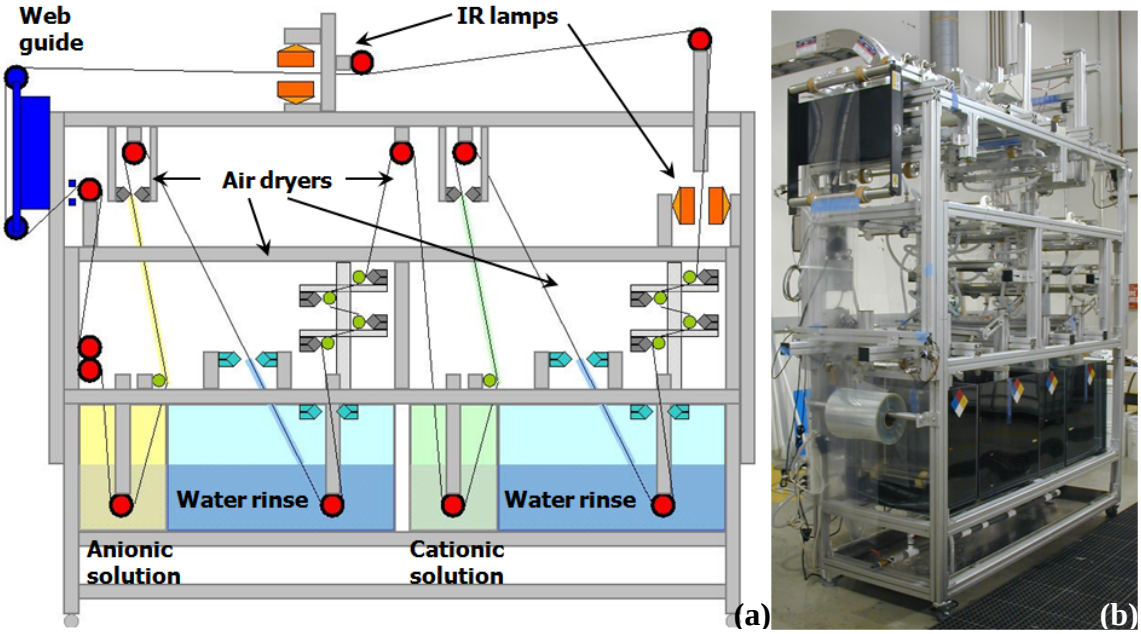

Figure 6.3. Schematic continuous roll-to-roll process (a) and an actual pilot scale production unit for continuous layer-by-layer assembly (b).

REFERENCES AND NOTES

1. Karter, M. J., Jr. NFPA Reports: U.S. Fire Loss for 2009. *NFPA Journal*® **2010**, September/October.

2. Levchik, S. V., Introduction to Flame Retardancy and Polymer Flammability. In *Flame Retardant Polymer Nanocomposites*, Morgan, A. B.; Wilkie, C. A., Eds. John Wiley & Sons: Hoboken, NJ, 2007; pp 1-30.

3. Nelson, G. L.; Wilkie, C. A., Fire Retardancy in 2005. In *Fire and Polymer IV: Materials and Concepts for Hazard Prevention*, Wilkie, C. A.; Nelson, G. L., Eds. ACS Symposium Series 922; American Chemical Society: Washington, DC, 2006; pp 1-5.

4. Wang, J. Q.; Chow, W. K. A Brief Review on Fire Retardants for Polymeric Foams. *J. Appl. Polym. Sci.* **2005**, *97*, 366-376.

5. Camino, G.; Costa, L.; Dicortemiglia, M. P. L. Overview of Fire Retardant Mechanisms. *Polym. Degrad. Stab.* **1991**, *33*, 131-154.

6. Guo, G.; Park, C. B.; Lee, Y. H.; Kim, Y. S.; Sain, M. Flame Retarding Effects of Nanoclay on Wood-Fiber Composites. *Polym. Eng. Sci.* **2007**, *47*, 330-336.

7. Gilman, J. W.; Harris, R. H.; Shields, J. R.; Kashiwagi, T.; Morgan, A. B. A Study of the Flammability Reduction Mechanism of Polystyrene-Layered Silicate Nanocomposite: Layered Silicate Reinforced Carbonaceous Char. *Polym. Adv. Technol.* **2006**, *17*, 263-271.

8. Zhu, J.; Start, P.; Mauritz, K. A.; Wilkie, C. A. Thermal Stability and Flame Retardancy of Poly(Methyl Methacrylate)-Clay Nanocomposites. *Polym. Degrad. Stab.* **2002**, *77*, 253-258.

9. Peeterbroeck, S.; Laoutid, F.; Swoboda, B.; Lopez-Cuesta, J. M.; Moreau, N.; Nagy, J. B.; Alexandre, M.; Dubois, P. How Carbon Nanotube Crushing Can Improve Flame Retardant Behaviour in Polymer Nanocomposites? *Macromol. Rapid Commun.* **2007**, *28*, 260-264.

10. Schartel, B.; Potschke, P.; Knoll, U.; Abdel-Goad, M. Fire Behaviour of Polyamide 6/Multiwall Carbon Nanotube Nanocomposites. *Eur. Polym. J.* **2005**, *41*, 1061-1070.

11. Kashiwagi, T.; Du, F. M.; Douglas, J. F.; Winey, K. I.; Harris, R. H.; Shields, J. R. Nanoparticle Networks Reduce the Flammability of Polymer Nanocomposites. *Nat. Mater.* **2005**, *4*, 928-933.

12. Ray, S. S.; Okamoto, M. Polymer/Layered Silicate Nanocomposites: A Review from Preparation to Processing. *Prog. Polym. Sci.* **2003**, *28*, 1539-1641.

13. Zanetti, M.; Kashiwagi, T.; Falqui, L.; Camino, G. Cone Calorimeter Combustion and Gasification Studies of Polymer Layered Silicate Nanocomposites. *Chem. Mater.* **2002**, *14*, 881-887.

14. Ariga, K.; Hill, J. P.; Ji, Q. Layer-by-Layer Assembly as a Versatile Bottom-up Nanofabrication Technique for Exploratory Research and Realistic Application. *Phys. Chem. Chem. Phys.* **2007**, *9*, 2319-2340.

15. Decher, G., Polyelectrolyte Multilayers, an Overview. In *Multilayer Thin Films: Sequential Assembly of Nanocomposite Materials*, Decher, G.; Schlenoff, J. B., Eds. Wiley-VCH: Weinheim, Germany, 2003; pp 1-46.

16. Bertrand, P.; Jonas, A.; Laschewsky, A.; Legras, R. Ultrathin Polymer Coatings by Complexation of Polyelectrolytes at Interfaces: Suitable Materials, Structure and Properties. *Macromol. Rapid Commun.* **2000**, *21*, 319-348.

17. Podsiadlo, P.; Shim, B. S.; Kotov, N. A. Polymer/Clay and Polymer/Carbon Nanotube Hybrid Organic-Inorganic Multilayered Composites Made by Sequential Layering of Nanometer Scale Films. *Coord. Chem. Rev.* **2009**, *253*, 2835-2851.

18. Sun, J. Q.; Wu, T.; Liu, F.; Wang, Z. Q.; Zhang, X.; Shen, J. C. Covalently Attached Multilayer Assemblies by Sequential Adsorption of Polycationic Diazo-Resins and Polyanionic Poly(Acrylic Acid). *Langmuir* **2000**, *16*, 4620-4624.

19. Bergbreiter, D. E.; Chance, B. S. "Click"-Based Covalent Layer-by-Layer Assembly on Polyethylene Using Water-Soluble Polymeric Reagents. *Macromolecules* **2007**, *40*, 5337-5343.

20. Bergbreiter, D. E.; Tao, G. L.; Franchina, J. G.; Sussman, L. Polyvalent Hydrogen-Bonding Functionalization of Ultrathin Hyperbranched Films on Polyethylene and Gold. *Macromolecules* **2001**, *34*, 3018-3023.

21. Lv, F.; Peng, Z. H.; Zhang, L. L.; Yao, L. S.; Liu, Y.; Xuan, L. Photoalignment of Liquid Crystals in a Hydrogen-Bonding-Directed Layer-by-Layer Ultrathin Film. *Liq. Cryst.* **2009**, *36*, 43-51.

22. Krogman, K. C.; Lowery, J. L.; Zacharia, N. S.; Rutledge, G. C.; Hammond, P. T. Spraying Asymmetry into Functional Membranes Layer-by-Layer. *Nat. Mater.* **2009**, *8*, 512-518.

23. Lee, Y. M.; Park, D. K.; Choe, W. S.; Cho, S. M.; Han, G. Y.; Park, J.; Yoo, P. J. Spin-Assembled Layer-by-Layer Films of Weakly Charged Polyelectrolyte Multilayer. *J. Nanosci. Nanotechnol.* **2009**, *9*, 7467-7472.

24. Song, S. L.; Hu, N. F. Ph-Controllable Bioelectrocatalysis Based on "On-Off" Switching Redox Property of Electroactive Probes for Spin-Assembled Layer-by-Layer Films Containing Branched Poly(Ethyleneimine). *J. Phys. Chem. B* **2010**, *114*, 3648-3654.

25. Shiratori, S. S.; Rubner, M. F. pH-Dependent Thickness Behavior of Sequentially Adsorbed Layers of Weak Polyelectrolytes. *Macromolecules* **2000**, *33*, 4213-4219.

26. Bieker, P.; Schonhoff, M. Linear and Exponential Growth Regimes of Multi Layers of Weak Polyelectrolytes in Dependence on pH. *Macromolecules* **2010**, *43*, 5052-5059.

27. Wong, J. E.; Diez-Pascual, A. M.; Richtering, W. Layer-by-Layer Assembly of Polyelectrolyte Multilayers on Thermoresponsive P(NIPAM-co-MAA) Microgel: Effect of Ionic Strength and Molecular Weight. *Macromolecules* **2009**, *42*, 1229-1238.

28. Sui, Z. J.; Salloum, D.; Schlenoff, J. B. Effect of Molecular Weight on the Construction of Polyelectrolyte Multilayers: Stripping Versus Sticking. *Langmuir* **2003**, *19*, 2491-2495.

29. Tan, H. L.; McMurdo, M. J.; Pan, G. Q.; Van Patten, P. G. Temperature Dependence of Polyelectrolyte Multilayer Assembly. *Langmuir* **2003**, *19*, 9311-9314.

30. Chang, L.; Kong, X.; Wang, F.; Wang, L.; Shen, J. Layer-by-Layer Assembly of Poly(N-Acryloyl-N'-Propylpiperazine) and Poly (Acrylic Acid): Effect of pH and Temperature. *Thin Solid Films* **2008**, *516*, 2125-2129.

31. Yu, H. H.; Cao, T.; Zhou, L. D.; Gu, E. D.; Yu, D. S.; Jiang, D. S. Layer-by-Layer Assembly and Humidity Sensitive Behavior of Poly(Ethyleneimine)/Multiwall Carbon Nanotube Composite Films. *Sens. Actuators, B* **2006**, *119*, 512-515.

32. Aoki, P. H. B.; Volpati, D.; Riul, A.; Caetano, W.; Constantino, C. J. L. Layer-by-Layer Technique as a New Approach to Produce Nanostructured Films Containing Phospholipids as Transducers in Sensing Applications. *Langmuir* **2009**, *25*, 2331-2338.

33. Cui, H. F.; Cui, Y. H.; Sun, Y. L.; Zhang, K.; Zhang, W. D. Enhancement of Dopamine Sensing by Layer-by-Layer Assembly of PVI-DMEOS and Nafion on Carbon Nanotubes. *Nanotechnology* **2010**, *21*, 5601-5608.

34. Dvoracek, C. M.; Sukhonosova, G.; Benedik, M. J.; Grunlan, J. C. Antimicrobial Behavior of Polyelectrolyte-Surfactant Thin Film Assemblies. *Langmuir* **2009**, *25*, 10322-10328.

35. He, Q.; Cui, Y.; Li, J. B. Molecular Assembly and Application of Biomimetic Microcapsules. *Chem. Soc. Rev.* **2009**, *38*, 2292-2303.

36. Boudou, T.; Crouzier, T.; Ren, K. F.; Blin, G.; Picart, C. Multiple Functionalities of Polyelectrolyte Multilayer Films: New Biomedical Applications. *Adv. Mater.* **2010**, *22*, 441-467.

37. Chien, H. W.; Chang, T. Y.; Tsai, W. B. Spatial Control of Cellular Adhesion Using Photo-Crosslinked Micropatterned Polyelectrolyte Multilayer Films. *Biomaterials* **2009**, *30*, 2209-2218.

38. Yang, M.; Lu, S. F.; Lu, J. L.; Jiang, S. P.; Xiang, Y. Layer-by-Layer Self-Assembly of PDDA/PWA-Nafion Composite Membranes for Direct Methanol Fuel Cells. *Chem. Commun.* **2010**, *46*, 1434-1436.

39. Wang, F.; Alazemi, M.; Dutta, I.; Blunk, R. H.; P., A. A. Layer-by-Layer Assembly of Hybrid Nanoparticle Coatings for Proton Exchange Membrane Fuel Cell Bipolar Plates. *J. Power Sources* **2010**, *195*, 7054-7060.

40. Zhao, Y.; Tang, Y. W.; Wang, X. G.; Lin, T. Superhydrophobic Cotton Fabric Fabricated by Electrostatic Assembly of Silica Nanoparticles and Its Remarkable Buoyancy. *Appl. Surf. Sci.* **2010**, *256*, 6736-6742.

41. Ashcraft, J. N.; Argun, A. A.; Hammond, P. T. Structure-Property Studies of Highly Conductive Layer-by-Layer Assembled Membranes for Fuel Cell PEM Applications. *J. Mater. Chem.* **2010**, *20*, 6250-6257.

42. Jang, W. S.; Rawson, I.; Grunlan, J. C. Layer-by-Layer Assembly of Thin Film Oxygen Barrier. *Thin Solid Films* **2008**, *516*, 4819-4825.

43. Priolo, M. A.; Gamboa, D.; Holder, K. M.; Grunlan, J. C. Super Gas Barrier of Transparent Polymer-Clay Multi Layer Ultrathin Films. *Nano Lett.* **2010**, *10*, 4970-4974.

44. Wakelyn, P. J.; Bertoniere, N. R.; French, A. D.; Thibodeaux, D., *Cotton Fiber Chemistry and Technology*. CRC Press Taylor and Francis Group: Boca Raton, 2007.

45. Oulton, D. P., Fire-Retardant Textiles. In *Chemistry of the Textiles Industry*, Carr, C. M., Ed. Springer-Verlag: New York, 1995; pp 103-124.

46. Price, D.; Anthony, G.; Carty, P., Introduction: Polymer Combustion, Condensed Phase Pyrolysis and Smoke Formation. In *Fire Retardnat Materials*, Horrocks, A. R.; Price, D., Eds. Woodhead Publishing: Cambridge, 2001, pp 1-30.

47. Troitzsch, J., *International Plastics Flammability Handbook, Principles - Regulations -Testing and Approval.* 2nd ed.; Hanser Publications: Munich, 1990.

48. van Krevelen, D. W. Some Basic Aspects of Flame Resistance of Polymeric Materials. *Polymer* **1975**, *16*, 615-620.

49. van Krevelen, D. W.; Wise, H.; Millier, J., *Properties of Polymers*. Elsevier Scientific Publishing: New York, 1976.

50. Lewin, M.; Weil, E. D., Mechanisms and Modes of Action in Flame Retardancy of Polymers. In *Fire Retardant Materials*, Horrocks, A. R.; Price, D., Eds. Woodhead Publishing: Cambridge, 2001; pp 31-68.

51. Schmidt, W. G., Flame-Retardant Additives in Plastics and Recent Related Patents. *Inst. Plastics Ind., Trans.* **1965**, *12*, 247-255.

52. Georlette, P.; Simons, J., Halogen-Containing Fire-Retardant Compounds. In *Fire Retardancy of Polymeric Materials*, Grand, A. F.; Wilkie, C. A., Eds. Marcel Dekker: New York, 2000; pp 245-284.

53. Bocchini, S.; Camino, G., Halogen-Containing Flame Retardants. In *Fire Retardancy of Polymeric Materials*, 2nd ed.; Wilkie, C. A.; Morgan, A. B., Eds. CRC Press Taylor & Francis Group: Boca Raton, 2010; pp 75-106.

54. de Wit, C. A. An Overview of Brominated Flame Retardants in the Environment. *Chemosphere* **2002**, *46*, 583-624.

55. Lewin, M., Physical and Chemical Mechanisms of Flame Retarding of Polymers. In *Fire Retardancy of Polymers: The Use of Intumescence*, Le Bras, M.; Camino, G.; Bourbigot, S.; Delobel, R., Eds. Royal Society of Chemistry: London, 1998; pp 3-32.

56. Levchik, S. V.; Wilkie, C. A., Char Formation. In *Fire Retardancy of Polymeric Materials*, Grand, A. F.; Wilkie, C. A., Eds. Marcel Dekker: New York, 2000, pp 171-216.

57. Green, J., Phosphorus-Containing Flame Retardants. In *Fire Retardancy of Polymeric Materials*, Grand, A. F.; Wilkie, C. A., Eds. Marcel Dekker: New York, 2000; pp 147-170.

58. Green, J. A Review of Phosphorus-Containing Flame Retardants. *J. Fire Sci.* **1996**, *14*, 353-366.

59. Annakutty, K. S.; Kishore, K. Synthesis and Properties of Flame-Retardant Polyphosphate Esters - A Review. *J. Sci. Ind. Res.* **1989**, *48*, 479-493.

60. Aseeva, R. M.; Zaikov, G. E., *Combustion of Polymer Materials*. Carl Hanser Verlag: Munich, 1986.

61. Kandola, B. K.; Horrocks, A. R.; Price, D.; Coleman, G. V. Flame-Retardant Treatments of Cellulose and Their Influence on the Mechanism of Cellulose Pyrolysis. *J. Macromol. Sci., Rev. Macromol. Chem. Phys.* **1996**, *C36*, 721-794.

62. Isaacs, P.; Lewin, M.; Sello, S. B.; Stevens, C. V. Flame-Resistant Cellulose Esters. *Text. Res. J.* **1974**, *44*, 700-707.

63. Ermolenko, I. N.; Lyubliner, I. P.; Gulko, N. V., *Chemically Modified Carbon Fibers*. VCH Publishers: New York, 1990.

64. Babushok, V.; Tsang, W. Inhibitor Rankings for Alkane Combustion. *Combust. Flame* **2000**, *123*, 488-506.

65. Bourbigot, S.; Duquesne, S., Intumescence and Nanocomposites: A Novel Route for Flame-Retarding Polymeric Materials. In *Flame Retardant Polymer Nanocomposites*, Morgan, A. B.; Wilkie, C. A., Eds. John Wiley & Sons: Hoboken, 2007; pp 131-162.

66. Camino, G.; Delobel, R., Intumescence. In *Fire Retardancy of Polymeric Materials*, Grand, A.; Wilkie, C. A., Eds. Marcel Dekker: New York, 2000; pp 217-244.

67. Reeves, W. A.; Perkins, R. M.; Piccolo, B.; Drake, G. L. Some Chemical and Physical Factors Influencing Flame Retardancy. *Text. Res. J.* **1970**, *40*, 223-231.

68. Lewin, M.; Isaacs, P.; Stevens, C.; Sello, S. B. Flame Retardant Modification of Cellulose. *Textilveredlung* **1973**, *8*, 158-161.

69. Langley, J. T.; Drews, M. J.; Barker, R. H. Pyrolysis and Combustion of Cellulose. 7. Thermal-Analysis of the Phosphorylation of Cellulose and Model Carbohydrates During Pyrolysis in the Presence of Aromatic Phosphates and Phosphoramides. *J. Appl. Polym. Sci.* **1980**, *25*, 243-262.

70. Zhu, W. M.; Weil, E. D.; Mukhopadhyay, S. Intumescent Flame-Retardant System of Phosphates and 5,5,5'5',5",5"-Hexamethyltris(1,3,2-Dioxaphosphorinanemethan)Amine 2,2',2"-Trioxide for Polyolefins. *J. Appl. Polym. Sci.* **1996**, *62*, 2267-2280.

71. Hendrix, J. E.; Barker, R. H.; Drake, G. L. Pyrolysis and Combustion of Cellulose. 2. Thermal-Analysis of Mixtures of Methyl Alpha-D-Glucopyranoside and Levoglucosan with Model Phosphate Flame Retardants. *J. Appl. Polym. Sci.* **1972**, *16*, 41-59.

72. Walter, M. D.; Wajer, M. T., Magnesium Hydroxide: A Viable Alternative in Flame Retardants. In *Functional Fillers Conference*, Amsterdam, 1996.

73. Hornsby, P. R. The Application of Hydrated Mineral Fillers as Fire Retardant and Smoke Suppressing Additives for Polymers. *Macromol. Symp.* **1996**, *108*, 203-219.

74. Horn, W. E., Jr., Inorganic Hydroxides and Hydroxycarbonates: Their Function and Use as Flame Retardant Additives. In *Fire Retardancy of Polymeric Materials*, Grand, A. F.; Wilkie, C. A., Eds. Marcel Dekker: New York, 2000; pp 285-352.

75. Blumstein, A. Polymerization of Absorbed Monolayers. I. Preparation of the Caly-Polymer Complex. *J. Polym. Sci. Part A.* **1963**, *3*, 2653-2664.

76. Blumstein, A. Polymerization of Absorbed Monolayers. II. Thermal Degradation of the Inserted Polymer. *J. Polym. Sci. Part A.* **1963**, *3*, 2655-2672.

77. Wilkie, C. A.; Morgan, A. B., Nanocomposite I: Current Developments in Nanocomposites as Novel Flame Retardants. In *Advances in Fire Retardant Materials*, Horrocks, A. R.; Price, D., Eds. Woodhead Publishing: Cambridge, 2008; pp 95-123.

78. Jiang, D. D., Polymer Nanocomposites. In *Fire Retardancy of Polymeric Materials*, 2nd ed.; Wilkie, C. A.; Morgan, A. B., Eds. CRC Press Taylor & Francis Group: Boca Raton, 2010; pp 261-300.

79. Zammarano, M.; Franceschi, M.; Bellayer, S.; Gilman, J. W.; Meriani, S. Preparation and Flame Resistance Properties of Revolutionary Self-Extinguishing Epoxy Nanocomposites Based on Layered Double Hydroxides. *Polymer* **2005**, *46*, 9314-9328.

80. Sue, H. J.; Gam, K. T.; Bestaoui, N.; Spurr, N.; Clearfield, A. Epoxy Nanocomposites Based on the Synthetic Alpha-Zirconium Phosphate Layer Structure. *Chem. Mater.* **2004**, *16*, 242-249.

81. Sukpirom, N.; Lerner, M. M. Preparation of Organic-Inorganic Nanocomposites with a Layered Titanate. *Chem. Mater.* **2001**, *13*, 2179-2185.

82. Gilman, J. W. Flammability and Thermal Stability Studies of Polymer Layered-Silicate (Clay) Nanocomposites. *Appl. Clay Sci.* **1999**, *15*, 31-49.

83. Alexandre, M.; Dubois, P. Polymer-Layered Silicate Nanocomposites: Preparation, Properties and Uses of a New Class of Materials. *Mater. Sci. Engin. Rep.* **2000**, *28*, 1-63.

84. Kojima, Y.; Usuki, A.; Kawasumi, M.; Okada, A.; Fukushima, Y.; Kurauchi, T.; Kamigaito, O. Mechanical-Properties of Nylon 6-Clay Hybrid. *J. Mater. Res.* **1993**, *8*, 1185-1189.

85. Giannelis, E. P. Polymer Layered Silicate Nanocomposites. *Adv. Mater.* **1996**, *8*, 29-35.

86. Oya, A.; Kurokawa, Y.; Yasuda, H. Factors Controlling Mechanical Properties of Clay Mineral/Polypropylene Nanocomposites. *J. Mater. Sci.* **2000**, *35*, 1045-1050.

87. Tyan, H. L.; Leu, C. M.; Wei, K. H. Effect of Reactivity of Organics-Modified Montmorillonite on the Thermal and Mechanical Properties of Montmorillonite/Polyimide Nanocomposites. *Chem. Mater.* **2001**, *13*, 222-226.

88. Lu, C. S.; Mai, Y. W. Influence of Aspect Ratio on Barrier Properties of Polymer-Clay Nanocomposites. *Phys. Rev. Lett.* **2005**, *95*, 088303.

89. Yano, K.; Usuki, A.; Okada, A.; Kurauchi, T.; Kamigaito, O. Synthesis and Properties of Polyimide Clay Hybrid. *J. Polym. Sci., Part A: Polym. Chem.* **1993**, *31*, 2493-2498.

90. Osman, M. A.; Mittal, V.; Lusti, H. R. The Aspect Ratio and Gas Permeation in Polymer-Layered Silicate Nanocomposites. *Macromol. Rapid Commun.* **2004**, *25*, 1145-1149.

91. Gilman, J. W.; Jackson, C. L.; Morgan, A. B.; Harris, R.; Manias, E.; Giannelis, E. P.; Wuthenow, M.; Hilton, D.; Phillips, S. H. Flammability Properties of Polymer - Layered-Silicate Nanocomposites. Polypropylene and Polystyrene Nanocomposites. *Chem. Mater.* **2000**, *12*, 1866-1873.

92. Camino, G.; Tartaglione, G.; Frache, A.; Manferti, C.; Costa, G. Thermal and Combustion Behaviour of Layered Silicate-Epoxy Nanocomposites. *Polym. Degrad. Stab.* **2005**, *90*, 354-362.

93. Ras, R. H. A.; Umemura, Y.; Johnston, C. T.; Yamagishi, A.; Schoonheydt, R. A. Ultrathin Hybrid Films of Clay Minerals. *Phys. Chem. Chem. Phys.* **2007**, *9*, 918-932.

94. Mitchell, C. A.; Bahr, J. L.; Arepalli, S.; Tour, J. M.; Krishnamoorti, R. Dispersion of Functionalized Carbon Nanotubes in Polystyrene. *Macromolecules* **2002**, *35*, 8825-8830.

95. Kim, D.; Kim, Y.; Choi, K.; Grunlan, J. C.; Yu, C. H. Improved Thermoelectric Behavior of Nanotube-Filled Polymer Composites with Poly(3,4-Ethylenedioxythiophene) Poly(Styrenesulfonate). *ACS Nano* **2010**, *4*, 513-523.

96. Moniruzzaman, M.; Winey, K. I. Polymer Nanocomposites Containing Carbon Nanotubes. *Macromolecules* **2006**, *39*, 5194-5205.

97. Coleman, J. N.; Khan, U.; Blau, W. J.; Gun'ko, Y. K. Small but Strong: A Review of the Mechanical Properties of Carbon Nanotube-Polymer Composites. *Carbon* **2006**, *44*, 1624-1652.

98. Chatterjee, A.; Deopura, B. L. High Modulus and High Strength PP Nanocomposite Filament. *Composites Part A* **2006**, *37*, 813-817.

99. Dyke, C. A.; Tour, J. M. Unbundled and Highly Functionalized Carbon Nanotubes from Aqueous Reactions. *Nano Lett.* **2003**, *3*, 1215-1218.

100. Kashiwagi, T.; Grulke, E.; Hilding, J.; Harris, R.; Awad, W.; Douglas, J. Thermal Degradation and Flammability Properties of Poly(Propylene)/Carbon Nanotube Composites. *Macromol. Rapid Commun.* **2002**, *23*, 761-765.

101. Kashiwagi, T.; Grulke, E.; Hilding, J.; Groth, K.; Harris, R.; Butler, K.; Shields, J.; Kharchenko, S.; Douglas, J. Thermal and Flammability Properties of Polypropylene/Carbon Nanotube Nanocomposites. *Polymer* **2004**, *45*, 4227-4239.

102. Harrison, P. G. Silicate Cages: Precursors to New Materials. *J. Organomet. Chem.* **1997**, *542*, 141-183.

103. Kuo, S. W.; Lin, H. C.; Huang, W. J.; Huang, C. F.; Chang, F. C. Hydrogen Bonding Interactions and Miscibility between Phenolic Resin and Octa(Acetoxystyryl) Polyhedral Oligomeric Silsesquioxane (AS-POSS) Nanocomposites. *J. Poly. Sci. Part B: Poly. Phys.* **2006**, *44*, 673-686.

104. Misra, R.; Fu, B. X.; Morgan, S. E. Surface Energetics, Dispersion, and Nanotribomechanical Behavior of POSS/PP Hybrid Nanocomposites. *J. Poly. Sci. Part B: Poly. Phys.* **2007**, *45*, 2441-2455.

105. Feng, Y.; Jia, Y.; Guang, S. Y.; Xu, H. Y. Study on Thermal Enhancement Mechanism of POSS-Containing Hybrid Nanocomposites and Relationship between Thermal Properties and Their Molecular Structure. *J. Appl. Polym. Sci.* **2010**, *115*, 2212-2220.

106. Tseng, M. C.; Liu, Y. L. Preparation, Morphology, and Ultra-Low Dielectric Constants of Benzoxazine-Based Polymers/Polyhedral Oligomeric Silsesquioxane (POSS) Nanocomposites. *Polymer* **2010**, *51*, 5567-5575.

107. Liu, L.; Hu, Y.; Song, L.; Nazare, S.; He, S. Q.; Hull, R. Combustion and Thermal Properties of Octatma-POSS/PS Composites. *J. Mater. Sci.* **2007**, *42*, 4325-4333.

108. Devaux, E.; Rochery, M.; Bourbigot, S. Polyurethane/Clay and Polyurethane/POSS Nanocomposites as Flame Retarded Coating for Polyester and Cotton Fabrics. *Fire Mater.* **2002**, *26*, 149-154.

109. Image from Hybrid Plastics, http://www.hybridplastics.com/ (accessed on 03/2011).

110. Wang, D. Y.; Zhu, J.; Yao, Q.; Wilkie, C. A. A Comparison of Various Methods for the Preparation of Polystyrene and Poly(Methyl Methacrylate) Clay Nanocomposites. *Chem. Mater.* **2002**, *14*, 3837-3843.

111. Chen, B.; Evans, J. R. G.; Greenwell, H. C.; Boulet, P.; Coveney, P. V.; Bowden, A. A.; Whiting, A. A Critical Appraisal of Polymer-Clay Nanocomposites. *Chem. Soc. Rev.* **2008**, *37*, 568-594.

112. Paul, D. R.; Robeson, L. M. Polymer Nanotechnology: Nanocomposites. *Polymer* **2008**, *49*, 3187-3204.

113. Kashiwagi, T.; Harris, R. H.; Zhang, X.; Briber, R. M.; Cipriano, B. H.; Raghavan, S. R.; Awad, W. H.; Shields, J. R. Flame Retardant Mechanism of Polyamide 6-Clay Nanocomposites. *Polymer* **2004**, *45*, 881-891.

114. Lewin, M.; Pearce, E. M.; Levon, K.; Mey-Marom, A.; Zammarano, M.; Wilkie, C. A.; Jang, B. N. Nanocomposites at Elevated Temperatures: Migration and Structural Changes. *Polym. Adv. Technol.* **2006**, *17*, 226-234.

115. Hao, J. W.; Lewin, M.; Wilkie, C. A.; Wang, J. Q. Additional Evidence for the Migration of Clay Upon Heating of Clay-Polypropylene Nanocomposites from X-Ray Photoelectron Spectroscopy (XPS). *Polym. Degrad. Stab.* **2006**, *91*, 2482-2485.

116. Qin, H. L.; Zhang, S. M.; Zhao, C. G.; Hu, G. J.; Yang, M. S. Flame Retardant Mechanism of Polymer/Clay Nanocomposites Based on Polypropylene. *Polymer* **2005**, *46*, 8386-8395.

117. Kandola, B. K., Flame Retardancy Design for Textile. In *Fire Retardancy of Polymeric Materials*, 2 ed.; Wilkie, C. A.; Morgan, A. B., Eds. CRC Press Taylor and Francis Group: Boca Raton, 2010; pp 725-762.

118. Horrocks, A. R., Textiles. In *Fire Retardant Materials*, Horrocks, A. R.; Price, D., Eds. Woodhead Publishing: Cambridge, 2001; pp 128-181.

119. Solarski, S.; Ferreira, M.; Devaux, E.; Fontaine, G.; Bachelet, P.; Bourbigot, S.; Delobel, R.; Coszach, P.; Murariu, M.; Ferreira, A. D. S.; Alexandre, M.; Degee, P.; Dubois, P. Designing Polylactide/Clay Nanocomposites for Textile Applications: Effect of Processing Conditions, Spinning, and Characterization. *J. Appl. Polym. Sci.* **2008**, *109*, 841-851.

120. Horrocks, A. R.; Kandola, B. K.; Smart, G.; Zhang, S.; Hull, T. R. Polypropylene Fibers Containing Dispersed Clays Having Improved Fire Performance. I. Effect of Nanoclays on Processing Parameters and Fiber Properties. *J. Appl. Polym. Sci.* **2007**, *106*, 1707-1717.

121. Smart, G.; Kandola, B. K.; Horrocks, A. R.; Nazare, S.; Marney, D. Polypropylene Fibers Containing Dispersed Clays Having Improved Fire Performance. Part II: Characterization of Fibers and Fabrics from PP-Nanoclay Blends. *Polym. Adv. Technol.* **2008**, *19*, 658-670.

122. Bourbigot, S.; Devaux, E.; Flambard, X. Flammability of Polyamide-6/Clay Hybrid Nanocomposite Textiles. *Polym. Degrad. Stab.* **2002**, *75*, 397-402.

123. Bourbigot, S.; Le Bras, M.; Flambard, X.; Rochery, M.; Devaux, E.; Lichtenhan, J. D., Polyhedral Oligomeric Silsesquioxanes: Application to Flame Retardant Textiles.

In *Fire Retardancy of Polymers: New Applications of Mineral Fillers*, Le Bras, M.; S., B.; Wilkie, C. A., Eds. Royal Society of Chemistry: Cambridge, 2005; pp 189-201.

124. Weil, E. D.; Levchik, S. Current Practice and Recent Commercial Developments in Flame Retardancy of Polyamides. *J. Fire Sci.* **2004**, *22*, 251-264.

125. Bourbigot, S., Flame Retardancy of Textiles: New Approaches. In *Advances in Fire Retardant Materials*, Horrocks, A. R.; Price, D., Eds. CRC Press: Boca Raton, 2008; pp 9-40..

126. Tang, M.; Yu, Z. J.; Yu, Y. X.; Zhang, L. T.; Chen, L. F. Preparation of Silicon Carbide Fibers from the Blend of Solid and Liquid Polycarbosilanes. *J. Mater. Sci.* **2009**, *44*, 1633-1640.

127. Fukatsu, K. Kinetic and Thermogravimetric Analysis of Thermal-Degradation of Polychlal Fiber Polyester Fiber Blend. *J. Appl. Polym. Sci.* **1993**, *47*, 2117-2123.

128. Fukatsu, K. Thermal Degradation Behaviour of Aromatic Polyamide Fiber Blended with Cotton Fiber. *Polym. Degrad. Stab.* **2002**, *75*, 479-484.

129. Bajaj, P., Heat and Flame Protection. In *Handbook of Technical Textiles*, Horrocks, A. R.; Anand, S. C., Eds. Woodhead Publishing: Cambridge, 2000; pp 223-263.

130. Weil, E. D.; Levchik, S. V. Flame Retardants in Commercial Use or Development for Textiles. *J. Fire Sci.* **2008**, *26*, 243-281.

131. Horrocks, A. R., Flame Retardant/Resistant Textile Coatings and Laminates. In *Advances in Fire Retardant Materials*, Horrocks, A. R.; Price, D., Eds. CRC Press: Boca Raton, 2008; pp 159-187.

132. Wang, M. Y.; Horrocks, A. R.; Horrocks, S.; Hall, M. E.; Pearson, J. S.; Clegg, S. Flame Retardant Textile Back-Coatings. Part 1: Antimony-Halogen System Interactions and the Effect of Replacement by Phosphorus-Containing Agents. *J. Fire Sci.* **2000**, *18*, 265-294.

133. Horrocks, A. R.; Wang, M. Y.; Hall, M. E.; Sunmonu, F.; Pearson, J. S. Flame Retardant Textile Back-Coatings. Part 2. Effectiveness of Phosphorus-Containing Flame Retardants in Textile Back-Coating Formulations. *Polym. Int.* **2000**, *49*, 1079-1091.

134. Horrocks, A. R.; Davies, P. J.; Kandola, B. K.; Alderson, A. The Potential for Volatile Phosphorus-Containing Flame Retardants in Textile Back-Coatings. *J. Fire Sci.* **2007**, *25*, 523-540.

135. Giraud, S.; Bourbigot, S.; Rochery, M.; Vrornan, I.; Tighzert, L.; Delobel, R.; Poutch, F. Flame Retarded Polyurea with Microencapsulated Ammonium Phosphate for Textile Coating. *Polym. Degrad. Stab.* **2005**, *88*, 106-113.

136. Saihi, D.; Vroman, I.; Giraud, S.; Bourbigot, S. Microencapsulation of Ammonium Phosphate with a Polyurethane Shell Part 1: Coacervation Technique. *React. Funct. Polym.* **2005**, *64*, 127-138.

137. Horrocks, A. R., Smart Flame Retardant Textile Coatings and Laminates. In *Smart Textile Coatings and Laminates*, Smith, W. C., Ed. Woodhead Publishing: Cambridge, 2010; pp 264-294.

138. Simionescu, C. I.; Macoveanu, M. M.; Cazacu, G. Grafting of Synthetic-Fibers by Acrylamide in Cold High-Frequency Plasma. *Acta Polym.* **1981**, *32*, 715-718.

139. Simionescu, C. I.; Denes, F.; Macoveanu, M. M.; Totolin, M.; Cazacu, G. Polymerization of Some Potential Grafting-Monomers for Natural and Synthetic-Fibers in Cold-Plasma Conditions. *Acta Polym.* **1982**, *33*, 26-30.

140. Tsafack, M. J.; Levalois-Grutzmacher, J. L. Plasma-Induced Graft-Polymerization of Flame Retardant Monomers onto PAN Fabrics. *Surf. Coat. Technol.* **2006**, *200*, 3503-3510.

141. Huang, C. J. Room-Temperature Formation of Tantalum Oxide Films by Liquid Phase Deposition. *Thin Solid Films* **2005**, *478*, 332-337.

142. Chen, X. D.; Lenhert, S.; Hirtz, M.; Lu, N.; Fuchs, H.; Chi, L. F. Langmuir-Blodgett Patterning: A Bottom-up Way to Build Mesostructures over Large Areas. *Acc. Chem. Res.* **2007**, *40*, 393-401.

143. Balasubramanian, G.; Dionysiou, D. D.; Suidan, M. T.; Subramanian, Y.; Baudin, I.; Laine, J. M. Titania Powder Modified Sol-Gel Process for Photocatalytic Applications. *J. Mater. Sci.* **2003**, *38*, 823-831.

144. Singh, J.; Wolfe, D. E. Nanostructured Component Fabrication by Electron Beam-Physical Vapor Deposition. *J. Mater. Eng. Perform.* **2005**, *14*, 448-459.

145. Fahlman, B. D. Recent Advances in Chemical Vapor Deposition. *Curr. Org. Chem.* **2006**, *10*, 1021-1033.

146. Luzinov, I., Nanofabrication of Thin Polymer Films. In *Nanofibers and Nanotechnology in Textiles*, Brown, P. J.; Stevens, K., Eds. Woodhead Publishing: Cambridge, 2007; pp 448-469.

147. Minko, S.; Motornov, M., Hybrid Polymer Nanolayers for Surface Modification of Fibers. In *Nanofibers and Nanotechnology in Textiles*, Brown, P. J.; Stevens, K., Eds. Woodhead Publishing: Cambridge, 2007; pp 470-492.

148. Hyde, K.; Dong, H.; Hinestroza, J. P. Effect of Surface Cationization on the Conformal Deposition of Polyelectrolytes over Cotton Fibers. *Cellulose* **2007**, *14*, 615-623.

149. Iler, R. K. Multilayers of Colloidal Particles. *J. Colloid Interf. Sci.* **1966**, *21*, 569-594.

150. Decher, G.; Hong, J. D.; Schmitt, J. Buildup of Ultrathin Multilayer Films by a Self-Assembly Process .3. Consecutively Alternating Adsorption of Anionic and Cationic Polyelectrolytes on Charged Surfaces. *Thin Solid Films* **1992**, *210*, 831-835.

151. Lvov, Y.; Decher, G.; Mohwald, H. Assembly, Structural Characterization, and Thermal-Behavior of Layer-by-Layer Deposited Ultrathin Films of Poly(Vinyl Sulfate) and Poly(Allylamine). *Langmuir* **1993**, *9*, 481-486.

152. Lvov, Y.; Ariga, K.; Onda, M.; Ichinose, I.; Kunitake, T. A Careful Examination of the Adsorption Step in the Alternate Layer-by-Layer Assembly of Linear Polyanion and Polycation. *Colloids Surf., A* **1999**, *146*, 337-346.

153. Fou, A. C.; Onitsuka, O.; Ferreira, M.; Rubner, M. F.; Hsieh, B. R. Fabrication and Properties of Light-Emitting Diodes Based on Self-Assembled Multilayers of Poly(Phenylene Vinylene). *J. Appl. Phys.* **1996**, *79*, 7501-7509.

154. Cheung, J. H.; Fou, A. F.; Rubner, M. F. Molecular Self-Assembly of Conducting Polymers. *Thin Solid Films* **1994**, *244*, 985-989.

155. Tsukruk, V. V. Dendritic Macromolecules at Interfaces. *Adv. Mater.* **1998**, *10*, 253-255.

156. Lvov, Y.; Ariga, K.; Kunitake, T. Layer-by-Layer Assembly of Alternate Protein Polyion Ultrathin Films. *Chem. Lett.* **1994**, 2323-2326.

157. Caruso, F.; Furlong, D. N.; Ariga, K.; Ichinose, I.; Kunitake, T. Characterization of Polyelectrolyte-Protein Multilayer Films by Atomic Force Microscopy, Scanning Electron Microscopy, and Fourier Transform Infrared Reflection-Absorption Spectroscopy. *Langmuir* **1998**, *14*, 4559-4565.

158. Jessel, N.; Oulad-Abdeighani, M.; Meyer, F.; Lavalle, P.; Haikel, Y.; Schaaf, P.; Voegel, J. C. Multiple and Time-Scheduled in Situ DNA Delivery Mediated by Beta-Cyclodextrin Embedded in a Polyelectrolyte Multilayer. *Proc. Natl. Acad. Sci. U. S. A.* **2006**, *103*, 8618-8621.

159. Lvov, Y.; Onda, M.; Ariga, K.; Kunitake, T. Ultrathin Films of Charged Polysaccharides Assembled Alternately with Linear Polyions. *J. Biomater. Sci., Polym. Ed.* **1998**, *9*, 345-355.

160. Lvov, Y.; Haas, H.; Decher, G.; Mohwald, H.; Mikhailov, A.; Mtchedlishvily, B.; Morgunova, E.; Vainshtein, B. Successive Deposition of Alternate Layers of Polyelectrolytes and a Charged Virus. *Langmuir* **1994**, *10*, 4232-4236.

161. Ariga, K.; Lvov, Y.; Onda, M.; Ichinose, I.; Kunitake, T. Alternately Assembled Ultrathin Film of Silica Nanoparticles and Linear Polycations. *Chem. Lett.* **1997**, 125-126.

162. Kotov, N. A.; Dekany, I.; Fendler, J. H. Layer-by-Layer Self-Assembly of Polyelectrolyte-Semiconductor Nanoparticle Composite Films. *J. Phys. Chem.* **1995**, *99*, 13065-13069.

163. Zucolotto, V.; Gattas-Asfura, K. M.; Tumolo, T.; Perinotto, A. C.; Antunes, P. A.; Constantino, C. J. L.; Baptista, M. S.; Leblanc, R. M.; Jr., O. N. O. Nanoscale Manipulation of Cdse Quantum Dots in Layer-by-Layer Films: Influence of the Host Polyelectrolyte on the Luminescent Properties. *Appl. Surf. Sci.* **2005**, *246*, 397-402.

164. Kotov, N. A.; Magonov, S.; Tropsha, E. Layer-by-Layer Self-Assembly of Alumosilicate-Polyelectrolyte Composites: Mechanism of Deposition, Crack Resistance, and Perspectives for Novel Membrane Materials. *Chem. Mater.* **1998**, *10*, 886-895.

165. Podsiadlo, P.; Kaushik, A. K.; Arruda, E. M.; Waas, A. M.; Shim, B. S.; Xu, J.; Nandivada, H.; Pumplin, B. G.; Lahann, J.; Ramamoorthy, A.; Kotov, N. A. Ultrastrong and Stiff Layered Polymer Nanocomposites. *Science* **2007**, *318*, 80-83.

166. Chen, X.; Lei, Y.; Yang, W. S. Fabrication of Free-Standing Layer-by-Layer Films of Layered Double Hydroxide Nanosheets and Polyelectrolytes. *Chem. Lett.* **2008**, *37*, 1050-1051.

167. N'gom, M.; Ringnalda, J.; Mansfield, J. F.; Agarwal, A.; Kotov, N.; Zaluzec, N. J.; Norris, T. B. Single Particle Plasmon Spectroscopy of Silver Nanowires and Gold Nanorods. *Nano Lett.* **2008**, *8*, 3200-3204.

168. Gole, A.; Murphy, C. J. Biotin-Streptavidin-Induced Aggregation of Gold Nanorods: Tuning Rod-Rod Orientation. *Langmuir* **2005**, *21*, 10756-10762.

169. Wang, Y.; Tang, Z. Y.; Podsiadlo, P.; Elkasabi, Y.; Lahann, J.; Kotov, N. A. Mirror-Like Photoconductive Layer-by-Layer Thin Films of Te Nanowires: The Fusion of Semiconductor, Metal, and Insulator Properties. *Adv. Mater.* **2006**, *18*, 518-522.

170. Jain, V.; Yochum, H. M.; Montazami, R.; Heflin, J. R.; Hu, L. B.; Gruner, G. Modification of Single-Walled Carbon Nanotube Electrodes by Layer-by-Layer Assembly for Electrochromic Devices. *J. Appl. Phys.* **2008**, *103*, 074504.

171. Yan, X. B.; Chen, X. J.; Tay, B. K.; Khor, K. A. Transparent and Flexible Glucose Biosensor Via Layer-by-Layer Assembly of Multi-Wall Carbon Nanotubes and Glucose Oxidase. *Electrochem. Commun.* **2007**, *9*, 1269-1275.

172. Ariga, K.; Lvov, Y.; Kunitake, T. Assembling Alternate Dye-Polyion Molecular Films by Electrostatic Layer-by-Layer Adsorption. *J. Am. Chem. Soc.* **1997**, *119*, 2224-2231.

173. Park, Y. M.; Kim, Y. S.; Kim, B. S.; Lee, C. S.; Son, Y. A. Self-Assembly Multi-Layer of 1,3-Bisdicyanovinylindane and Its Spectral Sensing Properties. *J. Nanosci. Nanotechnol.* **2009**, *9*, 1160-1163.

174. Kim, B. S.; Park, S. W.; Hammond, P. T. Hydrogen-Bonding Layer-by-Layer Assembled Biodegradable Polymeric Micelles as Drug Delivery Vehicles from Surfaces. *ACS Nano* **2008**, *2*, 386-392.

175. Tang, Z. Y.; Wang, Y.; Podsiadlo, P.; Kotov, N. A. Biomedical Applications of Layer-by-Layer Assembly: From Biomimetics to Tissue Engineering. *Adv. Mater.* **2006**, *18*, 3203-3224.

176. Caruso, F.; Caruso, R. A.; Mohwald, H. Nanoengineering of Inorganic and Hybrid Hollow Spheres by Colloidal Templating. *Science* **1998**, *282*, 1111-1114.

177. Caruso, R. A.; Susha, A.; Caruso, F. Multilayered Titania, Silica, and Laponite Nanoparticle Coatings on Polystyrene Colloidal Templates and Resulting Inorganic Hollow Spheres. *Chem. Mater.* **2001**, *13*, 400-409.

178. Liang, Z. J.; Susha, A. S.; Yu, A. M.; Caruso, F. Nanotubes Prepared by Layer-by-Layer Coating of Porous Membrane Templates. *Adv. Mater.* **2003**, *15*, 1849-1853.

179. Hyde, G. K.; Hinestroza, J. P., Electrostatic Self-Assembled Nanolayer Films on Cotton Fibers. In *Nanofibers and Nanotechnology in Textiles*, Brown, P. J.; Stevens, K., Eds. Woodhead Publishing: Cambridge, 2007, pp 428-447.

180. Lin, Z. Y.; Renneckar, S.; Hindman, D. P. Nanocomposite-Based Lignocellulosic Fibers 1. Thermal Stability of Modified Fibers with Clay-Polyelectrolyte Multilayers. *Cellulose* **2008**, *15*, 333-346.

181. Lee, J. A.; Krogman, K. C.; Ma, M. L.; Hill, R. M.; Hammond, P. T.; Rutledge, G. C. Highly Reactive Multilayer-Assembled TiO_2 Coating on Electrospun Polymer Nanofibers. *Adv. Mater.* **2009**, *21*, 1252-1256.

182. Dubas, S. T.; Kumlangdudsana, P.; Potiuaraj, P. Layer-by-Layer Deposition of Antimicrobial Silver Nanoparticles on Textile Fibers. *Colloids Surf., A* **2006**, *289*, 105-109.

183. Ou, R. Q.; Zhang, J. G.; Deng, Y. L.; Ragauskas, A. J. Polymer Clay Self-Assembly Complexes on Paper. *J. Appl. Polym. Sci.* **2007**, *105*, 1987-1992.

184. Hyde, K.; Rusa, M.; Hinestroza, J. Layer-by-Layer Deposition of Polyelectrolyte Nanlayers on Natural Fibres: Cotton. *Nanotechnology* **2005**, *16*, S422-S428.

185. Janssens, M., Fundamentals of Fire Testing and What Tests Measure. In *Fire Retardancy of Polymeric Materials*, 2nd ed.; Wilkie, C. A.; Morgan, A. B., Eds. CRC Press Taylor & Francis Group: Boca Raton, 2010; pp 349-386.

186. Images are from Govmark, Inc., http://www.govmark.com/, and ASTM international, http://www.astm.org/, standard D6413 and D5132 (accessed on 03/2011).

187. Image is from Agricultural Research Magazine April 2002, United States Department of Agriculture, Agricultural Research Service. Cotton carpeting that fights off flames http://www.ars.usda.gov/is/AR/archive/apr02/carpet0402.pdf (accessed on 03/2011).

188. Image from ASTM international, http://www.astm.org/Standards/E1354.htm (accessed on 03/2011).

189. Image from ASTM international, http://www.astm.org/Standards/D7309.htm (accessed on 03/2011).

190. Podsiadlo, P.; Kaushik, A. K.; Arruda, E. M.; Waas, A. M.; Shim, B. S.; Xu, J. D.; Nandivada, H.; Pumplin, B. G.; Lahann, J.; Ramamoorthy, A.; Kotov, N. A. Ultrastrong and Stiff Layered Polymer Nanocomposites. *Science* **2007**, *318*, 80-83.

191. Podsiadlo, P.; Michel, M.; Lee, J.; Verploegen, E.; Kam, N. W. S.; Ball, V.; Lee, J.; Qi, Y.; Hart, A. J.; Hammond, P. T.; Kotov, N. A. Exponential Growth of Lbl Films with Incorporated Inorganic Sheets. *Nano Lett.* **2008**, *8*, 1762-1770.

192. Kleinfeld, E. R.; Ferguson, G. S. Rapid, Reversible Sorption of Water from the Vapor by a Multilayered Composite Film: A Nanostructured Humidity Sensor. *Chem. Mater.* **1995**, *7*, 2327-2331.

193. van Duffel, B.; Schoonheydt, R. A.; Grim, C. P. M.; De Schryver, F. C. Multilayered Clay Films: Atomic Force Microscopy Study and Modeling. *Langmuir* **1999**, *15*, 7520-7529.

194. Glinel, K.; Laschewsky, A.; Jonas, A. M. Ordered Polyelectrolyte "Multilayers". 4. Internal Structure of Clay-Based Multilayers. *J. Phys. Chem. B* **2002**, *106*, 11246-11252.

195. Malwitz, M. M.; Lin-Gibson, S.; Hobbie, E. K.; Butler, P. D.; Schmidt, G. Orientation of Platelets in Multilayered Nanocomposite Polymer Films. *J. Poly. Sci. Part B: Poly. Phys.* **2003**, *41*, 3237-3248.

196. Vuillaume, P. Y.; Glinel, K.; Jonas, A. M.; Laschewsky, A. Ordered Polyelectrolyte "Multilayers". 6. Effect of Molecular Parameters on the Formation of Hybrid Multilayers Based on Poly(Diallylammonium) Salts and Exfoliated Clay. *Chem. Mater.* **2003**, *15*, 3625-3631.

197. Lee, H. C.; Lee, T. W.; Kim, T. H.; Park, O. O. Fabrication and Characterization of Polymer/Nanoclay Hybrid Ultrathin Multilayer Film by Spin Self-Assembly Method. *Thin Solid Films* **2004**, *458*, 9-14.

198. Lutkenhaus, J. L.; Olivetti, E. A.; Verploegen, E. A.; Cord, B. M.; Sadoway, D. R.; Hammond, P. T. Anisotropic Structure and Transport in Self-Assembled Layered Polymer-Clay Nanocomposites. *Langmuir* **2007**, *23*, 8515-8521.

199. Thompson, D. W.; Butterworth, J. T. The Nature of Laponite and Its Aqueous Dispersions. *J. Colloid Interf. Sci.* **1992**, *151*, 236-243.

200. Cummins, H. Z. Liquid, Glass, Gel: The Phases of Colloidal Laponite. *J. Non-Cryst. Solids* **2007**, *353*, 3891-3905.

201. Ploehn, H. J.; Liu, C. Y. Quantitative Analysis of Montmorillonite Platelet Size by Atomic Force Microscopy. *Ind. Eng. Chem. Res.* **2006**, *45*, 7025-7034.

202. Li, Y.-C.; Schulz, J.; Grunlan, J. C. Polyelectrolyte/Nanosilicate Thin-Film Assemblies: Influence of pH on Growth, Mechanical Behavior, and Flammability. *ACS Appl. Mater. Interfaces* **2009**, *1*, 2338-2347.

203. Owens, D. K. The Mechanism of Corona and Ultraviolet Light-Induced Self-Adhesion of Poly(Ethylene Terephthalate) Film. *J. Appl. Polym. Sci.* **1975**, *19*, 3315-3326.

204. Zhang, D.; Sun, Q.; Wadsworth, L. C. Mechanism of Corona Treatment on Polyolefin Films. *Polym. Eng. Sci.* **1998**, *38*, 965-970.

205. Diz, H. M. M.; Rand, B. The Variable Nature of the Isoelectric Point of the Edge Surface of Kaolinite. *Brit. Ceram. Trans. J.* **1989**, *88*, 162-166.

206. Saunders, J. M.; Goodwin, J. W.; Richardson, R. M.; Vincent, B. A Small-Angle X-Ray Scattering Study of the Structure of Aqueous Laponite Dispersions. *J. Phys. Chem. B* **1999**, *103*, 9211-9218.

207. Schoeler, B.; Kumaraswamy, G.; Caruso, F. Investigation of the Influence of Polyelectrolyte Charge Density on the Growth of Multilayer Thin Films Prepared by the Layer-by-Layer Technique. *Macromolecules* **2002**, *35*, 889-897.

208. Vertlib, V.; Dietiker, M.; Plotze, M.; Yezek, L.; Spolenak, R.; Puzrin, A. M. Fast Assembly of Bio-Inspired Nanocomposite Films. *J. Mater. Res.* **2008**, *23*, 1026-1035.

209. Le Luyer, C.; Lou, L.; Bovier, C.; Plenet, J. C.; Dumas, J. G.; Mugnier, J. A Thick Sol-Gel Inorganic Layer for Optical Planar Waveguide Applications. *Opt. Mater.* **2001**, *18*, 211-217.

210. Kehlbeck, J. D.; Hagerman, M. E.; Cohen, B. D.; Eliseo, J.; Fox, M.; Hoek, W.; Karlin, D.; Leibner, E.; Nagle, E.; Nolan, M.; Schaefer, I.; Toney, A.; Topka, M.; Uluski, R.; Wood, C. Directed Self-Assembly in Laponite/CdSe/Polyaniline Nanocomposites. *Langmuir* **2008**, *24*, 9727-9738.

211. Pawar, N.; Bohidar, H. B. Hydrophobic Hydration Mediated Universal Self-Association of Colloidal Nanoclay Particles. *Colloids Surf., A* **2009**, *333*, 120-125.

212. Oliver, W. C.; Pharr, G. M. An Improved Technique for Determining Hardness and Elastic-Modulus Using Load and Displacement Sensing Indentation Experiments. *J. Mater. Res.* **1992**, *7*, 1564-1583.

213. Sepeur, S.; Kunze, N.; Werner, B.; Schmidt, H. UV Curable Hard Coatings on Plastics. *Thin Solid Films* **1999**, *351*, 216-219.

214. Wu, L. Y. L.; Soutar, A. M.; Zeng, X. T. Increasing Hydrophobicity of Sol-Gel Hard Coatings by Chemical and Morphological Modifications. *Surf. Coat. Technol.* **2005**, *198*, 420-424.

215. Gui, H.; Zhang, X. H.; Liu, Y. Q.; Dong, W. F.; Wang, Q. G.; Gao, J. M.; Song, Z. H.; Lai, J. M.; Qiao, J. L. Effect of Dispersion of Nano-Magnesium Hydroxide on the

Flammability of Flame Retardant Ternary Composites. *Compos. Sci. Technol.* **2007**, *67*, 974-980.

216. Li, Y.-C.; Schulz, J.; Mannen, S.; Delhom, C.; Condon, B.; Chang, S.; Zammarano, M.; Grunlan, J. C. Flame Retardant Behavior of Polyelectrolyte-Clay Thin Film Assemblies on Cotton Fabric. *ACS Nano* **2010**, *4*, 3325-3337.

217. Priolo, M. A.; Gamboa, D.; Grunlan, J. C. Transparent Clay-Polymer Nano Brick Wall Assemblies with Tailorable Oxygen Barrier. *ACS Appl. Mater. Interfaces* **2010**, *2*, 312-320.

218. Schartel, B.; Pawlowski, K. H.; Lyon, R. E. Pyrolysis Combustion Flow Calorimeter: A Tool to Assess Flame Retarded PC/ABS Materials? *Thermochim. Acta* **2007**, *462*, 1-14.

219. Lyon, R. E.; Walters, R. N. Pyrolysis Combustion Flow Calorimetry. *J. Anal. Appl. Pyrolysis* **2004**, *71*, 27-46.

220. Hergenrother, P. M.; Thompson, C. M.; Smith, J. G.; Connell, J. W.; Hinkley, J. A.; Lyon, R. E.; Moulton, R. Flame Retardant Aircraft Epoxy Resins Containing Phosphorus. *Polymer* **2005**, *46*, 5012-5024.

221. Suh, M. W. A Study of Shrinkage of Plain Knitted Cotton Fabric Based on Structural Changes of Loop Geometry Due to Yarn Swelling and Deswelling. *Text. Res. J.* **1967**, *37*, 417-431.

222. Zeronian, S. H.; Bertoniere, N. R.; Alger, K. W.; Duffin, J. L.; Kim, M. S.; Dubuque, L. K.; Collins, M. J.; Xie, C. Effect of Dimethyloldihydroxyethyleneurea on the Properties of Cellulosic Fibers. *Text. Res. J.* **1989**, *59*, 484-492.

223. Tunega, D.; Gerzabek, M. H.; Lischka, H. *Ab Initio* Molecular Dynamics Study of a Monomolecular Water Layer on Octahedral and Tetrahedral Kaolinite Surfaces. *J. Phys. Chem. B* **2004**, *108*, 5930-5936.

224. Mantz, R. A.; Jones, P. F.; Chaffee, K. P.; Lichtenhan, J. D.; Gilman, J. W.; Ismail, I. M. K.; Burmeister, M. J. Thermolysis of Polyhedral Oligomeric Silsesquioxane (POSS) Macromers and POSS-Siloxane Copolymers. *Chem. Mater.* **1996**, *8*, 1250-1259.

225. Schwab, J. J.; Lichtenhan, J. D. Polyhedral Oligomeric Silsesquioxane (POSS)-Based Polymers. *Appl. Organomet. Chem.* **1998**, *12*, 707-713.

226. Gupta, S. K.; Schwab, J. J.; Lee, A.; Fu, B. X.; Hsiao, B. S., POSS Reinforced Fire Retarding EVE Resins, in *Affordable Materials Technology-Platform to Global Value and Performance*. *Sampe Pub.*, Rasmussen, B. M.; Pilato, L. A.; Lkliger, H. S., Eds. **2002**, *47*, 1571-1526.

227. Hsiue, G. H.; Liu, Y. L.; Liao, H. H. Flame-Retardant Epoxy Resins: An Approach from Organic-Inorganic Hybrid Nanocomposites. *J. Polym. Sci., Part A: Polym. Chem.* **2001**, *39*, 986-996.

228. Fina, A.; Tabuani, D.; Camino, G. Polypropylene-Polysilsesquioxane Blends. *Eur. Polym. J.* **2010**, *46*, 14-23.

229. Cassagneau, T.; Caruso, F. Oligosilsesquioxanes as Versatile Building Blocks for the Preparation of Self-Assembled Thin Films. *J. Am. Chem. Soc.* **2002**, *124*, 8172-8180.

230. Wang, X. M.; Ding, H. M.; Shan, Y. K.; He, M. Y. Fabrication of Layer-by-Layer Films of Polyhedral Oligomeric Silsesquioxanes. *Chin. Chem. Lett.* **2004**, *15*, 1227-1229.

231. Carroll, J. B.; Frankamp, B. L.; Srivastava, S.; Rotello, V. M. Electrostatic Self-Assembly of Structured Gold Nanoparticle/Polyhedral Oligomeric Silsesquioxane (POSS) Nanocomposites. *J. Mater. Chem.* **2004**, *14*, 690-694.

232. Li, Y.-C.; Mannen, S.; Schulz, J.; Grunlan, J. C. Growth and Fire Protection Behavior of POSS-Based Multilayer Thin Films *J. Mater. Chem.* **2011**, *21*, 3060-3069.

233. Wu, G. J.; Su, Z. H. Polyhedral Oligomeric Silsesquioxane Nanocomposite Thin Films Via Layer-by-Layer Electrostatic Self-Assembly. *Chem. Mater.* **2006**, *18*, 3726-3732.

234. Liu, Y. L.; Liu, C. S.; Chen, W. H.; Chen, S. Y.; Wang, K. S.; Hwu, M. J. Ultra-Low-*k* Thin Films of Polyhedral Oligomeric Silsesquioxane/Epoxy Nanocomposites Via Covalent Layer-by-Layer Assembly. *J. Nanosci. Nanotechnol.* **2009**, *9*, 1839-1843.

235. Marsh, D. H.; Riley, D. J.; York, D.; Graydon, A. Sorption of Inorganic Nanoparticles in Woven Cellulose Fabrics. *Particuology* **2009**, *7*, 121-128.

236. Blanchard, E. J.; Graves, E. E.; Salame, P. A. Flame Resistant Cotton/Polyester Carpet Materials. *J. Fire Sci.* **2000**, *18*, 151-164.

237. Xiao, Z. L.; Han, C. Y.; Welp, U.; Wang, H. H.; Kwok, W. K.; Willing, G. A.; Hiller, J. M.; Cook, R. E.; Miller, D. J.; Crabtree, G. W. Fabrication of Alumina Nanotubes and Nanowires by Etching Porous Alumina Membranes. *Nano Lett.* **2002**, *2*, 1293-1297.

238. Bae, C. D.; Kim, S. Y.; Ahn, B. Y.; Kim, J. Y.; Sung, M. M.; Shin, H. J. Template-Directed Gas-Phase Fabrication of Oxide Nanotubes. *J. Mater. Chem.* **2008**, *18*, 1362-1367.

239. Mei, Y. F.; Thurmer, D. J.; Deneke, C.; Kiravittaya, S.; Chen, Y. F.; Dadgar, A.; Bertram, F.; Bastek, B.; Krost, A.; Christen, J.; Reindl, T.; Stoffel, M.; Coric, E.; Schmidt, O. G. Fabrication, Self-Assembly, and Properties of Ultrathin ALN/GAN Porous Crystalline Nanomembranes: Tubes, Spirals, and Curved Sheets. *ACS Nano* **2009**, *3*, 1663-1668.

240. Park, M. H.; Kim, M. G.; Joo, J.; Kim, K.; Kim, J.; Ahn, S.; Cui, Y.; Cho, J. Silicon Nanotube Battery Anodes. *Nano Lett.* **2009**, *9*, 3844-3847.

241. Shen, D. K.; Gu, S. The Mechanism for Thermal Decomposition of Cellulose and Its Main Products. *Bioresour. Technol.* **2009**, *100*, 6496-6504.

242. Horrocks, A. R. An Introduction to the Burning Behavior of Cellulosic Fibers. *J. Soc. Dyers Colour.* **1983**, *99*, 191-197.

243. Delobel, R.; Lebras, M.; Ouassou, N.; Alistiqsa, F. Thermal Behaviors of Ammonium Polyphosphate-Pentaerythritol and Ammonium Pyrophosphate-Pentaerythritol Intumescent Additives in Polypropylene Formulations. *J. Fire Sci.* **1990**, *8*, 85-108.

244. Zhang, S.; Horrocks, A. R. Substantive Intumescence from Phosphorylated 1,3-Propanediol Derivatives Substituted on to Cellulose. *J. Appl. Polym. Sci.* **2003**, *90*, 3165-3172.

245. Bourbigot, S.; Lebras, M.; Delobel, R. Fire Degradation of an Intumescent Flame-Retardant Polypropylene Using the Cone Calorimeter. *J. Fire Sci.* **1995**, *13*, 3-22.

246. Kandola, B. K.; Horrocks, A. R. Complex Char Formation in Flame-Retarded Fibre-Intumescent Combinations - IV. Mass Loss and Thermal Barrier Properties. *Fire Mater.* **2000**, *24*, 265-275.

247. Horrocks, A. R.; Kandola, B. K.; Davies, P. J.; Zhang, S.; Padbury, S. A. Developments in Flame Retardant Textiles - A Review. *Polym. Degrad. Stab.* **2005**, *88*, 3-12.

248. Cini, N.; Tulun, T.; Decher, G.; Ball, V. Step-by-Step Assembly of Self-Patterning Polyelectrolyte Films Violating (Almost) All Rules of Layer-by-Layer Deposition. *J. Am. Chem. Soc.* **2010**, *132*, 8264-8265.

249. Kharlampieva, E.; Kozlovskaya, V.; Sukhishvili, S. A. Layer-by-Layer Hydrogen-Bonded Polymer Films: From Fundamentals to Applications. *Adv. Mater.* **2009**, *21*, 3053-3065.

250. Flambard, X.; Bourbigot, S.; Kozlowski, R.; Muzyczek, M.; Mieleniak, B.; Ferreira, M.; Vermeulen, B.; Poutch, F. Progress in Safety, Flame Retardant Textiles and Flexible Fire Barriers for Seats in Transportation. *Polym. Degrad. Stab.* **2005**, *88*, 98-105.

251. Tsuyumoto, I.; Oshio, T. Development of Fire Resistant Laminated Wood Using Concentrated Sodium Polyborate Aqueous Solution. *J. Wood Chem. Technol.* **2009**, *29*, 277-285.

252. Bourbigot, S.; Duquesne, S., Intumescence-Based Fire Retardants. In *Fire Retardnacy of Polymeric Materials*, 2nd ed.; Wilkie, C. A.; Morgan, A. B., Eds. CRC Press Taylor & Francis Group: Boca Raton, 2010; Chapter 6.

253. Tong, W. J.; Gao, C. Y.; Mohwald, H. Stable Weak Polyelectrolyte Microcapsules with pH-Responsive Permeability. *Macromolecules* **2006**, *39*, 335-340.

254. American Association of Textile Chemists and Colorists test method 124, smoothness appearance of fabrics after repeated home laundering, http://www.aatcc.org/Technical/Test_Methods/scopes/tm124.cfm (accessed on 03/2011).

255. Krogman, K. C.; Zacharia, N. S.; Schroeder, S.; Hammond, P. T. Automated Process for Improved Uniformity and Versatility of Layer-by-Layer Deposition. *Langmuir* **2007**, *23*, 3137-3141.

VITA

Yu-Chin Li was born in Taipei, Taiwan. She received her Bachelor of Science degree in chemistry from the National Taiwan University in 2002 and directly entered the graduate program at the same school, earning her Master of Science degree, also in chemistry, in 2004. After working as a researcher at Academia Sinica in Taipei for a year, she entered the doctoral program at Texas A&M University, where in May 2011 she received her Ph.D. degree, in materials science & engineering. Her research interests include flame retardant materials and polymer nanocomposites. Her permanent address is 4F, No.14, Ln.204, Song-Shan Rd, Taipei, 110, Taiwan. Her email address is yuchin1024@gmail.com.